論文 / 著書情報
Article / Book Information

題目(和文)	共鳴的に相互作用する 1 次元量子系の普遍的性質
Title(English)	Universal Properties of Resonantly Interacting Quantum Systems in One Dimension
著者(和文)	関野裕太
Author(English)	Yuta Sekino
出典(和文)	学位:博士(理学), 学位授与機関:東京工業大学, 報告番号:甲第11041号, 授与年月日:2019年3月26日, 学位の種別:課程博士, 審査員:西田 祐介,西森 秀稔,笹本 智弘,古賀 昌久,上妻 幹旺
Citation(English)	Degree:Doctor (Science), Conferring organization: Tokyo Institute of Technology, Report number:甲第11041号, Conferred date:2019/3/26, Degree Type:Course doctor, Examiner:,,,,
学位種別(和文)	博士論文
Type(English)	Doctoral Thesis

Dissertation

Universal Properties of Resonantly Interacting Quantum Systems in One Dimension

Yuta Sekino

Department of Physics, Tokyo Institute of Technology, Japan

February 14, 2019

Abstract

Understanding quantum many-body systems with interactions is an important problem common to various fields of physics, such as atomic physics, condensed matter physics, nuclear physics, and particle physics. Among others, ultracold atoms have provided ideal grounds to study strongly interacting systems and to explore exotic quantum states because of their high controllability. We can widely control the strengths of the interactions from weak to strong as well as the geometry of the systems. In order to deepen our understanding of quantum many-body systems with interactions, we in this thesis investigate two types of one-dimensional (1D) systems realizable with ultracold atoms; bosons and spinless fermions near two-body resonances and bosons near a three-body resonance.

One-dimensional systems near two-body resonances have been intensively studied because, in the homogeneous cases, they are exactly solvable systems. The energy spectra and thermodynamic quantities exactly obtained by the Bethe ansatz have greatly contributed to deepening our comprehension of many-body systems in 1D. On the other hand, the exact computations of correlation functions, which encode information about excitations of the systems, are in general much more complicated even in the integrable systems.

Motivated by this background, we derive a series of exact relations for correlation functions in bosons and fermions near two-body resonances. These relations called universal relations originate from the universal properties of the resonant systems: Their properties depend on the interactions only through the scattering lengths characterizing the low-energy scattering. The universal relations are strong constraints on the systems because the relations hold for any particle number, scattering length, temperature, and with or without a trapping potential. The relations include the asymptotic behaviors of correlation functions in high-energy regime as well as the energy relations, in which the energies are expressed in term of the momentum distributions. The universal relations involve two- and three-body contacts, which are the integrals of local pair and triad correlations, respectively.

Firstly we derive, in both bosons and fermions, universal relations for static correlation functions such as static structure factors and momentum distributions within the first-quantized formalisms. The power laws of the static correlation functions for large momentum and the energy relations are obtained. The coefficients in these power-law behaviors are proportional to the two-body contact. We clarify that the three-body contact makes no contribution to the bosonic energy relation, but it plays a crucial role in the fermionic one.

Secondly, we derive universal relations for dynamic correlation functions for bosons. Using the operator product expansion (OPE) in the field theoretical formalism, we obtain the large-energy-momentum behaviors of the dynamic structure factor, the dynamic current correlation, and the single-particle spectral density as well as the quasiparticle energy and the scattering rate in high-energy regime. While the behaviors of the dynamic structure factor and the current correlation are proportional to the two-body contact, that of the single-particle spectral density is proportional to the number density. Because of the interrelation between 1D bosons and fermions near two-body resonances, the results of the dynamic structure factor and the current

correlation for bosons also hold for the fermions.

Thirdly, the quantum field theory for fermions near a two-body resonance is studied to derive universal relations for the single-particle spectral density. Unlike for bosons, the regularization is necessary for the field theory for fermions. Performing a renormalization group analysis, we find that not only two-body but also three-body couplings are renormalized and clarify that the renormalization of the three-body coupling is associated with the appearance of the three-body contact in the fermionic energy relation. Applying OPE to the constructed field theory, we investigate the large-energy-momentum behavior of the single-particle spectral density. As a result, the behavior is found to be proportional to the number density.

The high controllability of ultracold atoms allows us to extinguish their two-body interaction, leading to the realization of unique systems governed by the three-body interaction, which is otherwise hidden behind the two-body interaction. In such systems, novel bound states, which are not stabilized by two-body interactions, are expected to appear. From this perspective, 1D bosons with a resonant three-body interaction are investigated in this thesis. We reveal that they form few-body bound states as well as a many-body droplet stabilized by the quantum mechanical effect. Their binding energies relative to that of three bosons are all universal and the ground-state energy of the dilute droplet is found to grow exponentially as $E_N/E_3 \to \exp(8N^2/3\pi)$ with increasing particle number $N \gg 1$. This exponential growth of E_N results from the asymptotic freedom associated with the three-body interaction in 1D.

While our studies of the resonantly interacting systems in 1D are motivated by highly tunable ultracold atoms, the properties of the systems are universal in the sense that they are independent of microscopic details of the interaction potentials. Accordingly, our result can be applied not only to ultracold atomic gases in elongated traps but also other 1D quantum systems in which microscopic length scales associated with interactions are much smaller than other length scales such as the scattering lengths, thermal de Broglie wavelengths, and mean interparticle distances.

List of Publications

1. Yuta Sekino and Yusuke Nishida, "Quantum droplet of one-dimensional bosons with a three-body attraction," Phys. Rev. A **97**, 011602(R) (2018).

2. Yuta Sekino, Shina Tan, and Yusuke Nishida, "Comparative study of one-dimensional Bose and Fermi gases with contact interactions from the viewpoint of universal relations for correlation functions," Phys. Rev. A **97**, 013621 (2018).

Acknowledgement

I would like to express my deepest gratitude to my supervisor Prof. Yusuke Nishida for his encouragement and support. The studies could not been accomplished without his insightful advice and fruitful discussions. I also thank Prof. Shina Tan for giving a meaningful advice on the study of one-dimensional fermions we co-authored. I would like to express my gratitude to the members of the Nishida group and all colleagues who share the room with me in Tokyo Institute of Technology for providing me an exciting life. In particular, I would like to thank Dr. Kazutaka Takahashi, Dr. Yoshitaka Fujimoto, Takato Yoshimura, Takaaki Anzai, Manaka Okuyama, and Keisuke Fujii for stimulating discussions. Finally, I would like to show my gratitude for my family for their unfailing support.

Contents

Chapter 1

Introduction

1.1 Strongly correlated many-body systems

Strongly correlated many-body systems appear in a variety of fields of physics, such as atomic physics, condensed matter physics, nuclear physics, and particle physics. These systems include strongly correlated electron systems such as high-T_c superconductors [1], superfluid nuclear matters expected to be realized in neutron stars [2, 3], and strongly interacting quark–gluon plasmas produced in heavy ion collisions [4–7]. While the strongly correlated systems exhibit many interesting phenomena, understanding of their physical properties is always challenging. Among others, ultracold atoms are highly tunable systems, where we can widely control their quantum statistics, interaction, and spatial dimensionality [8–10]. This high controllability allows us to systematically investigate quantum many-body systems from a weakly-interacting regime to a strongly correlated regime. Therefore, the ultracold atoms have been providing ideal grounds to deepen our knowledge of strongly interacting many-body systems.

1.2 Ultracold atoms and universal properties near resonances

Ultracold atoms are atomic gases produced by laser cooling [11] and evaporative cooling [12]. Typically, these gases have densities n between 10^{12} and 10^{15} atoms per cm^3 and they are maintained at temperatures T in the nanokelvin range. The atomic gases reach the quantum degenerate regime $T \lesssim 0.1T_{\rm deg}$, where $T_{\rm deg} = \hbar^2 n^{2/3}/(k_B m)$ is the quantum degeneracy temperature with m being the mass of the atoms. Since there are a variety of atomic species and isotopes, we can obtain ultracold Bose or Fermi gases as well as mixtures of bosons and fermions. For instance, ^{7}Li, ^{23}Na, ^{39}K, ^{87}Rb, ^{133}Cs, and ^{174}Yb are bosonic atoms, while ^{6}Li, ^{40}K, ^{86}Rb, and ^{173}Yb are fermionic ones. Since atoms have various hyperfine states, we can also choose the number of internal states.

For ultracold bosonic atoms or fermionic atoms with two internal states, the s-wave scattering length a_s, which characterizes the low-energy scattering amplitude of two particles, can be tuned by an external magnetic field B near a Feshbach resonance [13]. Near the resonance, the scattering length can be parametrized as a simple function of B [14], $a_s = a_{\rm bg}[1 - \Delta/(B - B_0)]$,

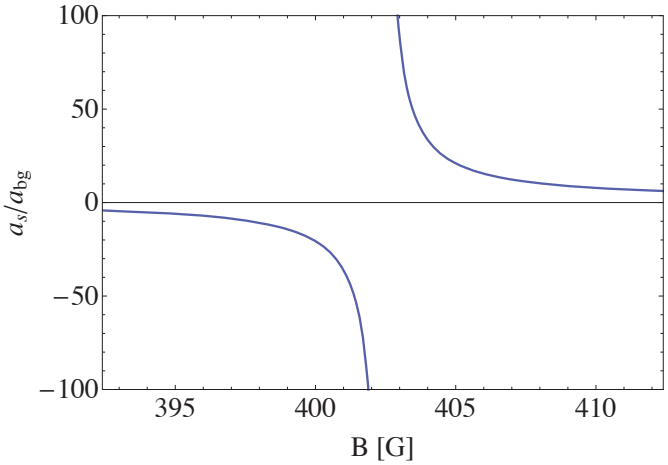

Figure 1.1: Scattering length a_s near a Feshbach resonance for ^{39}K. The resonance position $B_0 = 402.4$ G and the resonance width $\Delta = -52$ G are determined by the experiment in Ref. [15].

where $a_{\rm bg}$ denotes the off-resonant value of the scattering length, B_0 is the resonance position, at which a_s is divergent, and Δ is the resonance width. Figure 1.1 shows that a_s takes arbitrary values from $-\infty$ to ∞. In the case of a single-component Fermi gas, the s-wave scattering is forbidden by Fermi-Dirac statistics, and thus the p-wave scattering is dominant. The p-wave scattering can also be magnetically controlled via a p-wave Feshbach resonance [16].

The van der Waals interaction between atoms is short ranged and its range is typically $r_0 \sim 1$ nm. In the case of ultracold atoms with mass m near a s-wave resonance, r_0 is much smaller than the thermal de Broglie wavelength $\lambda_T = h/\sqrt{2\pi m k_B T}$ and the mean interatomic distance $n^{-1/3}$ as well as the absolute value of the scattering length:

$$r_0 \ll \lambda_T,\, n^{-1/3},\, |a_s|. \tag{1.1}$$

In this resonant regime, the scattering length is the only relevant length scale associated with the interaction potential, so that the system has universal properties: A variety of physical quantities depend on the interaction only through the scattering length, i.e., become independent of microscopic details of the interaction potential. For example, in the unitary limit $a_s \to \infty$, the Fermi gas becomes a strongly interacting system called the unitary Fermi gas, and the number density n is the only dimensionful scale of the system [17]. Therefore, the thermodynamic function of the unitary Fermi gas is given by a function of a single variable $1/n\lambda_T^3$, which is independent of the interaction potential. Another example is the existence of a series of three-body bound states called Efimov trimers for identical bosons near a s-wave resonance [18–21]. The binding energy of the n-th Efimov trimer follows the universal scaling law $B^{(n)} \sim (22.7)^{-2n}$. The experimental signature of the Efimov trimers has been also observed with ultracold atoms such as ^{133}Cs [22]. The universal physics near resonances including the unitary Fermi gas and the Efimov trimers can be described by the zero-range models, where the short-range interactions are reduced to contact interactions with $r_0 \to 0$.

Since such universal properties appear as long as systems are in the resonant regime in Eq. (1.1), the studies of the universal properties can be applied not only to ultracold atoms but also other resonant systems. Accordingly, such studies play an important role as a bridge among various subfields of physics. In nuclear physics, the neutron-neutron s-wave scattering length $a_s \simeq -18.5$ fm is much larger than the range of the nuclear force $r_0 \simeq 1$ fm [23]. A dilute neutron matter at low temperature, which is expected to be realized in the inner crust of neutron stars, reaches the regime in Eq. (1.1) [24], and thus the neutron matter shares the universal properties with ultracold Fermi gases near s-wave resonances. On the other hand, the physics of the Efimov trimers is studied not only from the perspectives of atomic and molecular physics [22, 25], but also from the point of views of nuclear physics [26] and condensed matter physics [27].

Recently, a series of exact relations, called *universal relations*, for a system near a resonance have received much attention [28–30]. The universal relations are strong constraints on the system because they hold for any number of particles, scattering length, temperature, and with or without a trapping potential. In particular, it is valuable that these relations provide exact information of the system even in the strongly correlated regime. In the relations, various quantities including power-law tails of correlation functions in frequency-momentum space, the energy, and the derivative of a free energy with respect to a coupling constant are related to so-called contact parameters, which measure short-range correlations of the system. While the universal relations were originally found in a 3D Fermi gas with an s-wave interaction [28–30], they have been generalized to various systems such as Bose gases [31, 32], lower-dimensional gases [32–35], and quantum gases with higher partial-wave interactions [36–38] as well as to nuclear systems [39]. The relations have also been verified experimentally in 3D Fermi gases with s-wave and p-wave interactions [40, 41].

1.3 One-dimensional systems near two-body resonances

The 1D counterparts of the zero-range models have been intensively studied since 1960s and greatly contributed to the advancement of our understanding of strongly interacting many-body systems in 1D because, in the homogeneous cases, they are exactly solvable systems [42, 43]. Among others, the zero-range model for 1D bosons in the absence of a trapping potential has a long history [44, 45]. In 1960, Girardeau investigated 1D bosons with an infinitely strong repulsion and found that their energy eigenstates are related to those for spinless free fermions through the Bose-Fermi mapping [46]. These strongly interacting bosons are called the Tonks-Girardeau gas. Because of the existence of the Bose-Fermi mapping, various physical quantities such as thermodynamic quantities are identical between the Tonks-Girardeau and the noninteracting Fermi gases. In this sense, the Tonks-Girardeau gas is frequently referred to as "fermionized" bosons. After three years of the Girardeau's work, Lieb and Liniger studied the zero-range model of bosons with a delta-function interaction potential, which is now called the Lieb-Liniger model [44]. For a finite repulsive interaction, Lieb and Liniger exactly computed the ground state energy in the thermodynamic limit as well as the excitation spectrum by using the Bethe

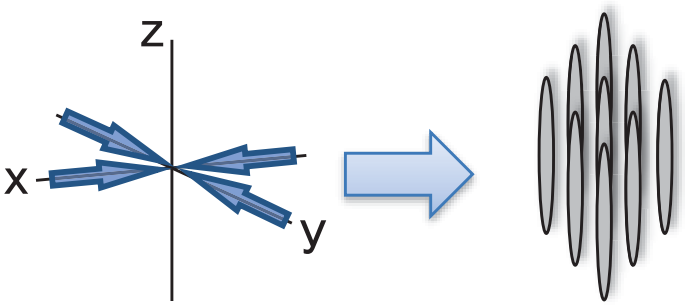

Figure 1.2: (Left) Configuration of two pairs of counter-propagating laser beams to produce a 2D optical potential which is periodic in the x and y directions. (Right) Atoms in a 2D optical periodic potential with a large amplitude. The atoms can freely move only along the z-axis, leading to an array of 1D tubes. The optical potential around its each minimum can be well approximated by a tightly confining harmonic oscillator potential along the transverse direction.

ansatz method and revealed the existence of the gapless excitation. Thermodynamic quantities and the excitation spectrum at finite temperature was studied by Yang and Yang in 1969 [47]. On the other hand, in the case of attractive interaction, McGuire found that the ground state of N-bosons is a cluster-like bound state, whose binding energy grows as N^3 with increasing particle number [48].

Until about two decades ago, such 1D bosons had been mainly studied from a purely theoretical perspective. This situation changed with a proposal to realize 1D atomic systems by Olshanii in 1998 [49]. He showed that 1D systems with a delta-function interaction potential can be obtained by confining a 3D ultracold atomic gas with a contact s-wave interaction in a highly elongated harmonic trap. Such a 1D confinement can be realized by using a 2D optical lattice (see Fig. 1.2). Six years later, 1D Bose gases were experimentally realized with ultracold ^{87}Rb and the fermionized properties of the Tonks-Girardeau gas were observed [50]. This experimental achievement has stimulated many theoretical and experimental studies of 1D systems near resonances [45].

On the other hand, 1D spinless fermions near a resonance can be obtained by confining a 3D Fermi gas near a p-wave resonance in a highly elongated harmonic trap [51]. These fermions can be described by the fermionic zero-range model [52]. Cheon and Shigehara found that all energy eigenstates of the fermionic zero-range model are mapped into those of the bosonic zero-range model and vice versa via the Girardeau's Bose-Fermi mapping [52]. This Bose-Fermi correspondence is a natural generalization of the interrelation between the Tonks-Girardeau gas and the free fermions. As a consequence of the Bose-Fermi correspondence, the energy spectrum, thermodynamics and density correlation functions are identical between bosons and fermions related to each other through the Bose-Fermi mapping. Accordingly, many results derived in the bosonic model can be directly applied to the fermionic one. However, some correlation functions such as a momentum distribution and a single-particle spectral density are different between bosons and fermions, and these correlation functions for fermions have been much less revealed

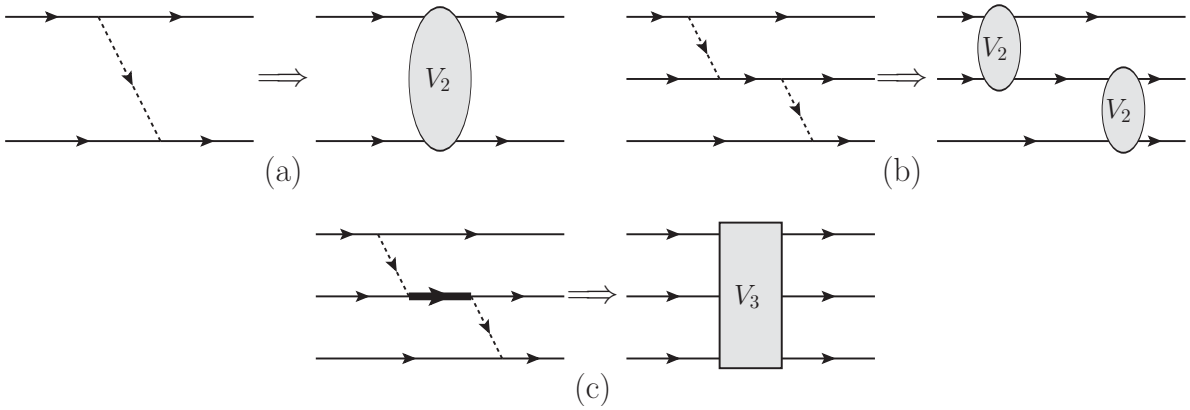

Figure 1.3: Mechanism of the emergence of two- and three-body interactions among nucleons due to virtual pions and delta particles. The solid, dotted, and bold solid lines indicate the propagations of a nucleon, a pion, and a delta particle, respectively. Figure (a) denotes the one-pion exchange process leading to the two-body potential V_2 between nucleons, while Figs. (b) and (c) denote two-pion exchange processes without and with a virtual delta excitation, respectively. Because of the virtual excitation, the process (c) gives rise to the three-nucleon interaction V_3.

than those for bosons.

While the thermodynamic quantities in the zero-range models can be exactly computed by the Bethe ansatz, the exact calculations of correlation functions are in general much more complicated even in integrable systems [54]. One of the great successes in such a problem is Haldane's theory of quantum liquids, where the low-energy behaviors of correlation functions at zero temperature were found to be universal [55]. These universal properties of correlation functions originate from the quantum many-body fluctuation in 1D. In this thesis, we investigate another kind of universal properties i.e., universal relations for correlation functions, which is effectively determined by few-body physics. Although these universal relations are powerful by themselves, the relations combined with the Bose-Fermi correspondence and the exact contact parameters obtained by the Bethe ansatz provide us more detailed information about correlation functions.

1.4 Three-body interactions

Most of the physical systems we are interested in consist of two or more constituents interacting with each other. The key to understanding of such systems is to clarify how interparticle interactions affect their properties. While interactions between atoms, molecules, or nucleons (proton and neutron) are usually treated as pairwise ones, interactions among three or more particles which cannot be expressed in terms of the pairwise potentials, in general, appear [56–59]. However, the three and higher-body interactions are usually so weak that they are hidden behind two-body ones [60].

Three- and higher-body interactions often result from virtual excitations. Here we explain

the mechanism of the emergence of two- and three-body interactions in the case of three-nucleon systems [59]. Within the low-energy effective theory of nucleons, virtual particles other than nucleons are integrated out and replaced with interaction potentials. Figure (a) indicates that the exchange of one virtual pion between two nucleons gives the pairwise Yukawa potential V_2. A two-pion exchange process with the propagation of a virtual nucleon [depicted in Fig. 1.3 (b)] can be expressed in terms of V_2 because it can be separated into two one-pion exchange processes [shown in Fig. 1.3 (a)] by cutting the virtual nucleon line. On the other hand, there is another two-pion exchange process shown in Fig. 1.3 (c), in which an excited state called a delta particle appears as a virtual state. This process cannot be separated into the one-pion exchange depicted in Fig. 1.3 (a), and thus it provides the three-body interaction V_3, which cannot be expressed as the sum of the two-body interactions.

As mentioned in the previous sections, ultracold atoms provide ideal grounds where interatomic interactions are widely tunable. Taking advantage of these features, we can make a two-body interaction so week that the system is governed by a three-body interaction. Recently, various proposals to independently tune two- and three-body interactions in ultracold atomic systems have been put forward [61–71]. It is predicted that the systems with three-body interactions exhibit many interesting phenomena [61–71]. For example, a weakly interacting Bose-Einstein condensate with a two-body attraction and a three-body repulsion is predicted to be formed into a self-binding droplet [72]. Three-body repulsions are also expected to stabilize paired bosonic superfluids [64, 73–76] and the Pfaffian state, whose excitations called anyons obey the non-Abelian statistics and have received much attention in the context of topological quantum computations [77].

Resonant three-body interactions have been studied in dimensions higher than one. In 3D bosons, such a three-body interaction is predicted for large and negative s-wave scattering lengths when a Efimov trimer crossed the three-particle threshold [61, 72]. In 2D bosons, it was found that a resonant three-body attraction stabilizes a series of exotic four-body bound states called semisuper Efimov tetramers, whose sizes follow a universal scaling law [78]. In this thesis, we investigate what bound states are formed because of the interplay of the resonant three-body interaction and the one-dimensionality.

1.5 Purposes and outline of this thesis

In order to deepen our understanding of interacting quantum many-body systems in various fields of physics, we in this thesis investigate two types of 1D systems from the viewpoint of the universal properties near resonances; bosons and spinless fermions near two-body resonances and bosons near a three-body resonance.

This thesis is organized as follows. In Chapter 2, we review previous works related to our study. In particular, we introduce how to describe universal properties near two-body resonances, details of the Bose-Fermi correspondence and of the Bethe ansatz, and how to realize a 1D system governed by a resonant three-body interaction. Chapters 3, 4, and 5 are devoted to deriving universal relations in bosons and fermions near two-body resonances. In Chapter 3,

we derive universal relations for static correlation functions including a static structure factor and a momentum distribution. Universal relations for dynamic correlation functions are studied for bosons in Chapter 4 and for fermions in Chapter 5. In Chapter 6, we investigate universal properties of bound states of bosons with a resonant three-body interaction. We summarize this this thesis in Chapter 7. Throughout this thesis, we set $\hbar = 1$.

Chapter 2

Review of resonantly interacting systems in 1D

In this chapter, we review previous works in resonantly interacting quantum systems in 1D. First, we review the universal properties of bosons and fermions near two-body resonances in Section 2.1. Section 2.2 is devoted to the review of the Bethe ansatz to exactly solve the Schrödinger equations in the homogeneous cases. In Section 2.3, we introduce how to realize 1D bosons with a resonant three-body interaction. In the end of this chapter, we summarize the chapter.

2.1 Universalities near two-body resonances in 1D

We begin by reviewing 1D scattering problems for two identical particles with short-range interactions to understand the universalities of low-energy physics with large scattering length and how to describe the universal properties. We follow Refs [30, 79] below.

Suppose that two identical particles with their mass m interact with each other via a potential $U(x)$, which is symmetric $U(x) = U(-x)$ and has a range r_0, i.e., $U(x) = 0$ for $|x| > r_0$. Because of statistics of particles, a wave function for relative motion satisfies $\psi_B(-x) = \psi_B(x)$ for spinless bosons and $\psi_F(-x) = -\psi_F(x)$ for spinless fermions. For $|x| > r_0$, $\psi_B(x)$ and $\psi_F(x)$ solve the free Schrödinger equation, and thus they can be expressed as

$$\psi_B(x) = \cos(kx) + f_e\,(k)\, e^{ik|x|}, \tag{2.1a}$$

$$\psi_F(x) = i\sin(kx) + f_o(k)\mathrm{sgn}(x)e^{ik|x|}, \tag{2.1b}$$

where $\mathrm{sgn}(x) \equiv x/|x|$, $k > 0$ is a relative momentum, and $f_e(k)$ and $f_o(k)$ are even- and odd-wave scattering amplitudes,[1] respectively. These scattering wave functions can be also written

[1] For distinguishable particles in 1D, a wave function outside the range takes the form of $\psi(x) = e^{ikx} + f_{1\mathrm{D}}\,(k;\mathrm{sgn}(x))\, e^{ik|x|}$, which is in analogy to a 3D scattering state $\psi(\mathbf{r}) = e^{i\mathbf{k}\cdot\mathbf{r}} + f_{3\mathrm{D}}(k,\theta)e^{ikr}/r$. Futhermore, the 1D scattering amplitude can be separated into even- and odd-parity parts: $f_{1\mathrm{D}}\,(k;\mathrm{sgn}(x)) = f_e(k) + f_o(k)\mathrm{sgn}(x)$, which is in analogy to the partial wave expansion in 3D; $f_{3\mathrm{D}}(k,\theta) = \sum_{l=0}^{\infty} f_l(k)P_l(\cos\theta)$. Here $P_l(\cos\theta)$ is a the Legendre polynomial.

in terms of phase shifts:

$$\psi_B(x) = e^{i\delta^e_{1\mathrm{D}}(k)} \cos\left[k|x| + \delta^e_{1\mathrm{D}}(k)\right], \tag{2.2a}$$

$$\psi_F(x) = -ie^{i\delta^o_{1\mathrm{D}}(k)} \mathrm{sgn}(x) \sin\left[k|x| + \delta^e_{1\mathrm{D}}(k)\right]. \tag{2.2b}$$

The scattering amplitudes are thus related to the phase shifts by the following relations:

$$f_e(k) = \frac{1}{-i\cot\delta^e_{1\mathrm{D}}(k) - 1}, \tag{2.3a}$$

$$f_o(k) = \frac{1}{-i\cot\delta^o_{1\mathrm{D}}(k) - 1}. \tag{2.3b}$$

For sufficiently low energy $kr_0 \ll 1$, $\cot\delta^e_{1\mathrm{D}}(k)$ and $\cot\delta^o_{1\mathrm{D}}(k)$ can be expanded as

$$\cot\delta^e_{1\mathrm{D}}(k) = ka^e_{1\mathrm{D}} + O(k^3), \tag{2.4a}$$

$$\cot\delta^o_{1\mathrm{D}}(k) = \frac{1}{ka^o_{1\mathrm{D}}} + O(k), \tag{2.4b}$$

where real-valued parameters $a^e_{1\mathrm{D}}$ and $a^o_{1\mathrm{D}}$ are 1D scattering lengths in even-wave and odd-wave channels, respectively. Using Eqs. (2.2) and (2.4), we can find that, for $kr_0 \ll 1$, wave functions at $x = r_0$ satisfy the following equations:

$$\psi_B(r_0) + (a^e_{1\mathrm{D}} - r_0)\psi'_B(r_0) \simeq 0, \tag{2.5a}$$

$$\psi_F(r_0) + (a^o_{1\mathrm{D}} - r_0)\psi'_F(r_0) \simeq 0. \tag{2.5b}$$

Here $\psi'(x)$ denotes the derivative of $\psi(x)$.

When the scattering lengths are much larger than the range, $|a^e_{1\mathrm{D}}|, |a^o_{1\mathrm{D}}| \gg r_0$, low-energy properties of the systems depend on the interactions only through the scattering lengths. These universal properties of two-body physics originate from the existence of the well-defined zero-range limit $r_0 \to +0$. In this limit, interparticle interactions can be treated as contact interactions. The contact interactions lead to the contact boundary conditions, which are obtained by taking the zero-range limit of Eqs. (2.5):

$$\psi_B(+0) + a^e_{1\mathrm{D}}\psi'_B(+0) = 0, \tag{2.6a}$$

$$\psi_F(+0) + a^o_{1\mathrm{D}}\psi'_F(+0) = 0. \tag{2.6b}$$

From these boundary conditions, phase shifts for bosons and fermions in this limit are found to be

$$\cot\delta^e_{1\mathrm{D}}(k) = ka^e_{1\mathrm{D}}, \tag{2.7a}$$

$$\cot\delta^o_{1\mathrm{D}}(k) = \frac{1}{ka^o_{1\mathrm{D}}}, \tag{2.7b}$$

respectively. The models in which the phase shifts in the forms of Eqs. (2.7) hold for any k are called zero-range models. In the zero-range models, the scattering lengths are the only length

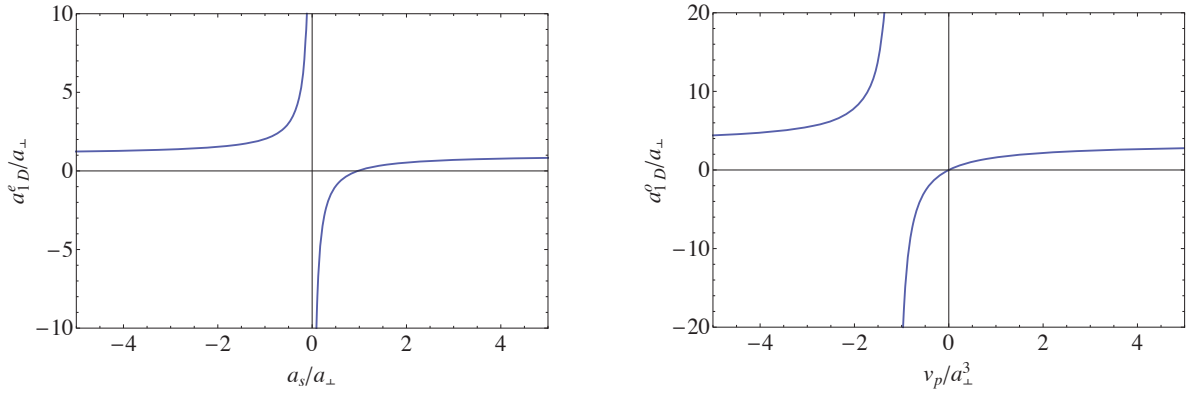

(a) (b)

Figure 2.1: One-dimensional scattering lengths (a) for bosons and (b) for fermions.

scales which arise from interactions. Therefore, the zero-range models are found to describe effective theories of 1D systems near resonances ($|a^e_{1D}|$, $|a^o_{1D}| \gg r_0$). One way to represent the zero-range models is to use the free Schrödinger equation for $|x| > 0$ combined with the contact boundary conditions in Eqs. (2.6). We take advantage of this formalism to clarify essential properties of 1D bosons and fermions near resonances in the next section. Two other representations of the zero-range models are also introduced in Section 2.1.2.

Before proceeding to the next section, we note that, in the case of ultracold atoms, the 1D scattering lengths a^e_{1D} and a^o_{1D} are related to parameters controllable via Feshbach resonances. As mentioned in Section 1.3, 1D bosons (fermions) with a contact interaction can be realized by confining 3D bosons (fermions) with an s-wave (a p-wave) interaction in a highly elongated harmonic trap, $V(x,y,z) = \frac{1}{2}m\omega_x^2 x^2 + \frac{1}{2}m\omega_\perp^2(y^2+z^2)$ with $\omega_x \ll \omega_\perp$ [49, 51]. The transverse motion of the trapped atoms is "frozen" to the zero point oscillation, and thus they can freely move only along the x-axis. For bosons, a^e_{1D} can be expressed in terms of the transverse oscillator length $a_\perp = \sqrt{\hbar/(m\omega_\perp)}$ and the 3D scattering length a_s [49]:

$$a^e_{1D} = a_\perp \left(\frac{|\zeta(1/2)|}{\sqrt{2}} - \frac{a_\perp}{a_s} \right), \tag{2.8}$$

where $\zeta(x)$ is the zeta function. On the other hand, a^o_{1D} for fermions can be expressed in terms of $a_\perp = \sqrt{\hbar/(m\omega_\perp)}$ and the 3D scattering volume v_p, which characterizes the p-wave scattering amplitude at low energy [51]:

$$a^o_{1D} = \frac{3v_p}{a_\perp^2} \left(1 + \frac{3|\zeta(3/2)|}{2\sqrt{2}\pi} \frac{v_p}{a_\perp^3} \right)^{-1}. \tag{2.9}$$

By tuning a_s and v_p via magnetic Feshbach resonances, a^e_{1D} and a^e_{1D} can be widely controlled [see Figs. (a) and (b)].

2.1.1 Contact boundary conditions and Bose-Fermi correspondence

The expressions of the zero-rage models with Eqs. (2.6) allow us to easily find an excellent and practical relation between bosons and fermions [46, 51–53]. When we set $a^e_{1\mathrm{D}} = a^e_{1\mathrm{D}} = a$, both bosonic and fermionic wave functions satisfy the same contact boundary condition,

$$\psi(+0) + a\psi'(+0) = 0, \tag{2.10}$$

as well as the free Schrödinger equation for $|x| > 0$:

$$-\frac{1}{m}\frac{d^2}{dx^2}\psi(x) = E\psi(x). \tag{2.11}$$

Although bosons and fermions obey the different statistics, all bosonic energy eigenstates $\psi_B(x)$ are mapped to fermionic ones $\psi_F(x)$ in one-to-one via

$$\psi_F(x) = \mathrm{sgn}(x)\psi_B(x). \tag{2.12}$$

Since Eq. (2.11) determines energy eigenvalues and $\frac{d}{dx}\mathrm{sgn}(x) = 0$ for $|x| > 0$, this mapping preserves the energy eigenvalues between bosons and fermions. This interrelation between bosons and fermions is called *Bose-Fermi correspondence*. This is a natural generalization of the well-known correspondence between impenetrable bosons and free fermions with $a^e_B = a^o_F = -0$ [46]. The Bose-Fermi correspondence originates from the special property of 1D, in which the anti-symmetrizing factor has the simple form of $\mathrm{sgn}(x)$. In order to clarify the consequences of the Bose-Fermi correspondence, we set $a^e_{1\mathrm{D}} = a^o_{1\mathrm{D}} = a$ in the rest of this thesis.

The representation through Eqs. (2.10) and (2.11) also allows us to find another property of the zero-range models. When two particles approach each other, $x \to 0$, wave functions behave non-analytically [see Fig. 2.2]:

$$\psi_\alpha(x) = \phi^{(2)}_\alpha(x)\psi_\alpha(+0) + O(x^2), \tag{2.13}$$

where $\alpha = B$, F labels statistics of particles and

$$\phi^{(2)}_B(x) = (1 - |x|/a), \tag{2.14a}$$

$$\phi^{(2)}_F(x) = (\mathrm{sgn}(x) - x/a), \tag{2.14b}$$

are the dimensionless two-body scattering-state wave functions with zero energy. Figure 2.3 shows how the scattering length a controls the non-analyticity of the wave functions. Recalling that a wave function of free particles are a smooth plane wave, we can see that bosons (fermions) become non-interacting for $a \to \pm\infty$ ($a \to -0$).

The zero-range models with the contact boundary conditions can be easily generalized to N-body physics. The zero-range models with N particles describe 1D quantum many-body systems in the resonant regime, where the interaction range r_0 is much smaller than other length scales such as a scattering length a, a mean interparticle distance l_{mean}, and a thermal de Broglie wavelength $\lambda_T \sim 1/\sqrt{mk_BT}$. In ultracold atom experiments, particles are often trapped by a

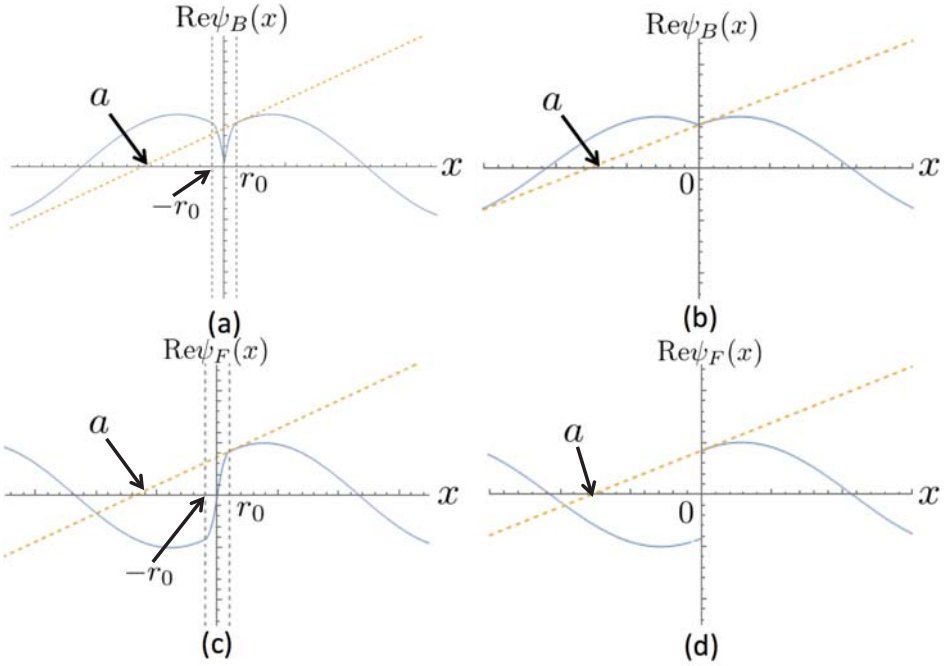

Figure 2.2: Real part of bosonic (fermionic) wave function (a) [(c)] for a finite range $r_0 \ll |a|, k^{-1}$ and (b) [(d)] in the zero-range limit $r_0 \to +0$. The positions of the scattering length a are determined by Eqs. (2.5a), (2.5b), and (2.10).

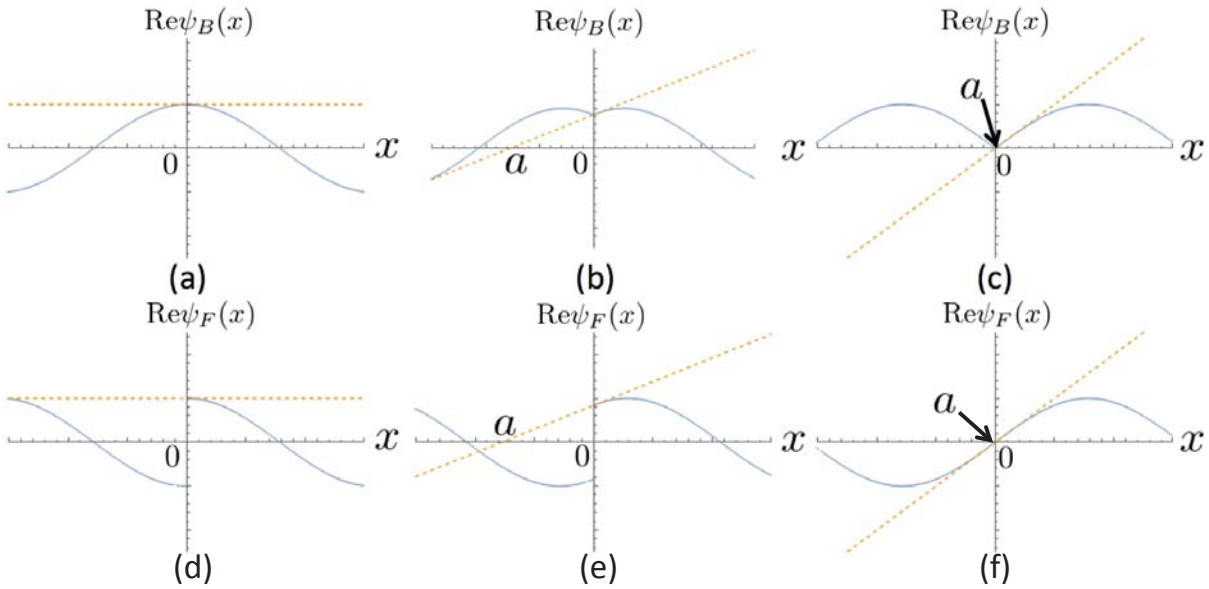

Figure 2.3: Real part of bosonic (fermionic) wave functions in the zero-range models for (a) [(d)] $a \to \pm\infty$, (b) [(e)] $a < 0$, and (c) [(f)] $a \to -0$. Smooth wave functions correspond to free particles.

smooth potential $V(x)$. For this reason, we take a trapping potential into account. The N-body energy eigenfunctions of both zero-range models solve the free Schrödinger equation over the domain where all particles are separated from each other:

$$\sum_{i=1}^{N}\left[-\frac{1}{2m}\frac{\partial^2}{\partial x_i^2}+V(x_i)\right]\Psi(x_1,\cdots,x_N)=E\,\Psi(x_1,\cdots,x_N) \tag{2.15}$$

with $x_{ij}\equiv x_i-x_j\neq 0$ for any $1\leq i<j\leq N$. When each pair of particles $1\leq i<j\leq N$ come into contact with each other, the eigenfunctions satisfy the contact boundary conditions:

$$\lim_{x_{ij}\to+0}\left(1+a\partial_{x_{ij}}\right)\Psi(x_1,\cdots,x_N)=0. \tag{2.16}$$

Energy eigenfunctions for bosons (fermions) are solutions totally symmetric (antisymmetric) in the exchange of particles. The Bose-Fermi correspondence in Eq. (2.12) is generalized to N-body problems as follows: For any bosonic solution $\Psi_B(x_1,\cdots,x_N)$ with energy E, the corresponding fermionic solution $\Psi_F(x_1,\cdots,x_N)$ with the same energy always exists, and they are related to each other through the Girardeau's Bose-Fermi mapping[2] [46]

$$\Psi_F(x_1,\cdots,x_N)=A(x_1,\cdots,x_N)\Psi_B(x_1,\cdots,x_N). \tag{2.17}$$

Here the N-body mapping factor $A(x_1,\cdots,x_N)$ is given by

$$A(x_1,\cdots,x_N)=\prod_{1\leq i<j\leq N}\mathrm{sgn}(x_{ij}). \tag{2.18}$$

The non-analytic behaviors of two-body wave functions in Eqs. (2.13) are also generalized to many-body wave functions: From Eqs. (2.15) and (2.16), we can see that, when two particles $i<j$ come close to each other with their center-of-mass coordinate $X_{ij}=(x_i+x_j)/2$ fixed, Ψ_α becomes proportional to the non-analytic two-body wave functions $\phi_\alpha^{(2)}(x_{ij})$ in Eq. (2.14):

$$\Psi_\alpha(x_1,\cdots,x_N)=\phi_\alpha^{(2)}(x_{ij})\Phi_{\alpha;ij}(X_{ij};\{x_k\}_{k\neq i,j})+O(x_{ij}^2), \tag{2.19}$$

where

$$\Phi_{\alpha;ij}(X_{ij};\{x_k\}_{k\neq i,j})\equiv\lim_{x_{ij}\to+0}\Psi_\alpha(x_1,\cdots,x_N) \tag{2.20}$$

is a smooth function of X_{ij}. In Chapter 3, we prove that the non-analytic behaviors in Eqs.(2.19) lead to universal relations for correlation functions.

The Bose-Fermi correspondence is known to make a variety of physical quantities identical between bosons and fermions with the same scattering length $a_{1\mathrm{D}}^e=a_{1\mathrm{D}}^o=a$. Since the energy spectrum $\{E_i\}_i$ is identical between bosons and fermions, the partition function $\mathcal{Z}=\sum_i\exp[-E_i/(k_BT)]$ at temperature T is also identical. As a result, with a and T fixed, bosons and fermions have the same thermodynamics.

[2] When bosons and fermions with periodic (or more generally twisted) boundary conditions are considered, there is a subtle issue in the Bose-Fermi mapping as mentioned in Section 3.3.

The Bose-Fermi correspondence also makes some correlation functions for bosons the same as those for fermions. Since $|A(x_1, \cdots, x_N)| = 1$, the absolute value of the wave function Ψ_F in Eq. (2.17) is the same as that of Ψ_B. Consequently, both states have the same probability distribution of finding M particles at the positions $x_1, \ldots, x_M$:

$$g_M(x_1, \ldots, x_M) = \frac{N!}{(N-M)!} \int dx_{M+1} \cdots dx_N \, |\Psi_\alpha(x_1, \ldots, x_N)|^2, \tag{2.21}$$

where $\alpha = B, F$ labels statistics of particles and Ψ_α is normalized as $\int dx_1 \cdots dx_N |\Psi_\alpha|^2 = 1$. Hereafter, we abbreviate the label $\alpha = B, F$ for quantities identical between Ψ_B and Ψ_F. Because of the correspondence of $g_M(x_1, \ldots, x_M)$, the following quantities are also identical for Ψ_B and Ψ_F: the density profile $n(x) = g_1(x)$, the static structure factor

$$S(k) = 1 + \frac{1}{N} \int dx_1 dx_2 \, e^{-ik(x_1 - x_2)} [g_2(x_1, x_2) - n(x_1) n(x_2)], \tag{2.22}$$

and the two- and three-body contact densities

$$\mathcal{C}_2(x) \equiv g_2(x, x), \qquad \mathcal{C}_3(x) \equiv g_3(x, x, x), \tag{2.23}$$

which measure the probabilities that two and three particles come into contact with each other at the position x, respectively. The two- and three-body contacts are given by the integrals of $\mathcal{C}_2(x)$ and $\mathcal{C}_3(x)$ over x:

$$C_2 \equiv \int dx \, \mathcal{C}_2(x), \qquad C_3 \equiv \int dx \, \mathcal{C}_3(x). \tag{2.24}$$

The correspondence of C_2 was previously pointed out in Ref. [80]. As shown in Chapters 3–5, C_2 and C_3 play roles as contact parameters in universal relations.

The correspondence of $g_M(x_1, \ldots, x_M)$ for bosons and fermions is naturally generalized to systems at nonzero temperature T. With a and T fixed, the canonical ensemble average of $g_M(x_1, \ldots, x_M)$ is identical between bosons and fermions. In particular, the two-body contact plays an important role in the thermodynamics of bosons and fermions. By using the Hellmann-Feynman theorem, one can find that C_2 is the thermodynamic quantity conjugate to the inverse scattering length [81],

$$\left(\frac{\partial F}{\partial(-1/a)} \right)_T = \frac{C_2}{m}, \tag{2.25}$$

where F is the free energy.

While some correlation functions including $S(k)$ are, by definition, identical between Ψ_B and Ψ_F, other correlation functions are different between them. One of representative examples is a momentum distribution

$$\rho_\alpha(k) = N \int dx_2 \cdots dx_N \left| \int dx_1 e^{-ikx_1} \Psi_\alpha(x_1, \ldots, x_N) \right|^2. \tag{2.26}$$

Although $\rho_B(k)$ and $\rho_F(k)$ are not identical with each other, we show in the next chapter that there are two nontrivial connections between them resulting from the Bose-Fermi correspondence.

2.1.2 Other representations of the zero-range models

In the previous section, we define the zero-range models by combining the contact boundary conditions in Eq. (2.16) with the free Schrödinger equation [Eq. (2.15)] over the domain where all particles are separated from each other. However, in many cases in quantum mechanics, we usually start with a Hamiltonian or a Lagrangian. Using the method of pseudopotentials, Eqs. (2.15) and (2.16) can be written as a single Schrödinger equation. In this framework, bosons and fermions with contact interactions can be described by the following first-quantized Hamiltonians [44, 53]:

$$H_B = \sum_{i=1}^{N} \left[-\frac{1}{2m} \frac{\partial^2}{\partial x_i^2} + V(x_i) \right] - \frac{2}{ma} \sum_{i<j} \delta(x_{ij}), \tag{2.27}$$

$$H_F = \sum_{i=1}^{N} \left[-\frac{1}{2m} \frac{\partial^2}{\partial x_i^2} + V(x_i) \right] - \frac{2a}{m} \sum_{i<j} \delta'(x_{ij}) D_{ij}, \tag{2.28}$$

where the regularized differential operator D_{ij} acts on a fermionic wave function as

$$D_{ij}\Psi_F = \lim_{x_{ij}=+0} \left[\frac{\partial}{\partial x_{ij}} \Psi_F(x_1, \cdots, x_N) \right] \tag{2.29}$$

with the center of mass coordinate $X_{ij} = (x_i + x_j)/2$ of the pair of fermions i, j and the other $N-2$ coordinates $\{x_k\}_{k\neq i,j}$ fixed.

The zero-range models are also described in second-quantized formalisms. The quantum field theory of bosons is given by the Lagrangian density

$$\mathcal{L}_B = \phi^\dagger \left(i\partial_t + \frac{\partial_x^2}{2m} - V(x) \right) \phi + \frac{1}{ma} \phi^\dagger \phi^\dagger \phi \phi, \tag{2.30}$$

where $\phi = \phi(t, x)$ is a complex bosonic field. If is straightforward to derive $\mathcal{L}_B$ from the first-quantized Hamiltonian H_B in Eq. (2.27). While the quantum field theory for bosons is well defined without a regularization, that for fermions requires a regularization procedure. In Ref. [80], it was found that the quantum field theory described by the Lagrangian density

$$\mathcal{L}_F = \psi^\dagger \left(i\partial_t + \frac{\partial_x^2}{2m} - V(x) \right) \psi + \frac{v_2}{2m} \left| \psi \partial_x \psi \right|^2 \tag{2.31}$$

with a fermionic field $\psi = \psi(t, x)$ reproduces a two-body problem in the fermionic zero-range model. However, this quantum field theory is not enough for three or more fermions: If three- or higher-body problems were considered, one would be faced with logarithmic ultraviolet divergences which cannot be canceled by the renormalization of v_2. This implies that additional terms which act on three- or higher-body states are required at low energy scale in order to express the fermionic zero-range model within a field theory framework. In Chapter 5, we construct the quantum field theory for fermions near a two-body resonance. One of advantages of field theoretical formalisms is that we can use the operator product expansion to derive universal relations for dynamic correlation functions for large energy and momentum.

2.2 Bethe ansatz

In this section, we review the Bethe ansatz method to solve the Schrödinger equations of the zero-range models without a trapping potential [44]. Here, we consider N bosons with an even-wave interactions described by the Hamiltonian

$$H_B = -\frac{1}{2m}\sum_{i=1}^{N}\frac{\partial^2}{\partial x_i^2} - \frac{2}{ma}\sum_{i<j}\delta(x_i - x_j). \tag{2.32}$$

The procedure shown below is also applicable to fermions with an odd-wave interaction. We impose periodic boundary conditions on a wave function

$$\Psi(x_1, \cdots, x_l, \cdots, x_N) = \Psi(x_1, \cdots, x_l + L, \cdots, x_N) \tag{2.33}$$

with a period L. Because of Bose-Einstein statistics, the wave function should be symmetric under the exchange of particles:

$$\Psi(x_1, \cdots, x_N) = \Psi(x_{P_1}, \cdots, x_{P_N}), \tag{2.34}$$

where P is a permutation

$$P = \begin{pmatrix} 1 & 2 & \cdots & N \\ P_1 & P_2 & \cdots & P_N \end{pmatrix}. \tag{2.35}$$

For this reason, it is sufficient to consider the wave function $\Psi_<(x_1, x_2, \cdots, x_N)$ over the domain $0 \le x_1 < x_2 < \cdots < x_N < L$. The boundary conditions (2.33) combined with Eq. (2.34) leads to the constraint on $\Psi_<(x_1, x_2, \cdots, x_N)$

$$\Psi_<(0, x_2, \cdots, x_{N-1}x_N) = \Psi_<(x_2, x_3, \cdots, x_N, L). \tag{2.36}$$

Over the domain $0 \le x_1 < x_2 < \cdots < x_N < L$, the Schrödinger equation reduces to that for free particles:

$$-\frac{1}{2m}\sum_{i=1}^{N}\frac{\partial^2}{\partial x_i^2}\Psi_<(x_1, x_2, \cdots, x_N) = E\Psi_<(x_1, x_2, \cdots, x_N). \tag{2.37}$$

We find a solution of the form

$$\Psi_<(x_1, x_2, \cdots, x_N) = \sum_P A_P \exp\left[i\sum_{j=1}^{N}\lambda_{P_j}x_j\right], \tag{2.38}$$

where $\{\lambda_j\}$ are quantum numbers called quasi momenta. This ansatz is called the Bethe ansatz, and the corresponding state is called the Bethe state. Here, all the $\{\lambda_j\}$ are assumed to be distinct. The Bethe state has a series of conserved charges

$$\mathcal{Q}_l \equiv \sum_{j=1}^{N}(\lambda_j)^l \qquad (l = 0, 1, 2, \cdots). \tag{2.39}$$

For example, the number of particles N, total momentum P, and energy E are given by

$$N = \mathcal{Q}_0, \quad P = \mathcal{Q}_1 = \sum_{j=1}^{N} \lambda_j, \quad E = \frac{\mathcal{Q}_2}{2m} = \frac{1}{2m} \sum_{j=1}^{N} (\lambda_j)^2, \tag{2.40}$$

respectively.

Let us now determine unknown quantities A_P and λ_j in Eq. (2.38). The contact interaction in the Hamiltonian (2.32) leads to the boundary conditions

$$\left(\frac{\partial}{\partial x_{j+1}} - \frac{\partial}{\partial x_j} + \frac{2}{a} \right) \Psi_<(x_1, x_2, \cdots, x_N) \Big|_{x_{j+1}=x_j+0^+} = 0. \tag{2.41}$$

Substituting (2.38) into this yields

$$\sum_P A_P (i\lambda_{P_{j+1}} - i\lambda_{P_j} + 2/a) \exp \left[i(\lambda_{P_{j+1}} + \lambda_{P_j}) x_j + i \sum_{k \neq j, j+1} \lambda_{P_k} x_k \right] = 0, \tag{2.42}$$

leading to

$$A_P (i\lambda_{P_{j+1}} - i\lambda_{P_j} + 2/a) + A_{P'} (i\lambda_{P_j} - i\lambda_{P_{j+1}} + 2/a) = 0 \tag{2.43}$$

with

$$P' \equiv \begin{pmatrix} 1 & 2 & \cdots & j-1 & j & j+1 & j+2 & \cdots & N \\ P_1 & P_2 & \cdots & P_{j-1} & P_{j+1} & P_j & P_{j+2} & \cdots & P_N \end{pmatrix}. \tag{2.44}$$

By introducing new notations

$$A_{P_1, P_2, \cdots, P_j, P_{j+1}, \cdots, P_N} = A_P, \tag{2.45}$$

$$A_{P_1, P_2, \cdots, P_{j+1}, P_j, \cdots, P_N} = A_{P'}, \tag{2.46}$$

$$S_{l,m} = \frac{\lambda_l - \lambda_m + 2i/a}{\lambda_l - \lambda_m - 2i/a}, \tag{2.47}$$

Eq. (2.43) leads to

$$\frac{A_{P'}}{A_P} = \frac{A_{P_1, P_2, \cdots, P_{j+1}, P_j, \cdots, P_N}}{A_{P_1, P_2, \cdots, P_j, P_{j+1}, \cdots, P_N}} = S_{P_j, P_{j+1}}. \tag{2.48}$$

Next, we evaluate the boundary condition (2.36). The left hand side of Eq. (2.36) equals

$$\Psi_<(0, x_2, \cdots, x_N) = \sum_P A_{P_1, P_2, \cdots, P_N} \exp \left[i(\lambda_{P_2} x_2 + \cdots + \lambda_{P_N} x_N) \right], \tag{2.49}$$

while the right hand side equals

$$\begin{aligned} \Psi_<(x_2, \cdots, x_N, L) &= \sum_Q A_Q \exp \left[i(\lambda_{Q_1} x_2 + \cdots + \lambda_{Q_{N-1}} x_N + \lambda_{Q_N} L) \right] \\ &= \sum_P A_{P_2, \cdots, P_N, P_1} e^{i\lambda_{P_1} L} \exp \left[i(\lambda_{P_2} x_2 + \cdots + \lambda_{P_N} x_N) \right]. \end{aligned} \tag{2.50}$$

Thus, we have

$$A_{P_1,P_2,\cdots,P_N} = A_{P_2,\cdots,P_N,P_1} e^{i\lambda_{P_1} L}. \tag{2.51}$$

By using Eq. (2.48) iteratively, the left hand side of this equation is rewritten as

$$\begin{aligned} A_{P_1,P_2,\cdots,P_N} &= \frac{A_{P_1,P_2,P_3,\cdots,P_N}}{A_{P_2,P_1,P_3\cdots,P_N}} \frac{A_{P_2,P_1,P_3,P_4\cdots,P_N}}{A_{P_2,P_3,P_1,P_4\cdots,P_N}} \cdots \frac{A_{P_2,\cdots,P_{N-1},P_1,P_N}}{A_{P_2,\cdots,P_{N-1},P_N,P_1}} \times A_{P_2,\cdots,P_N,P_1} \\ &= \left(\prod_{k=2}^{N} S_{P_k,P_1} \right) A_{P_2,\cdots,P_N,P_1}. \end{aligned} \tag{2.52}$$

Changing the index $P_1 \to j$ and using Eq. (2.47), Eq. (2.51) leads to the Bethe ansatz equations:

$$e^{i\lambda_j L} = \prod_{k\neq j} \frac{\lambda_j - \lambda_k - 2i/a}{\lambda_j - \lambda_k + 2i/a}. \tag{2.53}$$

2.2.1 Repulsive case

By recalling that the coupling constant in Eq. (2.32) is proportional to $-1/a$, a negative scattering length $a < 0$ leads to a repulsive interaction between bosons. In this case, all the quasi momenta $\{\lambda_j\}$ are real valued, which corresponds to the fact that there is no bound state. It is convenient to use a function

$$\theta(\lambda) \equiv i \ln \left(\frac{i + \frac{\lambda|a|}{2}}{i - \frac{\lambda|a|}{2}} \right) = 2 \tan^{-1} \left(\frac{\lambda|a|}{2} \right), \qquad -\pi \leq \theta(\lambda) \leq \pi. \tag{2.54}$$

Rewriting Eq. (2.53) as

$$e^{i\lambda_j L} = (-1)^{N-1} \prod_{k=1}^{N} \frac{i + \frac{(\lambda_j - \lambda_k)|a|}{2}}{i - \frac{(\lambda_j - \lambda_k)|a|}{2}} \tag{2.55}$$

and taking the logarithm of both sides, we obtain

$$\lambda_j L + \sum_{k=1}^{N} \theta(\lambda_j - \lambda_k) = 2\pi n_j. \tag{2.56}$$

Here, n_j defined by

$$n_j = \tilde{n}_j + \frac{N-1}{2} \qquad (\tilde{n}_j \in \mathbb{Z}) \tag{2.57}$$

is a half odd integer when N is even and an integer when N is odd. From Eq. (2.56), the proposition

$$n_j < n_k \qquad \Longrightarrow \qquad \lambda_j < \lambda_k, \tag{2.58}$$

$$n_j = n_k \qquad \Longrightarrow \qquad \lambda_j = \lambda_k, \tag{2.59}$$

can be proven by contradiction [54]. Since $\{\lambda_j\}$ are assumed to be distinct, we can take $\{n_j\}$ and $\{\lambda_j\}$ in ascending order

$$n_1 < n_2 < \cdots < n_N, \tag{2.60a}$$

$$\lambda_1 < \lambda_2 < \cdots < \lambda_N. \tag{2.60b}$$

If the set of n_j is given, a wave function is uniquely determined by solving Eq. (2.56). For instance, the ground state corresponds to the following set of n_j [86]:

$$n_j = -\frac{N-1}{2} + j - 1, \qquad (j = 1, 2, \cdots, N). \tag{2.61}$$

We now consider the thermodynamic limit of the ground state:

$$N \to \infty, \qquad L \to \infty, \qquad n = N/L = \text{fixed}. \tag{2.62}$$

We note that n denotes not an integer but the number density. The system is characterized only by a single dimensionless parameter $\gamma = 2/(n|a|) > 0$. The discrete variable n_j in Eq. (2.61) can be replaced by continuous one:

$$y_j = n_j/L \to y, \qquad \lambda_j \to \lambda(y). \tag{2.63}$$

Equations (2.60) make $\lambda(y)$ a monotonically increasing function in y, and thus the regions of y and λ are limited as

$$-\frac{n_N}{L} \le y \le \frac{n_N}{L}, \qquad \frac{n_N}{L} = \frac{N-1}{2L} \to \frac{n}{2}, \tag{2.64}$$

$$-K \le \lambda \le K, \tag{2.65}$$

where the cutoff K is an unknown parameter. Define the density of states in quasi-momentum space as

$$f(\lambda) \equiv \frac{dy}{d\lambda}. \tag{2.66}$$

Because of $\Delta y = \Delta n/L = (n_{j+1} - n_j)/L = 1/L$, the summation of a function $F(\lambda_j)$ is evaluated as

$$\begin{aligned}
\sum_{j=1}^{N} F(\lambda_j) &= L \sum_{-n/2 \le y_j \le n/2} \Delta y F(\lambda(y_j)) \\
&\simeq L \int_{-n/2}^{n/2} dy\, F(\lambda(y)) \\
&= L \int_{-K}^{K} d\lambda\, \frac{dy}{d\lambda} F(\lambda) \\
&= L \int_{-K}^{K} d\lambda\, f(\lambda) F(\lambda).
\end{aligned} \tag{2.67}$$

For example, the conserved charge in Eq. (2.39) is given by

$$\mathcal{Q}_l = \sum_{j=1}^{N} (\lambda_j)^l = L \int_{-K}^{K} d\lambda\, \lambda^l f(\lambda). \tag{2.68}$$

In the thermodynamic limit, the Bethe equations (2.56) reduce to

$$\frac{\lambda(y)}{2\pi} + \frac{1}{L} \sum_{k=1}^{N} \frac{1}{2\pi} \theta(\lambda(y) - \lambda_k) = y. \tag{2.69}$$

Equation (2.67) replaces this summation by an integral:

$$\frac{\lambda(y)}{2\pi} + \int_{-K}^{K} d\lambda' \, \frac{1}{2\pi} \theta(\lambda(y) - \lambda') f(\lambda') = y. \tag{2.70}$$

Differentiating the both sides with respect to λ, we obtain

$$\frac{1}{2\pi} + \int_{-K}^{K} \frac{d\lambda'}{2\pi} \frac{4|a|}{4 + (\lambda - \lambda')^2 a^2} f(\lambda') = f(\lambda). \tag{2.71}$$

On the other hand, Eq. (2.68) provides the number density $n = \mathcal{Q}_0/L$ in terms of $f(\lambda)$:

$$n = \int_{-K}^{K} d\lambda\, f(\lambda). \tag{2.72}$$

The unknown quantities K and $f(\lambda)$ for any $\gamma = 2/(n|a|) > 0$ are determined by numerically solving Eq. (2.71) combined with Eq. (2.72). Once K and $f(\lambda)$ are determined, we can obtain the ground-state energy density

$$\mathcal{E} = \frac{E}{L} = \frac{1}{2m} \int_{-K}^{K} d\lambda\, \lambda^2 f(\lambda). \tag{2.73}$$

By using the Hellmann-Feynman theorem, a two-body contact density is also obtained [81, 82]:

$$\mathcal{C}_2 \equiv \frac{C_2}{L} = m \frac{d\mathcal{E}}{d(-1/a)}. \tag{2.74}$$

For sufficiently small or large γ, the analytical expression of $\mathcal{C}_2$ is also obtained as

$$\mathcal{C}_2 \simeq \begin{cases} n^2 & \text{for} \quad \gamma \ll 1, \\ \frac{4}{3}\pi^2 \gamma^{-2} n^2 & \text{for} \quad \gamma \gg 1. \end{cases} \tag{2.75}$$

In the case of finite temperature $T > 0$, we can also exactly compute $\mathcal{C}_2$ by the method of the thermodynamic Bethe ansatz [81, 82]. In addition, the Bethe ansatz allows us to obtain the exact three-body contact density $\mathcal{C}_3 = C_3/L$ [82–85].

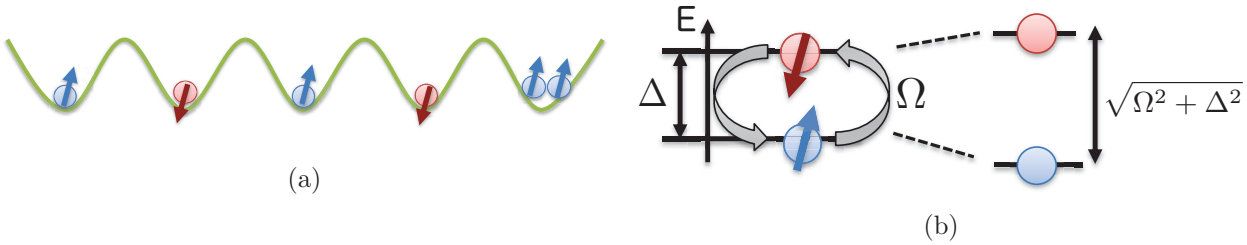

(a) (b)

Figure 2.4: (a) Two-component bosons in a 1D optical lattice. (b) Single-particle levels of bosons in the spin sector. The two states $|\uparrow\rangle$ and $|\downarrow\rangle$ are energetically separated by Δ and coupled to each other through the Rabi oscillation with a frequency Ω, leading to a level repulsion.

2.2.2 Attractive case

By recalling that the coupling constant in Eq. (2.32) is proportional to $-1/a$, a positive scattering length $a > 0$ leads to an attractive interaction between bosons. In this case, the ground state of N bosons is known to be a bound state with binding energy [48]

$$B_N = \frac{N(N^2-1)}{6ma^2}. \tag{2.76}$$

Because of $B_N \sim N^3$ for large N, we cannot take the thermodynamic limit of the ground state. The Bose-Fermi correspondence predicts that a N-fermion bound state with the same binding energy also exists for $a > 0$. In Chapter 5, we study two- and three-fermion bound states within a field theory framework.

2.3 Lattice realization of a three-body interaction

This section is devoted to the review to realize 1D bosons without two-body but with three-body interactions and to make the three-body interaction resonant. Our scheme is based on the proposal in Ref. [70], where ^{39}K atoms with two hyperfine states $|F, m_F\rangle = |1, -1\rangle \equiv |\uparrow\rangle$ and $|1, 0\rangle \equiv |\downarrow\rangle$ under the magnetic field $B = 58$ G are considered (see Fig. 2.4). As shown in Fig. 2.4(b), these two states are energetically separated by the detuning Δ and coupled to each other through the Rabi oscillation with a frequency Ω, where Δ and Ω are tunable in ultracold atom experiments [87]. Scattering lengths characterizing the intra- and intercomponent interactions in this system read $a_{\uparrow\uparrow} \approx 1.7$ nm, $a_{\downarrow\downarrow} \approx 9.4$ nm, and $a_{\uparrow\downarrow} \approx -2.8$ nm [15, 88]. The bosonic atoms are confined in an optical lattice with the lattice constant $l \equiv \lambda/2 = 532$ nm and the anisotropic intensities $V_x = V_{y,z}/4 = 15 \times 2\pi^2/m\lambda^2$, leading to the axial hopping parameter $t_x \approx 2\pi \times 30$ Hz with negligible radial ones $t_{y,z}$ as well as the on-site interaction strengths $g_{\uparrow\uparrow} \approx 2\pi \times 1.1$ kHz, $g_{\downarrow\downarrow} \approx 2\pi \times 6.1$ kHz, and $g_{\uparrow\downarrow} \approx -2\pi \times 1.8$ kHz within the harmonic

approximation[3] [8]. As a result, the system can be described by the lattice Hamiltonian in 1D:

$$H = -t_x \sum_{\sigma=\uparrow,\downarrow} \sum_i (b^\dagger_{\sigma i} b_{\sigma i+1} + b^\dagger_{\sigma i+1} b_{\sigma i}) + \sum_i H_i, \tag{2.77}$$

$$H_i = -\frac{\Delta}{2}(b^\dagger_{\uparrow i} b_{\uparrow i} - b^\dagger_{\downarrow i} b_{\downarrow i}) - \frac{\Omega}{2}(b^\dagger_{\uparrow i} b_{\downarrow i} + b^\dagger_{\downarrow i} b_{\uparrow i}) + \sum_{\sigma,\sigma'} \frac{g_{\sigma\sigma'}}{2} b^\dagger_{\sigma i} b^\dagger_{\sigma' i} b_{\sigma' i} b_{\sigma i}, \tag{2.78}$$

where $b_{\sigma i}$ and $b^\dagger_{\sigma i}$ are annihilation and creation operators of a boson with spin σ at the lattice point i, respectively. Diagonalizing H_i in the one-boson sector, we can see that the single-particle spinor eigenstates are energetically separated by the gap $\sqrt{\Omega^2 + \Delta^2}$.

We now consider the low-energy physics relative to the spin gap $\sqrt{\Omega^2 + \Delta^2}$. In this case, the relevant degrees of freedom are atoms in the lower-energy spin state. Virtual excitations to the higher-energy spin state lead to the emergence of effective three- and higher-body interactions in a similar way as in nucleon systems in Section 1.4. As shown above, the on-site coupling constants $|g_{\sigma\sigma'}| \sim$ kHz in Eq. (2.78) are much larger than the hopping parameter $t_x \approx 2\pi \times 30$ Hz. We assume that Δ and Ω are also much larger than t_x. This assumption allows us to treat effective multibody interactions as on-site interactions, leading to the effective single-component Hamiltonian

$$H_{\rm eff} = -t_x \sum_i (b^\dagger_i b_{i+1} + b^\dagger_{i+1} b_i) + \sum_i \hat{U}_{{\rm eff},i}, \tag{2.79}$$

$$\hat{U}_{{\rm eff},i} = \sum_{n=1}^{\infty} \frac{U_n}{n!} b_i^{\dagger n} b_i^n. \tag{2.80}$$

Here b_i and $b^\dagger_i$ are annihilation and creation operators of a boson in the lower-energy spin state at the lattice point i, respectively, and the effective N-body coupling constant U_N depends on the parameters (Δ, Ω) in the original Hamiltonian (2.77). We note that the "effective" interactions U_N do not have to be larger than t_x.

We now determine the dependence of U_N on (Δ, Ω). To achieve this, we can focus on single-site problems because t_x is much smaller than Δ, Ω, and $|g_{\sigma\sigma'}|$. Since the low-energy physics of the two-component system is described by the effective Hamiltonian of Eq. (2.79), the lowest eigenvalue of H_i has to be identical with the eigenvalue of $\hat{U}_{{\rm eff},i}$ in the N-boson sector,

$$\langle N|\hat{U}_{{\rm eff},i}|N\rangle = \sum_{n=1}^{N} \frac{U_n}{n!} \langle N|b_i^{\dagger n} b_i^n|N\rangle = \sum_{n=1}^{N} U_n \frac{N!}{n!(N-n)!}, \tag{2.81}$$

where $|N\rangle = \frac{1}{\sqrt{N}}(b^\dagger_i)^N|{\rm vac}\rangle$. The operator H_i in the N-boson sector has three types of non-

[3] Note the differences from Ref. [70] by the factor of 2 because our oscillator lengths are $\ell_x = \sqrt{2}\ell_{y,z} \approx 86$ nm.

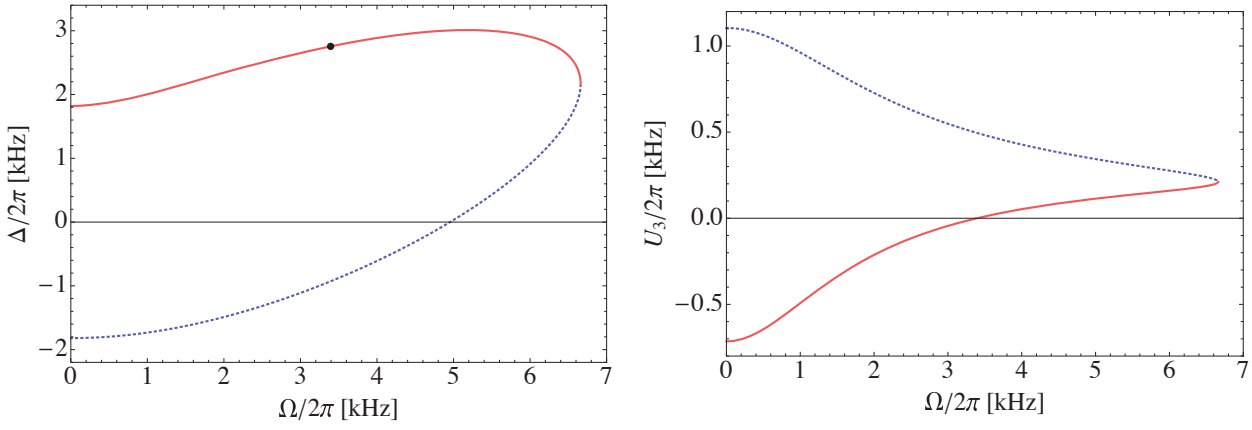

(a) (b)

Figure 2.5: (a) Curve in the plane of Rabi frequency Ω and detuning Δ along which the effective two-body interaction energy U_2 vanishes. The dot marks the point at which both U_2 and U_3 vanish. (b) Effective three-body interaction energy U_3 as a function of Ω with Δ simultaneously tuned to fix $U_2 = 0$. The solid (dotted) curve corresponds to Δ along the solid (dotted) curve in (a). These figures are taken from Ref. [89] © 2018 American Physical Society.

vanishing matrix elements:

$$\langle N_\uparrow, N_\downarrow | H_i | N_\uparrow, N_\downarrow \rangle = -\Delta \frac{N_\uparrow - N_\downarrow}{2} + g_{\uparrow\uparrow} \frac{N_\uparrow(N_\uparrow - 1)}{2} + g_{\downarrow\downarrow} \frac{N_\downarrow(N_\downarrow - 1)}{2} + g_{\uparrow\downarrow} N_\uparrow N_\downarrow, \tag{2.82}$$

$$\langle N_\uparrow, N_\downarrow | H_i | N_\uparrow - 1, N_\downarrow + 1 \rangle = -\Omega \frac{\sqrt{N_\uparrow(N_\downarrow + 1)}}{2}, \tag{2.83}$$

$$\langle N_\uparrow, N_\downarrow | H_i | N_\uparrow + 1, N_\downarrow - 1 \rangle = -\Omega \frac{\sqrt{(N_\uparrow + 1)N_\downarrow}}{2}, \tag{2.84}$$

where $|N_\uparrow, N_\downarrow\rangle = \frac{1}{\sqrt{N_\uparrow! N_\downarrow!}} (b_{\uparrow i}^\dagger)^{N_\uparrow} (b_{\downarrow i}^\dagger)^{N_\downarrow} |\mathrm{vac}\rangle$ with $N_\uparrow + N_\downarrow = N$. It is easy to numerically calculate the lowest eigenvalue of H_i in the N-boson sector. The obtained eigenvalue E_N should equal Eq. (2.81): $E_N = \sum_{n=1}^{N} U_n \frac{N!}{n!(N-n)!}$. Therefore, the effective coupling constants U_N are obtained as

$$U_1 = E_1 = -\frac{\sqrt{\Delta^2 + \Omega^2}}{2}, \tag{2.85}$$

$$U_2 = E_2 - 2U_1, \tag{2.86}$$

$$U_3 = E_3 - 3U_1 - 3U_2, \tag{2.87}$$

$$\cdots, \tag{2.88}$$

where the analytic expression of E_1 is used. Figure 2.5(b) shows the curve of the vanishing two-body interaction in the plane of (Ω, Δ) and Fig 2.5(b) shows U_3 as a function of Ω with $U_2 = 0$ fixed. At the point of $(\Omega, \Delta) \approx 2\pi \times (3.4, 2.8)$ kHz (shown by the dot in Fig 2.5(b)), both

of two- and three-body interactions vanish, so that U_3 along the curve of $U_2 = 0$ changes its sign at this point from attractive to repulsive with increasing Ω. As a result, we can realize 1D bosons without two-body but with tunable three-body interactions. We note that effective four- and higher-body interactions also appear but are negligible as far as the low energy physics is concerned.

2.3.1 Three-body resonance

In order to construct the effective theory of 1D bosons near a three-body resonance, we start with the problem of a three-body bound state without two-body but with attractive three-body interactions $U_3 < 0$ within the single-component model. From Eq. (2.79) with $U_2 = 0$, we can see that the binding energy $B_3 > 0$ is determined by the integral equation

$$\frac{1}{|U_3|} = \frac{\sqrt{3}}{16\pi^2}\int_0^{4\pi/\sqrt{3}} dp_1 \int_0^{4\pi} dp_2 \, \frac{1}{B_3 + 2t_x \sum_n [1 - \cos(\boldsymbol{p}\cdot\hat{\boldsymbol{e}}_n)]}, \tag{2.89}$$

where $\hat{\boldsymbol{e}}_1 = (\sqrt{3}, 1)/2$, $\hat{\boldsymbol{e}}_2 = (-\sqrt{3}, 1)/2$, and $\hat{\boldsymbol{e}}_3 = (0, -1)$ and $\boldsymbol{p} = (p_1, p_2)$ is a set of momenta conjugate to relative coordinates (Jacobi coordinates) of three bosons. In particular, B_3 in the weak attraction limit $U_3/t_x \to -0$ is found to be exponentially small [89]

$$B_3 \to 72\, t_x \exp\left(-4\sqrt{3}\pi \frac{t_x}{|U_3|}\right). \tag{2.90}$$

This behavior of B_3 shows that, when the three-body interaction is weakly attractive, the system is near a three-body resonance in the sense that the length scale associated with the three-body bound state

$$a_3 \equiv l\sqrt{\frac{2t_x}{B_3}} = \frac{l}{6}\exp\left(2\sqrt{3}\pi \frac{t_x}{|U_3|}\right) \gg l \tag{2.91}$$

becomes much larger than the microscopic length scale l. Near the three-body resonance, the long-range properties of the system depend on the interaction only through a_3 and thus become universal in a similar way to those near a two-body resonance. Hereafter, a_3 is referred to as a three-body scattering length.

To obtain the effective field theory describing the universal properties near this resonance, we take the continuum limit $l \to 0$ with $t_x l^2 = 1/2m$, $l \times i = x$, $b_i/\sqrt{l} = \phi(x)$, and $U_n l^2 = u_n/m$ fixed. Consequently, the lattice Hamiltonian in Eq. (2.79) with $U_2 = 0$ reduces to

$$H_{\rm cont} = \int dx \left(\frac{1}{2m}|\partial_x \phi(x)|^2 + \frac{u_3}{6m}[\phi^\dagger(x)]^3[\phi(x)]^3\right). \tag{2.92}$$

We note that the interaction terms corresponding to four- and higher-body couplings vanish in the limit of $l \to 0$ because all of them depend on positive powers of l. In the continuum limit, the binding energy B_3 can be expressed in terms of m and the three-body scattering length in Eq. (2.91) as

$$B_3 = \frac{1}{m a_3^2}. \tag{2.93}$$

In Chapter 6, this quantum field theory is investigated in detail.

2.4 Summary

This chapter was devoted to a review of previous works on resonantly interacting quantum systems in 1D. In Section 2.1, the zero-range models describing the universal properties of bosons and fermions near two-body resonance were introduced. By using contact boundary conditions, it was found that these two systems are related to each other via the Bose-Fermi mapping in Eq. (2.17). Because of the existence of this mapping, these systems have the same thermodynamics and static structure factor. In addition, contact interactions were found to provide non-analytic behaviors of wave functions when two particles come into contact with each other. We also reviewed representations of the zero-range models in first- and second-quantized formalisms. In Section 2.2, we introduced the Bethe ansatz, which is used to exactly solve the Schrödinger equations of the zero-range models without a trapping potential. In particular, the energy and contact densities in the thermodynamic limit for negative scattering length are found to be calculable. In Section 2.3, we introduced the way to realize a 1D system governed by a resonant three-body interaction. By tuning the detuning and Rabi frequency for two-component bosons in an optical lattice, we can make an effective two-body interaction vanishing and an effective three-body one resonant.

Chapter 3

Universal relations for static correlation functions

In this chapter, correlation functions for 1D bosons and fermions near two-body resonances are studied from the viewpoint of universal relations. In the zero-range models for bosons and fermions, we derive the power-law tails of the static structure factor and the momentum distribution in the large momentum regime in Section 3.1. We note that, because the interaction range r_0 is regarded as $r_0 \to 0$ in these models, the large momentum regime in the models corresponds to the following region:

$$\lambda_T^{-1},\, n,\, |a|^{-1} \ll |k| \ll r_0^{-1}, \tag{3.1}$$

where λ_T is the thermal de Broglie wavelength, n is the number density, and a is the 1D scattering length. The energy relations, in which the sums of kinetic and interaction energies are expressed in terms of momentum distributions and contact parameters, are derived in Section 3.2. We clarify the consequences of the Bose-Fermi correspondence in these universal relations and verify them for homogeneous systems. For simplicity, we focus on energy eigenstates without a trap in the thermodynamic limit or those of trapped gases in Sections 3.1 and 3.2. The results derived in these two sections are generalized to finite-size systems and statistical ensembles in Section 3.3. In Section 3.4, we exactly compute the momentum distribution for N fermions at infinite scattering length and demonstrate that the relations for fermions hold in this case. We conclude this chapter in Section 3.5.

3.1 Tails of correlation functions

In this section, we study asymptotic behaviors of static structure factors and momentum distributions in the large momentum limit. We start with the expression of the zero-range models with contact boundary conditions: When each pair of particles $1 \leq i < j \leq N$ come into contact with each other, bosonic and fermionic energy eigenfunctions, Ψ_B and Ψ_F, satisfy

$$\lim_{x_{ij} \to +0} \left(1 + a\partial_{x_{ij}}\right) \Psi_\alpha(x_1, \cdots, x_N) = 0 \tag{3.2}$$

with $\alpha = B, F$. Over the domain where all particles are separated from each other, both Ψ_B and Ψ_F solves the free Schrödinger equation:

$$\sum_{i=1}^{N} \left(-\frac{1}{2m}\frac{\partial^2}{\partial x_i^2} + V(x_i) \right) \Psi_\alpha(x_1, \cdots, x_N) = E\Psi_\alpha(x_1, \cdots, x_N), \tag{3.3}$$

where bosons and fermions have the same mass m and a trapping potential $V(x)$ is a smooth function of x. When two particles $i < j$ come close to each other, Ψ_α behaves as follows:

$$\Psi_\alpha(x_1, \cdots, x_N) = \phi_\alpha^{(2)}(x_{ij})\Phi_{\alpha;ij}(X_{ij}; \{x_k\}_{k\neq i,j}) + O(x_{ij}^2), \tag{3.4}$$

where $x_{ij} = x_i - x_j$ and $X_{ij} = (x_i + x_j)/2$ are relative and center-of-mass coordinates of particles i, j, respectively,

$$\phi_B^{(2)}(x) = (1 - |x|/a), \tag{3.5a}$$

$$\phi_F^{(2)}(x) = (\mathrm{sgn}(x) - x/a), \tag{3.5b}$$

are the zero-energy two-body scattering-state wave functions, and

$$\Phi_{\alpha;ij}(X_{ij}; \{x_k\}_{k\neq i,j}) \equiv \lim_{x_{ij}\to+0} \Psi_\alpha \left(x_1, \cdots, X_{ij} + \frac{x_{ij}}{2}, \cdots, X_{ij} - \frac{x_{ij}}{2}, , \cdots, x_N \right) \tag{3.6}$$

is smooth with respect to X_{ij}.

3.1.1 Static structure factors

We first turn to the large-momentum behaviors of static structure factors defined by

$$S(k) = 1 + \frac{1}{N}\int dx_1 dx_2 e^{-ik(x_1-x_2)}[g_2(x_1, x_2) - n(x_1)n(x_2)], \tag{3.7}$$

where

$$g_2(x_1, x_2) = N(N-1)\int dx_3 \cdots dx_N \, |\Psi_\alpha(x_1, \ldots, x_N)|^2 \tag{3.8}$$

and $n(x) = g_1(x)$. The key point to evaluate $S(k)$ for large k is that the Fourier transform of a function having discontinuities or discontinuous derivatives in isolated points obeys a power law at $|k| \to \infty$. The density profile $n(x)$ in Eq. (3.7) is a smooth function, so that its Fourier transformation rapidly vanishes for $|k| \to \infty$. On the other hand, substituting Eq. (3.4) into Eq. (3.8), we can see that the singularity of Ψ_α makes the pair correlation function $g_2(x_1, x_2)$ singular at short distance, $x_{12} \to 0$:

$$\begin{aligned} g_2(x_1, x_2) &= N(N-1)\int dx_3 \cdots dx_N \, |\phi_\alpha^{(2)}(x_{12})|^2 |\Phi_{\alpha;12}(X_{12}; \{x_k\}_{k\neq 1,2})|^2 + O(x_{12}^2) \\ &= |\phi_\alpha^{(2)}(x_{12})|^2 \, \mathcal{C}_2(X_{12}) + O(x_{12}^2), \end{aligned} \tag{3.9}$$

where

$$\mathcal{C}_2(X) \equiv g_2(X,X) = N(N-1)\int dx_3 \cdots dx_N \, |\Phi_{\alpha;12}(X;\{x_k\}_{k\neq 1,2})|^2 \tag{3.10}$$

was used. This singular term proportional to $|x_{12}|$ makes a dominant contribution to $S(k)$ in the large-k limit. By changing integration variables $x_1, x_2 \to x_{12}, X_{12}$, the large-$k$ behavior of $S(k)$ reads

$$\begin{aligned} S(k) &\simeq 1 + \frac{1}{N}\int dx_{12}\, e^{-ikx_{12}} |\phi_\alpha^{(2)}(x_{12})|^2 \int dX_{12}\, \mathcal{C}_2(X_{12}) \\ &= 1 + \frac{1}{N}\int dx_{12}\, e^{-ikx_{12}} (1 - 2|x_{12}|/a + x_{12}^2/a^2) C_2 \end{aligned} \tag{3.11}$$

with $C_2 = \int dX\, \mathcal{C}_2(X)$. Using the Fourier transforms, $\int dx\, e^{-ikx} = 2\pi\delta(k)$, $\int dx\, e^{-ikx}|x| = -2/k^2$, and $\int dx\, e^{-ikx}x^2 = -2\pi\delta''(k)$, we obtain the power-law tail of $S(k)$ for $|k| \to \infty$:

$$\lim_{|k|\to\infty} S(k) = 1 + \frac{4C_2}{Nak^2}. \tag{3.12}$$

We note that this result is derived from the boundary conditions (3.4) satisfied by all eigenstates of the zero-range models. Therefore, Eq. (3.12) holds for any eigenstate.

3.1.2 Momentum distributions

Next, let us turn to momentum distributions defined by

$$\rho_\alpha(k) = N\int dx_2 \cdots dx_N \left| \int dx_1 e^{-ikx_1} \Psi_\alpha(x_1, \ldots, x_N) \right|^2 \tag{3.13}$$

with normalization $\int dk/(2\pi)\, \rho_\alpha(k) = N$. In the case of bosons, the power-law tail of $\rho_B(k)$ at large k was derived by Olshanii and Dunjko in a similar way to that for $S(k)$ [90]. Their result is written as

$$\lim_{|k|\to\infty} \rho_B(k) = \frac{4C_2}{a^2k^4} \tag{3.14}$$

in our definition of C_2.

We now derive the tail of $\rho_F(k)$. The Fourier transform of Ψ_F with respect to x_1 at large k is dominated by the singularity in Eq. (3.4):

$$\int dx_1 e^{-ikx_1} \Psi_F(x_1, \ldots, x_N) \simeq \sum_{j=2}^{N} e^{-ikx_j} \Phi_{F;1j}(x_j; \{x_k\}_{k\neq 1,j}) \int dx_{1j} e^{-ikx_{1j}} \phi_F^{(2)}(x_{1j}), \tag{3.15}$$

where the change of variables $x_1 \to x_{1j}$ was performed. By using $\int dx\, e^{-ikx}\mathrm{sgn}(x) = -2i/k$ and $\int dx\, e^{-ikx}x = 2\pi i\, \delta'(k) = 0$ for $k \neq 0$, we obtain

$$\int dx_1 e^{-ikx_1} \Psi_F(x_1, \ldots, x_N) \simeq \frac{-2i}{k} \sum_{j=2}^{N} e^{-ikx_j} \Phi_{F;1j}(x_j; \{x_k\}_{k\neq 1,j}). \tag{3.16}$$

Substituting this into Eq. (3.13) yields

$$\rho_F(k) \simeq N \int dx_2 \cdots dx_N \left| \frac{-2i}{k} \sum_{j=2}^{N} e^{-ikx_j} \Phi_{F;1j}(x_j; \{x_k\}_{k\neq 1,j}) \right|^2 . \tag{3.17}$$

Recalling that $\Phi_{F;1j}(x_j; \{x_k\}_{k\neq 1,j})$ is a smooth function of x_j, we can see that the cross terms in the modulus squared are written as the Fourier transforms of functions continuous at $x_{jl} = 0$, where $j, l \neq 1$, with respect to x_{jl}. These terms thus rapidly vanish in the large-k limit, and Eq. (3.17) reduces to

$$\begin{aligned} \rho_F(k) &\simeq \frac{4}{k^2} \sum_{j=2}^{N} N \int dx_2 \cdots dx_N \left| \Phi_{F;1j}(x_j; \{x_k\}_{k\neq 1,j}) \right|^2 \\ &= \frac{4}{k^2} N(N-1) \int dx_2 \cdots dx_N \left| \Phi_{F;1j}(x_2; \{x_k\}_{k\neq 1,2}) \right|^2 , \end{aligned} \tag{3.18}$$

where the antisymmetry of the wave function was used in the last line. By using Eq. (3.10) and $C_2 = \int dx\, \mathcal{C}_2(x)$, $\rho_F(k)$ is found to have the following power-law tail:

$$\lim_{|k|\to\infty} \rho_F(k) = \frac{4C_2}{k^2}. \tag{3.19}$$

This is consistent with the result derived by using the operator product expansion [80].

Let us compare Eq. (3.19) with Eq. (3.14). As mentioned in the end of Section 2.1.1, the Bose-Fermi mapping (2.17) does not make $\rho_B(k)$ and $\rho_F(k)$ identical, and we indeed find that they obey different power laws at large momentum. Nevertheless, Eqs. (3.14) and (3.19) show that $\rho_B(k)$ and $\rho_F(k)$ are related to each other at $|k| \to \infty$ through the two-body contact: $\lim_{|k|\to\infty} a^2 k^4 \rho_B(k) = \lim_{|k|\to\infty} k^2 \rho_F(k) = 4C_2$. This is one of the nontrivial connections between $\rho_B(k)$ and $\rho_F(k)$ resulting from the Bose-Fermi correspondence.

At the end of this section, we apply Eqs. (3.12), (3.14), and (3.19) to the ground states of uniform Bose and Fermi gases with a negative scattering length. In this case, $n(x) = n = N/L$ and $\mathcal{C}_2(x) = \mathcal{C}_2 = C_2/L$ are constant with L being the system size. In the thermodynamic limit, the states are characterized only by the dimensionless parameter $\gamma = -2/(na) > 0$. As mentioned in Section 2.2.1, $\mathcal{C}_2$ can be numerically calculated for arbitrary $\gamma > 0$ by the Bethe ansatz [82]. This numerical result combined with Eqs. (3.12), (3.14), and (3.19) completely determines the large-k asymptotics of $S(k)$ and $\rho_\alpha(k)$ for arbitrary $\gamma > 0$. For sufficiently small or large γ, the analytical expression of $\mathcal{C}_2$ is also obtained as $\mathcal{C}_2 \simeq n^2$ for $\gamma \ll 1$ and $\mathcal{C}_2 \simeq \frac{4}{3}\pi^2\gamma^{-2}n^2$ for $\gamma \gg 1$. By substituting these expressions into Eqs. (3.12), (3.14), and (3.19), we obtain the explicit forms of the tails for $\gamma \ll 1$ and $\gamma \gg 1$, which are consistent with the large-k limit of the previous results in Refs. [91–93].

3.2 Energy relations

In order to derive the energy relations for 1D bosons and fermions, we use first-quantized Hamiltonians with pseudopotentials:

$$H_B = H_0 - \frac{2}{ma}\sum_{i<j}\delta(x_{ij}), \tag{3.20}$$

$$H_F = H_0 - \frac{2a}{m}\sum_{i<j}\delta'(x_{ij})D_{ij} \tag{3.21}$$

with

$$H_0 = \sum_{i=1}^{N}\left(-\frac{1}{2m}\frac{\partial^2}{\partial x_i^2} + V(x_i)\right). \tag{3.22}$$

Here, the linear operator D_{ij} acts on a fermionic wave function as $D_{ij}\Psi_F = \frac{\partial}{\partial x_{ij}}\Psi_F|_{x_{ij}=+0}$ with the center of mass coordinate $X_{ij} = (x_i + x_j)/2$ of the pair of fermions i, j and the other $N-2$ coordinates $\{x_k\}_{k\neq i,j}$ fixed.

The energy relation for bosons is easily derived by evaluating the expectation value of H_B with respect to Ψ_B [94]:

$$E - E_{\rm trap} = \int\frac{dk}{2\pi}\frac{k^2}{2m}\rho_B(k) - \frac{C_2}{ma}, \tag{3.23}$$

where $E_{\rm trap} = \int dx V(x)n(x)$ is a trapping energy. We note that the kinetic energy for bosons is ultraviolet convergent because of Eq. (3.14).

In the case of fermions, an appropriate regularization procedure is however required to derive the energy relation. If the expectation value of H_F with respect to Ψ_F was naively evaluated, one would be faced with divergences from both kinetic and interaction energies. Indeed, Eq. (3.19) provides

$$\frac{k^2}{2m}\rho_F(k) \simeq \frac{k^2}{2m}\frac{4C_2}{k^2} = \text{constant} \tag{3.24}$$

for $|k| \to \infty$, and thus the kinetic energy has an ultraviolet divergence. In this paper, we perform the regularization of the fermionic theory in the following way: First, we introduce a function $f_\epsilon(x)$ with a range $\epsilon > 0$, which is finite for $|x| < \epsilon$, rapidly vanishes for $|x| > \epsilon$, and approaches the derivative of the delta function in the zero-range limit, $\lim_{\epsilon\to 0} f_\epsilon(x) = \delta'(x)$. We then replace $\delta'(x)$ in Eq. (3.21) with $f_\epsilon(x)$:

$$H_F \to H_F^{(\epsilon)} = H_0 - \frac{2a}{m}\sum_{i<j}f_\epsilon(x_{ij})D_{ij}. \tag{3.25}$$

After evaluating the expectation value of $H_F^{(\epsilon)}$ with respect to Ψ_F, we take the zero-range limit $\epsilon \to 0$. Our approach is motivated by the method used in Ref. [95].

3.2.1 Kinetic and trapping energies

Let us evaluate the expectation value of H_0 with respect to Ψ_F. In the previous section, we show in the limit $\epsilon \to 0$ that $\rho_F(k)$ behaves as $1/k^2$ for large momentum. For finite $\epsilon > 0$, Eq. (3.19) holds as long as $|k|$ is much smaller than $1/\epsilon$ but much larger than the other momentum scales in the system. However, the momentum distribution rapidly vanishes for $|k| > \Lambda \sim 1/\epsilon$, which is easily demonstrated in the case of a simple finite-range potential such as a square-well potential. As a result, a contribution from the region $|k| > \Lambda$ to the kinetic energy is negligible. The expectation value of H_0 is thus found to be

$$\int dx_1 \cdots dx_N \Psi_F^* H_0 \Psi_F \simeq \int_{-\Lambda}^{\Lambda} \frac{dk}{2\pi} \frac{\hbar^2 k^2}{2m} \rho_F(k) + E_{\rm trap}, \tag{3.26}$$

where a trapping energy $E_{\rm trap} = \int dx V(x) n(x)$ is convergent in the limit $\epsilon \to 0$ and the same as that for bosons.

We next evaluate the interaction energy

$$U_F = -\frac{2a}{m} \sum_{i<j} \int dx_1 \cdots dx_N \, \Psi_F^* f_\epsilon(x_{ij}) D_{ij} \Psi_F. \tag{3.27}$$

The interaction energy has only two contributions, $U_F^{(2)}$ and $U_F^{(3)}$, remaining in the limit $\epsilon \to 0$. Here, the contribution $U_F^{(M)}$ comes from the configurations $R_{i_1,\cdots,i_M}$ where only M particles at $x_{i_1}, \cdots, x_{i_M}$ interact with each other.

3.2.2 Evaluation of $U_F^{(2)}$

In the region R_{12}, the wave function behaves as Eq. (3.4), leading to

$$-aD_{12}\Psi_F(x_1, \cdots, x_N) = \Phi_{F;12}(X_{12}; \{x_k\}_{k\neq 1,2}). \tag{3.28}$$

The integral region R_{12} can be rewritten as

$$\int_{R_{12}} dx_1 \cdots dx_N = \int_{-\epsilon}^{\epsilon} dx_{12} \int_{-\infty}^{\infty} dX_{12} \int_{R'_{12}} dx_3 \cdots dx_N, \tag{3.29}$$

where the symbol R'_{12} refers to the region where all fermions at $x_3, \ldots, x_N$ are not affected by the interaction, i.e., $|x_{1i}|, |x_{2i}| > \epsilon$ for $i = 3, \ldots, N$ and $|x_{jk}| > \epsilon$ for $3 \le j < k \le N$. By taking the antisymmetry of Ψ_F into account, $U_F^{(2)}$ is given by

$$\begin{aligned} U_F^{(2)} = {} & \frac{N(N-1)}{2} \times \frac{2}{m} \int_{-\epsilon}^{\epsilon} dx_{12} \, f_\epsilon(x_{12}) \phi_F^{(2)}(x_{12}) \\ & \times \int_{-\infty}^{\infty} dX_{12} \int_{R'_{12}} dx_3 \cdots dx_N |\Phi_{F;12}(X_{12}; \{x_k\}_{k\neq 1,2})|^2 + O(\epsilon). \end{aligned} \tag{3.30}$$

Because power counting with respect to ϵ provides $dx_{12} = O(\epsilon)$, $f_\epsilon(x_{12}) = O(\epsilon^{-2})$, $[\mathrm{sgn}(x_{12}) - x_{12}/a] = O(1)$ and $dX_{12} = O(1)$, we need to evaluate the integral over R'_{12} up to $O(\epsilon^2)$. It is

convenient to rewrite this integral as follows:

$$\int_{R'_{12}} dx_3 \cdots dx_N |\Phi_{F;12}(X_{12}; \{x_k\}_{k\neq 1,2})|^2 = \frac{\mathcal{C}_2(X_{12})}{N(N-1)} - \int_{S_{12}} dx_3 \cdots dx_N |\Phi_{F;12}(X_{12}; \{x_k\}_{k\neq 1,2})|^2, \tag{3.31}$$

where $S_{12} = \mathbb{R}^{N-2} - R'_{12}$ is the complement of R'_{12} and Eq. (3.10) was used. The last term is dominated by the region where only one of the remaining fermions approaches the pair of fermions 1, 2, and thus it reads

$$\begin{aligned} &\int_{S_{12}} dx_3 \cdots dx_N |\Phi_{F;12}(X_{12}; \{x_k\}_{k\neq 1,2})|^2 \\ &= (N-2) \int_{\min\{x_1,x_2\}-\epsilon}^{\max\{x_1,x_2\}+\epsilon} dx_3 \int_{\mathbb{R}^{N-3}} dx_4 \cdots dx_N |\Phi_{F;12}(X_{12}; X_{12}, x_4, \cdots, x_N)|^2 + O(\epsilon^2). \end{aligned} \tag{3.32}$$

Note $x_3 = X_{12} + O(\epsilon)$ in the integral region. Using Eq. (3.6) and the definition of $g_3(x_1, x_2, x_3)$,

$$g_3(x_1, x_2, x_3) \equiv N(N-1)(N-2) \int_{\mathbb{R}^{N-3}} dx_4 \cdots dx_N \, |\Psi_F(x_1, \cdots, x_N)|^2, \tag{3.33}$$

as well as $\mathcal{C}_3(X) = g_3(X, X, X)$, we obtain

$$\begin{aligned} \int_{S_{12}} dx_3 \cdots dx_N |\Phi_{F;12}(X_{12}; \{x_k\}_{k\neq 1,2})|^2 &= (N-2) \int_{\min\{x_1,x_2\}-\epsilon}^{\max\{x_1,x_2\}+\epsilon} dx_3 \, \frac{\mathcal{C}_3(X_{12})}{N(N-1)(N-2)} + O(\epsilon^2) \\ &= \frac{(2\epsilon + |x_{12}|)\, \mathcal{C}_3(X_{12})}{N(N-1)} + O(\epsilon^2). \end{aligned} \tag{3.34}$$

By using Eqs. (3.31) and (3.34), $U_F^{(2)}$ in Eq. (3.30) is found to be

$$U_F^{(2)} = \frac{1}{m} \int_{-\epsilon}^{\epsilon} dx_{12} \, f_\epsilon(x_{12}) \left[\mathrm{sgn}(x_{12})(C_2 - 2\epsilon C_3) - x_{12} \left(\frac{C_2}{a} + C_3 \right) \right] + O(\epsilon), \tag{3.35}$$

where $C_3 = \int dX \, \mathcal{C}_3(X)$ is the three-body contact.

3.2.3 Evaluation of $U_F^{(3)}$

We now evaluate the contribution $U_F^{(3)}$ given by

$$\begin{aligned} U_F^{(3)} &= \frac{N(N-1)(N-2)}{3 \cdot 2} \frac{-2a}{m} \int_{R_{123}} dx_1 \cdots dx_N \, \Psi_F^* \left[f_\epsilon(x_{12}) D_{12} + f_\epsilon(x_{13}) D_{13} + f_\epsilon(x_{23}) D_{23} \right] \Psi_F \\ &= \frac{N(N-1)(N-2)}{m} \int_{R_{123}} dx_1 \cdots dx_N \, \Psi_F^* f_\epsilon(x_{12}) [-a D_{12} \Psi_F]. \end{aligned} \tag{3.36}$$

The integral region can be rewritten as

$$\int_{R_{123}} dx_1 \cdots dx_N = \int_{-\epsilon}^{\epsilon} dx_{12} \int_{-\infty}^{\infty} dX_{12} \int_{\min\{x_1,x_2\}-\epsilon}^{\max\{x_1,x_2\}+\epsilon} dx_3 \int_{\mathbb{R}^{N-3}} dx_4 \cdots dx_N + O(\epsilon^3). \tag{3.37}$$

Over the region R_{123}, Ψ_F^* is evaluated as

$$\Psi_F^*(x_1,\cdots,x_N) = \phi_F^{(3)}(x_1,x_2,x_3)\Phi_{F;123}^*(X_{12};x_4,\cdots,x_N) + O(\epsilon), \tag{3.38}$$

where

$$\phi_F^{(3)}(x_1,x_2,x_3) \equiv \mathrm{sgn}(x_{12})\mathrm{sgn}(x_{13})\mathrm{sgn}(x_{23}), \tag{3.39}$$

$$\Phi_{F;123}(X;x_4,\cdots,x_N) \equiv \lim_{\epsilon',\epsilon''\to+0} \Psi_F(X+\epsilon',X,X-\epsilon'',x_4,\cdots,x_N). \tag{3.40}$$

Here, $\phi_F^{(3)}(x_1,x_2,x_3)$ is the zero-energy three-body scattering-state wave function and the product of three sign functions in $\phi_F^{(3)}(x_1,x_2,x_3)$ comes from the antisymmetry in the exchange of fermions at x_1, x_2, x_3. On the other hand, $-aD_{12}\Psi_F$ is evaluated as

$$\begin{aligned} -aD_{12}\Psi_F(x_1,\cdots,x_N) &= \Phi_{F;12}(X_{12};x_3,x_4,\cdots,x_N) + O(\epsilon) \\ &= \Phi_{F;123}(X_{12};x_4,\cdots,x_N) + O(\epsilon), \end{aligned} \tag{3.41}$$

where $x_3 = X_{12} + O(\epsilon)$ was used in the last line. As a result, Eq. (3.36) is found to be

$$\begin{aligned} U_F^{(3)} &= \frac{1}{m}\int_{-\epsilon}^{\epsilon} dx_{12}\, f_\epsilon(x_{12}) \int_{\min\{x_1,x_2\}-\epsilon}^{\max\{x_1,x_2\}+\epsilon} dx_3\, \phi_F^{(3)}(x_1,x_2,x_3) \\ &\quad \times \int_{-\infty}^{\infty} dX_{12} \underbrace{N(N-1)(N-2)\int_{\mathbb{R}^{N-3}} dx_4\cdots dx_N\, |\Phi_{F;123}(X_{12};x_4,\cdots,x_N)|^2}_{=\mathcal{C}_3(X_{12})} + O(\epsilon) \\ &= \frac{1}{m}\int_{-\epsilon}^{\epsilon} dx_{12}\, f_\epsilon(x_{12})[2\epsilon\,\mathrm{sgn}(x_{12}) - x_{12}]C_3 + O(\epsilon). \end{aligned} \tag{3.42}$$

3.2.4 Evaluation of the total energy

Summing up Eqs. (3.35) and (3.42) yields

$$\begin{aligned} U_F &= U_F^{(2)} + U_F^{(3)} + O(\epsilon) \\ &= \frac{C_2}{m}\int_{-\epsilon}^{\epsilon} dx_{12}\, f_\epsilon(x_{12})\,\mathrm{sgn}(x_{12}) - \frac{1}{m}\left(\frac{C_2}{a} + 2C_3\right)\int_{-\epsilon}^{\epsilon} dx_{12}\, f_\epsilon(x_{12})\, x_{12} + O(\epsilon). \end{aligned} \tag{3.43}$$

Since $f_\epsilon(x)$ rapidly vanishes for $|x| > \epsilon$, we can replace the integration region $[-\epsilon,\epsilon]$ with $(-\infty,\infty)$. In general, an integral $\int_{-\infty}^{\infty} dx\, F(x)G(x)$ can be rewritten in terms of the Fourier transforms $\tilde{F}(k) = \int_{-\infty}^{\infty} dk/(2\pi)\, F(x)$ and $\tilde{G}(k) = \int_{-\infty}^{\infty} dk/(2\pi)\, G(x)$ as follows:

$$\int_{-\infty}^{\infty} dx\, F(x)G(x) = \int_{-\infty}^{\infty} \frac{dk}{2\pi}\, \tilde{F}(k)[\tilde{G}(k)]^*. \tag{3.44}$$

Since $\lim_{\epsilon\to+0} f_\epsilon(x) = \delta'(x)$, the Fourier transform of $f_\epsilon(x)$ can be evaluated as that of $\delta'(x)$ for $|k| < \Lambda$ and rapidly vanishes for $|k| > \Lambda$. Combining this Fourier transform with that of the sign function, $-2i/k$, the integral in the first term in Eq. (3.43) reads

$$\int_{-\epsilon}^{\epsilon} dx_{12}\, f_\epsilon(x_{12})\,\mathrm{sgn}(x_{12}) = \int_{-\Lambda}^{\Lambda} \frac{dk}{2\pi}\, ik\left(\frac{-2i}{k}\right)^* = -\int_{-\Lambda}^{\Lambda} \frac{dk}{2\pi}\, 2. \tag{3.45}$$

On the other hand, the integral in the second term in Eq. (3.43) is evaluated as

$$\int_{-\epsilon}^{\epsilon} dx_{12}\, f_\epsilon(x_{12})\, x_{12} = \int_{-\infty}^{\infty} dx_{12}\, \delta'(x_{12})\, x_{12} + O(\epsilon) = -1 + O(\epsilon). \tag{3.46}$$

Substituting Eqs. (3.45) and (3.46) into Eq. (3.43) yields

$$U_F = -\int_{-\Lambda}^{\Lambda} \frac{dk}{2\pi} \frac{2C_2}{m} + \frac{C_2}{ma} + \frac{2C_3}{m} + O(\epsilon). \tag{3.47}$$

Combining this with Eq. (3.26) and taking the limit of $\epsilon \sim 1/\Lambda \to +0$, we arrive at the following energy relation:

$$E - E_{\rm trap} = \lim_{\Lambda\to\infty} \int_{-\Lambda}^{\Lambda} \frac{dk}{2\pi} \frac{k^2}{2m} \left(\rho_F(k) - \frac{4C_2}{k^2} \right) + \frac{C_2}{ma} + \frac{2C_3}{m}. \tag{3.48}$$

This is a novel universal relation including the three-body correlation in 1D. We note that Eq. (3.48) is similar to the energy relation for 3D bosons, where the Efimov effect takes place [18], in the sense that both of them involve the three-body contacts [31].

In Ref. [80], the energy relation for 1D fermions with an odd-wave interaction was proposed by using the quantum field theory described by the Lagrangian density in Eq. (2.31). However, the proposed relation does not include the three-body contribution. To demonstrate the necessity of this contribution, we apply Eq. (3.48) to the ground state of a uniform Fermi gas with $a \to -\infty$ in the thermodynamic limit. In this case, the Fermi gas corresponds to the ideal Bose gas and has $E = E_{\rm trap} = 0$, $C_2/N = n$, and $C_3/N = n^2$ with $n(x) = n$. The momentum distribution, $\rho_F(k)/N = 4n/(k^2 + 4n^2)$, is also exactly calculated [91, 92]. By substituting these into both sides of Eq. (3.48), one can see that Eq. (3.48) holds in this case and that the three-body contact makes an essential contribution to the energy of fermions.

We now compare the energy relations for bosons and fermions. Although the left-hand sides of Eqs. (3.23) and (3.48) are the same, the right-hand sides look quite different, in particular, in the absence or presence of a term proportional to C_3. Nevertheless, Eqs. (3.23) and (3.48) connect $\rho_B(k)$ and $\rho_F(k)$, which is the other nontrivial connection of $\rho_\alpha(k)$ resulting from the Bose-Fermi correspondence.

3.3 Generalization of results

The universal relations [Eqs. (3.12), (3.14), (3.19), (3.23), and (3.48)] presented in the previous sections can be generalized to bosons and fermions with a finite system size $L < \infty$. Although k is not continuous but quantized, the power-law tails of correlation functions [Eqs. (3.12), (3.14), and (3.19)] hold for these systems. The energy relations for these systems can be obtained by replacing the integrals in Eqs. (3.23) and (3.48) with the sum over k: $\int_{-\Lambda}^{\Lambda} dk/(2\pi) \to L^{-1} \sum_{|k|<\Lambda}$. In the next section, we demonstrate Eqs. (3.19) and (3.48) for a finite-size fermionic system at unitarity $a \to \infty$.

Here, we note that, when wave functions with periodic (or more generally twisted) boundary conditions are considered, the Bose-Fermi mapping sometimes makes boundary conditions for

the mapped state different from those for the original state [44, 52]. The Bose-Fermi mapping is given by

$$\Psi_F(x_1, \cdots, x_N) = A(x_1, \cdots, x_N)\Psi_B(x_1, \cdots, x_N), \tag{3.49}$$

where the mapping factor has the form

$$A(x_1, \cdots, x_N) = \prod_{1 \le i < j \le N} \mathrm{sgn}(x_{ij}) \tag{3.50}$$

with $0 \le x_l \le L$ for $l = 1, \cdots, N$. We can easily find the following property of $A(x_1, \cdots, x_N)$:

$$A(x_1, \cdots, 0, \cdots, x_N) = (-1)^{N-1} A(x_1, \cdots, L, \cdots, x_N). \tag{3.51}$$

This means that, if and only if N is even, $A(x_1, \cdots, x_N)$ makes boundary conditions for the mapped state opposite in sign from those for the original state. For example, Ψ_B with periodic boundary conditions corresponds to Ψ_F with antiperiodic (periodic) ones if N is even (odd). On the other hand, the mapping factor does not change hard wall boundary conditions [96, 97].

Since the universal relations hold for any energy eigenstates, any statistical ensemble of the bosonic eigenstates satisfies Eqs. (3.12), (3.14), and (3.23), while any statistical ensemble of the fermionic eigenstates satisfies Eqs. (3.12), (3.19), and (3.48). This set of the ensembles includes not only a canonical ensemble in thermal equilibrium but also a generalized Gibbs ensemble, which is expected to describe the stationary properties after a quantum quench in integrable systems [98].

3.4 Fermions at unitarity

In this section, we study the ground state of a finite number of spinless fermions in the limit of $a \to \infty$. For simplicity, we consider fermions corresponding to free bosons with periodic boundary conditions without an external potential:

$$\Psi_F(x_1, \ldots, x_N) = L^{-N/2} A(x_1, \ldots, x_N), \tag{3.52}$$

where $0 \le x_i < L$. This state has $E = E_{\mathrm{trap}} = 0$, $C_2 = N(N-1)/L$, and $C_3 = N(N-1)(N-2)/L^2$.

We now compute $\rho_F(k)$ for the ground state. Because the wave function in Eq. (3.52) satisfies periodic (antiperiodic) boundary conditions if N is odd (even), k is quantized as $k = 2l\pi/L$ $[k = (2l+1)\pi/L]$, where l is an integer. The momentum distribution is given by

$$\rho_F(k) = N \int_0^L dx_2 \cdots \int_0^L dx_N \left| \int_0^L dx_1 \, \Psi_F(x_1, x_2, \cdots, x_N) e^{-ikx_1} \right|^2 \tag{3.53}$$

with normalization $L^{-1}\sum_k \rho_F(k) = N$. By using Eq. (3.50), this reads

$$\begin{aligned} \rho_F(k) &= NL^{-N} \int_0^L dx_1 \int_0^L dx_1' \, e^{-ik(x_1 - x_1')} \prod_{j=2}^{N} \left[\int_0^L dx_j \, \mathrm{sgn}(x_1 - x_j)\mathrm{sgn}(x_1' - x_j) \right] \\ &= NL^{-N} \int_0^L dx_1 \int_0^L dx_1' \, e^{-ik(x_1 - x_1')} \left(L - 2|x_1 - x_1'| \right)^{N-1}. \end{aligned} \tag{3.54}$$

For $k = 0$, we can easily obtain $\rho_F(k = 0) = L$. To calculate $\rho_F(k)$ for $k \neq 0$, we introduce a indefinite integral $I_l(z; k)$ for convenience:

$$I_l(z;k) \equiv \int dz\, e^{ikz}(L+2z)^l = \sum_{s=0}^{l} \frac{(-2)^s}{(ik)^{s+1}} \frac{l!}{(l-s)!} e^{ikz}(L+2z)^{l-s}. \tag{3.55}$$

By changing the integration valuable $x_1' \to z = x_1' - x_1$, $\rho_F(k)$ for $k \neq 0$ can be evaluated as

$$\begin{aligned}
\rho_F(k \neq 0) &= NL^{-N} \int_0^L dx_1 \int_{-x_1}^{L-x_1} dz\, e^{ikz} \left(L - 2|z|\right)^{N-1} \\
&= NL^{-(N-1)} \left[I_{N-1}(0;k) + I_{N-1}(0;-k)\right] \\
&\quad - NL^{-N} \int_0^L dx_1 \left[I_{N-1}(-x_1;k) + I_{N-1}(x_1 - L;-k)\right].
\end{aligned} \tag{3.56}$$

Since $e^{ikL} = (-1)^{N-1}$, the integrand is found to be zero:

$$\begin{aligned}
I_{N-1}(-x_1;k) + I_{N-1}(x_1 - L;-k) &= \sum_{s=0}^{N-1} \frac{(-2)^s}{(ik)^{s+1}} \frac{(N-1)!}{(N-1-s)!} e^{-ikx_1}(L-2x_1)^{N-1-s} \\
&\quad \times \left[1 + e^{ikL}(-1)^N\right] \\
&= 0.
\end{aligned} \tag{3.57}$$

Substituting Eq. (3.55) into Eq. (3.56) yields

$$\rho_F(k \neq 0) = L \sum_{s=1}^{\lfloor N/2 \rfloor} (-1)^{s-1} \frac{N!}{(N-2s)!} \left(\frac{2}{kL}\right)^{2s}, \tag{3.58}$$

where the floor function $\lfloor N/2 \rfloor$ equals $(N-1)/2$ if N is odd and $N/2$ if N is even. Consequently, we obtain the momentum distribution

$$\frac{\rho_F(k)}{L} = \delta_{k,0} + (1 - \delta_{k,0}) \sum_{s=1}^{\lfloor N/2 \rfloor} \frac{(-1)^{s-1} N!}{(N-2s)!} \left(\frac{2}{kL}\right)^{2s}. \tag{3.59}$$

Note that the wavenumber k can take the value of $k = 0$ only when N is odd. Taking the large-k limit, we have $\rho_F(k) \to 4N(N-1)/(k^2 L)$, which is consistent with Eq. (3.19). In addition, we confirmed that the energy relation for a finite-size system holds,

$$\frac{1}{L} \sum_k \frac{\hbar^2 k^2}{2m} \left(\rho_F(k) - \frac{4C_2}{k^2}\right) + \frac{2\hbar^2 C_3}{m} = 0, \tag{3.60}$$

by using Mathematica.

3.5 Summary

We studied 1D bosons and fermions which are related to each other through the Bose-Fermi mapping (3.49) and derived the power-law tails of $S(k)$ and $\rho_\alpha(k)$ at large k and the energy relations. We found the following three facts in these universal relations: $S(k)$ has the identical tail between bosons and fermions; the Bose-Fermi correspondence results in two nontrivial connections between $\rho_B(k)$ and $\rho_F(k)$ through their tails and through the energy relations; and the three-body contact makes no contribution to the energy relation for bosons, but it makes an essential contribution to that for fermions. Furthermore, Eqs. (3.12), (3.14), and (3.19) together with the Bethe ansatz completely determine the large-k tails of $S(k)$ and $\rho_\alpha(k)$ for uniform Bose and Fermi gases at any temperature. We also computed $\rho_F(k)$ for the ground state of N fermions in the limit of $a \to \infty$ and confirmed Eqs. (3.19) and (3.48) in this case.

We can consider some applications and generalizations of the universal relations presented in this chapter. Our relations can be used as reliable tests on numerical studies of correlation functions [99–103]. One may compute higher-order corrections to Eqs. (3.12), (3.14), and (3.19) at large momentum in a similar way to 2D and 3D cases [31, 104]. It should be interesting to see whether and how C_3 appears in these corrections. One can also generalize energy relations to 1D bosons and fermions with finite effective ranges [105–107], where a three-body correlation will make an essential contribution in the fermionic case as in Eq. (3.48).

Chapter 4

Dynamic correlation functions for bosons

The previous chapter is devoted to deriving the exact relations for static correlation functions such as static structure factors and the momentum distributions for 1D bosons and fermions. In this chapter, we turn to dynamic correlation functions of bosons such as a dynamic structure factor and a single-particle spectral density. The dynamic correlation functions provide information about excitations of systems. The dynamic structure factor $S(\omega, k)$ encodes information about the degrees of freedom which can be excited by density perturbations with energy and momentum transfer (ω, k) and, in ultracold atom experiments, it can be measured with Bragg spectroscopy [108] or Fourier sampling of time-of-flight images [109]. The single-particle spectral density $\mathcal{A}_B(\omega, k)$ provides the probability that a particle or a hole with energy ω and momentum k propagate, and it is measurable using stimulated Raman transition combined with additional spin flips [109, 110].

We investigate the exact asymptotics of dynamic correlation functions in the high-energy regime of 1D bosons. To derive these asymptotic behaviors, the operator product expansion (OPE) based on a field theoretical formalism is more useful than the method used in Chapter 3. Throughout this chapter, we focus on a thermal equilibrium state which is spatially homogeneous, i.e., a trapping potential is absent.

The outline of this chapter is as follows: In Section 4.1, we introduce the quantum field theory for resonantly interacting bosons and explain OPE. By using OPE, we calculate the large-energy-momentum behaviors of dynamic correlation functions including a density correlation (Section 4.2), a current correlation (Section 4.3), and a single-particle Green function (Section 4.4). The summary of this chapter is given in the last section.

For simplicity, we use the following shorthand notations in the rest of this thesis:

$$X = (X_0, X_1) \equiv (t, x), \tag{4.1}$$

$$\partial_t = \frac{\partial}{\partial X_0}, \quad \partial_x = \frac{\partial}{\partial X_1}, \tag{4.2}$$

$$A \overset{\leftrightarrow}{\partial} B \equiv \frac{1}{2}[A\partial B - (\partial A)B], \tag{4.3}$$

$$K = (K_0, K_1) \equiv (\omega, k), \tag{4.4}$$

$$K \cdot X \equiv K_0 X_0 - K_1 X_1, \tag{4.5}$$

$$\int_X \equiv \int dX_0\, dX_1, \tag{4.6}$$

$$\int_K \equiv \int \frac{dK_0 dK_1}{(2\pi)^2}, \tag{4.7}$$

$$F(K) + (K \to -K) \equiv F(K) + F(-K) \tag{4.8}$$

with $X_0 = t$ being a time, $X_1 = x$ a spacial coordinate, $K_0 = \omega$ an energy, $K_1 = k$ a momentum. The symbol $\langle \mathcal{O} \rangle$ denotes the canonical ensemble average of an operator $\mathcal{O}$:

$$\langle \mathcal{O} \rangle = \frac{\mathrm{Tr}[\mathcal{O} e^{-H/(k_B T)}]}{\mathrm{Tr}[e^{-H/(k_B T)}]}. \tag{4.9}$$

4.1 Quantum field theory of bosons

We investigate the quantum field theory described by the Lagrangian density

$$\mathcal{L}_B = \phi^\dagger \left(i\partial_t + \frac{\partial_x^2}{2m} \right) \phi + \frac{1}{ma} \phi^\dagger \phi^\dagger \phi \phi, \tag{4.10}$$

where $\phi(X)$ is a bosonic field, a is a one-dimensional scattering length. In order to make calculations in this chapter simpler, we perform the Hubbard-Stratonovich transformation [111]: By using the path-integral formula for a complex bosonic field d,

$$\int \mathcal{D}(d, d^\dagger) e^{-\frac{i}{ma} \int_X |d - \phi^2|^2} = 1, \tag{4.11}$$

the partition function of the system reads

$$\int \mathcal{D}(\phi, \phi^\dagger) e^{i \int_X \mathcal{L}_B(\phi, \phi^\dagger)} = \int \mathcal{D}(\phi, \phi^\dagger, d, d^\dagger) e^{i \int_X \mathcal{L}'_B(\phi, \phi^\dagger, d, d^\dagger)} \tag{4.12}$$

with the new Lagrangian density

$$\mathcal{L}'_B = \phi^\dagger \left(i\partial_t + \frac{\partial_x^2}{2m} \right) \phi + \frac{1}{ma} (-d^\dagger d + d^\dagger \phi^2 + \phi^{\dagger 2} d). \tag{4.13}$$

Because the Euler-Lagrange equation for $d^\dagger$ leads to $d = \phi^2$, d is found to be an auxiliary dimer field. The term of $d^\dagger \phi^2$ in $\mathcal{L}'_B$ converts two bosons into a dimer, while $\phi^{\dagger 2} d$ a dimer into two bosons. In the field theoretical formalism, the two-body contact density can be expressed as

$$\mathcal{C}_2 = \langle \phi^\dagger \phi^\dagger \phi \phi \rangle = \langle d^\dagger d \rangle. \tag{4.14}$$

The propagator of a boson $iG(K)$ is given by

$$G(K) = \frac{1}{K_0 - \frac{K_1^2}{2m} + i0^+}. \tag{4.15}$$

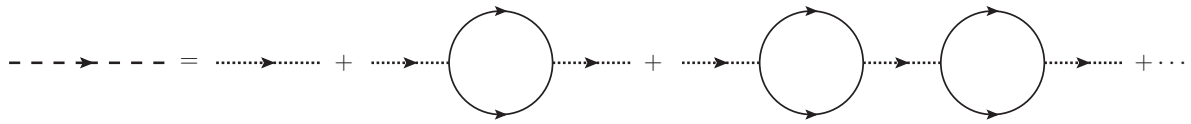

(a) $iD_B(K)$.

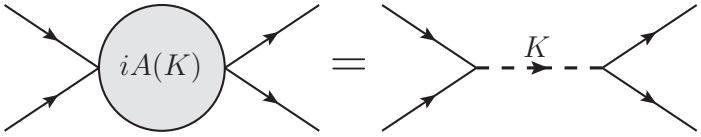

(b) $iA(K)$.

Figure 4.1: Feynman diagrams for (a) the full dimer propagator and (b) the two-body scattering amplitude. The solid, dotted, and dashed lines indicate $iG(K)$, $iD_B^{(0)}$, and $iD(K)$, respectively. The boson-dimer vertex is $2i/(ma)$.

On the other hand, the full propagator of a dimer $iD_B(K)$ is obtained by summing up all the bubble diagrams in Fig. 4.1(a):

$$\begin{aligned} iD_B(K) &= iD_B^{(0)} + iD_B^{(0)}\Pi_F(K)D_B^{(0)} + iD_B^{(0)}[\Pi_F(K)D_B^{(0)}]^2 + \cdots \\ &= \frac{i}{1/D_B^{(0)} - \Pi_B(K)}, \end{aligned} \tag{4.16}$$

where $D_B^{(0)} = -ma$ is the bare dimer propagator and

$$\Pi_B(K) = \frac{2i}{m^2a^2}\int_P G(K/2+P)G(K/2-P) \tag{4.17}$$

is the dimer self-energy. The integral in $\Pi_B(K)$ can be carried out by the residue theorem:

$$\begin{aligned} \Pi_B(K) &= \frac{2i}{m^2a^2}\int \frac{dP_0dP_1}{(2\pi)^2}\,\frac{1}{\frac{K_0}{2}+P_0-\frac{\left(\frac{K_1}{2}+P_1\right)^2}{2m}+i0^+}\,\frac{1}{\frac{K_0}{2}-P_0-\frac{\left(\frac{K_1}{2}-P_1\right)^2}{2m}+i0^+} \\ &= \frac{2i}{m^2a^2}(-i)\int\frac{dP_1}{2\pi}\,\frac{1}{K_0-\frac{\left(\frac{K_1}{2}+P_1\right)^2+\left(\frac{K_1}{2}-P_1\right)^2}{2m}+i0^+} \\ &= -\frac{1}{ma^2\beta_K} \end{aligned} \tag{4.18}$$

with $\beta_K \equiv \sqrt{K_1^2/4 - mK_0 - i0^+}$. Substituting this into Eq. (4.16), we obtain

$$D_B(K) = -\frac{ma}{1-1/(a\beta_K)}. \tag{4.19}$$

The scattering amplitude of two bosons $iA(K)$ depicted in Fig. 4.1(b) is related to the dimer propagator through

$$A(K) = -\frac{4}{m^2 a^2} D_B(K) = \frac{4}{m} \frac{1}{a - 1/\beta_K}, \tag{4.20}$$

where $K = (K_0, K_1)$ is a set of total energy K_0 and center-of-mass momentum K_1 of incoming atoms.

4.1.1 Operator product expansion

The operator product expansion (OPE) is one of field theoretical methods to investigate correlation functions. This method was invented independently by Kadanoff [112], Polyakov [113], and Wilson [114]. Recently, OPE in the context of atomic physics was also reviewed in Ref. [30]. The statement of OPE is that the operator product $A(X)B(0)$ can be given by a sum of local operators $\mathcal{O}_i(X)$:

$$A(X)B(0) = \sum_i \bar{W}_{AB}^{\mathcal{O}_i}(X)\mathcal{O}_i(0). \tag{4.21}$$

The quantities $\bar{W}_{AB}^{\mathcal{O}_i}(X)$ called Wilson coefficients are c-number functions of the separation X. The operators $\mathcal{O}_i(X)$ can be composed of field operators and their derivatives. In a quantum field theory framework, we often investigate the expectation value of a time-ordered product in Fourier transform:

$$\mathcal{G}_{AB}(K) \equiv -i \int d^2X \, e^{iK\cdot X} \mathcal{T}\left[A\left(X\right) B\left(0\right)\right], \tag{4.22}$$

where $\mathcal{T}$ denotes the time-ordering operator. According to OPE, this can be expressed as

$$\mathcal{G}_{AB}(K) = \sum_i W_{AB}^{\mathcal{O}_i}(K)\mathcal{O}_i. \tag{4.23}$$

Hereafter, a shorthand notation $\mathcal{O}_i \equiv \mathcal{O}_i(X = 0)$ is used. In general, the Wilson coefficient $W_{AB}^{\mathcal{O}_i}(K)$ has the form

$$W_{AB}^{\mathcal{O}_i}(K) = \frac{1}{K_1^{\Delta_{\mathcal{O}_i}+3-\Delta_A-\Delta_B}} f_{AB}^{\mathcal{O}_i}\left(\frac{K_1}{\sqrt{2mK_0}}\right), \tag{4.24}$$

where $f_{AB}^{\mathcal{O}_i}$ is a dimensionless function. Here, $\Delta_{\mathcal{O}}$ is the scaling dimension of $\mathcal{O}(X)$, which is defined so that the equal-time correlation function $\langle \mathcal{O}(0, X_1)\mathcal{O}^\dagger(0)\rangle$ with small separation X_1 behaves as $1/|X_1|^{2\Delta_{\mathcal{O}}}$. We note that, in a non-relativistic field theory, momentum has dimension 1 and energy has dimension 2 because of a parabolic dispersion relation.

Dynamic correlation functions studied in the rest of this chapter are given by the expectation values of operator products $\mathcal{G}_{AB}(K)$. Equation (4.24) shows that the large-K behavior of $\mathcal{G}_{AB}(K)$ is in general governed by Wilson coefficients of local operators with low scaling dimensions. If such Wilson coefficients are determined, OPE is available to the investigation of the

asymptotic behaviors of the coefficients for large energy K_0 and momentum K_1 in Fourier transforms. Because OPE is an operator identity, it is a natural method to derive universal relations for the correlation functions. By taking the expectation values of both sides of OPE (4.23) with respect to some state or ensemble of the system, the expression of $\langle \mathcal{G}_{AB}(K) \rangle$ for large K can be obtained. Since this expression holds for any state and ensemble, it is a universal relation.

In the case of resonantly interacting 1D systems with a scattering length a, the dimensionless function in Eq, (4.24) depends on the dimensionless coupling $1/(K_1 a)$ as well as $K_1/\sqrt{2mK_0}$. If the coefficient includes the large-K tail generated by a contact interaction, the function can be expanded at large K_1 with $K_1/\sqrt{2mK_0}$ and a fixed:

$$f_{AB}^{\mathcal{O}_i}\left(\frac{K_1}{\sqrt{2mK_0}}, \frac{1}{K_1 a}\right) = \left(\frac{1}{K_1 a}\right)^{N_{AB}^{\mathcal{O}_i}} g_{AB}^{\mathcal{O}_i}\left(\frac{K_1}{\sqrt{2mK_0}}\right) + \cdots . \tag{4.25}$$

As a result, Eq. (4.24) in the large-energy-momentum limit can be evaluated as

$$W_{AB}^{\mathcal{O}_i}(K) = \frac{1}{K_1^{\Delta_{\mathcal{O}_i}+3-\Delta_A-\Delta_B}} \left(\frac{1}{K_1 a}\right)^{N_{AB}^{\mathcal{O}_i}} g_{AB}^{\mathcal{O}_i}\left(\frac{K_1}{\sqrt{2mK_0}}\right) + \cdots . \tag{4.26}$$

This expression of $W_{AB}^{\mathcal{O}_i}(K)$ shows two essential facts: First, the large-K behavior of $W_{AB}^{\mathcal{O}_i}(K)$ is directly linked to its behavior for $1/|a| \ll 1$. Second, the exponent $N_{AB}^{\mathcal{O}_i}$ shifts the power-law decay of $W_{AB}^{\mathcal{O}_i}(K)$ at large K_1. Because the coupling constant for bosons is proportional to $-1/a$ [see Eq. (**??**)], the limit of $1/|a| \to 0$ corresponds to a non-interacting bosons. In this case, $\Delta_{\mathcal{O}}$ can be simply obtained by dimensional analysis. For example, a one-body operator defined by

$$\mathcal{O}_{a,b} \equiv \phi^\dagger (i \overleftrightarrow{\partial_t})^a (-i \overleftrightarrow{\partial_x})^b \phi \tag{4.27}$$

has $\Delta_{\mathcal{O}_{a,b}} = 2a + b + 1$ because of $\Delta_{\partial_x} = 1$, $\Delta_{\partial_t} = 2$, $\Delta_\phi = 1/2$. Because the large-K tail of $W_{AB}^{\mathcal{O}_i}(K)$ should vanish in a non-interacting theory, the exponent for bosons must be positive $N_{AB}^{\mathcal{O}_i} > 0$ and it can be determined by perturbative calculations combined with dimensional analysis. On the other hand, 1D fermions with a contact interaction is strongly interacting in the limit of $1/a \to 0$, and thus a non-perturbative treatment is necessary to determine $W_{AB}^{\mathcal{O}_i}(K)$ as shown in the next chapter.

In the rest of this chapter, we take advantage of OPE to clarify how the two-body contact density $\mathcal{C}_2 = \langle d^\dagger d \rangle$ affects dynamic correlation functions for bosons in the large-K limit. In order to determine the Wilson coefficient of $d^\dagger d$, we have to take the following local operators into account: the unit operator

$$1 \tag{4.28}$$

with $\Delta_1 = 0$, one-body operators

$$\mathcal{O}_{a,b} = \phi^\dagger (i \overleftrightarrow{\partial_t})^a (-i \overleftrightarrow{\partial_x})^b \phi \tag{4.29}$$

with $\Delta_{\mathcal{O}_{a,b}} = 2a + b + 1 \leq 4$, and a dimer density operator

$$d^\dagger d \sim \phi^\dagger \phi^\dagger \phi \phi \tag{4.30}$$

with $\Delta_{d^\dagger d} = 2$. As shown later, the other local operators makes higher-order contributions in powers of $1/K_1$ and $1/\sqrt{mK_0}$ or no contributions in a state which we are interested in.

The Wilson coefficients of above operators can be determined step by step by the following matching procedure [29].

- Step 1: Evaluate the expectation values of local operators in the right hand side of Eq. (4.23) with respect to a one-body state $|\phi_P\rangle$, which consists of one particle with a set of energy and momentum P. Note that only the unit and one-body operators have non-zero expectation values in this case.
- Step 2: Evaluate the expectation value of $\mathcal{G}_{AB}(K)$ in the left hand side of Eq. (4.23) with respect to $|\phi_P\rangle$.
- Step 3: Expand the expectation value $\langle\phi_P|\mathcal{G}_{AB}(K)|\phi_P\rangle$ in P.
- Step 4: Demand that both sides of the equation match up to order in P, to which we want to calculate the correlation function $\langle\mathcal{G}_{AB}(K)\rangle$. Finally, this matching for the one-body state determines the Wilson coefficients of the unit and one-body operators.
- Step 5: Repeat the same matching procedure for a two-body or a one-dimer state. In this case, only the unit, one-body, and two-body operators including $d^\dagger d$ survive in the right-hand side. Therefore, we can obtain the Wilson coefficient of $d^\dagger d$.

As mentioned in Section 2.2.1, the canonical ensemble average of $\mathcal{C}_2 = \langle d^\dagger d\rangle$ can be exactly computed by the Bethe ansatz. Combining this result with $W_{AB}^{d^\dagger d}(K)$ obtained by the matching procedure, we can completely determine the large-K behavior of the correlation function $\langle\mathcal{G}_{AB}(K)\rangle$ for any coupling constant and temperature.

4.2 Density correlation

In this section, we investigate the dynamic structure factor $S(K)$. We begin with a time-ordered product of the number density operators:

$$\mathcal{G}_{nn}(K) = -i\int d^2X\, e^{iK\cdot X}\mathcal{T}\left[n(X)n(0)\right] \tag{4.31}$$

with $n(X) = \phi^\dagger(X)\phi(X)$. The dynamic structure factor is given by the imaginary part of the expectation value of $\mathcal{G}_{nn}(K)$ [111]:

$$S(K) = -\frac{\mathrm{Im}[\langle\mathcal{G}_{nn}(K)\rangle]}{\pi(1+e^{-K_0/(k_BT)})}. \tag{4.32}$$

In the case of a thermal equilibrium state, $S(K)$ satisfies

$$S(K_0,K_1) = e^{K_0/(k_BT)}S(-K_0,-K_1), \tag{4.33}$$

$$S(K_0,K_1) = S(K_0,-K_1), \tag{4.34}$$

(a) (b) (c)

Figure 4.2: Diagrams for the expectations values of (a) $\langle\phi_P|1|\phi_P\rangle$, (b) $\langle\phi_P|\mathcal{O}_{a,b}|\phi_P\rangle$, and (c) $\langle\phi_P|\mathcal{G}_{nn}(K)|\phi_P\rangle$. The open dots in (b) and (c) denote operators at $X = 0$, while the filled dots in (c) the Fourier transform of $n(X)$. Energy and momentum are conserved at the filled dots.

so that we can assume $K_0 > 0$, $K_1 > 0$ without loss of generality. For large K, Eq. (4.31) can be expanded in terms of local operators:

$$\mathcal{G}_{nn}(K) = \sum_i W_{nn}^{\mathcal{O}_i}(K)\mathcal{O}_i. \tag{4.35}$$

Inserting this OPE in Eq. (4.32) yields

$$S(K) = -\frac{1}{\pi}\sum_i \mathrm{Im}\left[W_{nn}^{\mathcal{O}_i}(K)\right]\langle\mathcal{O}_i\rangle + \left(e^{-K_0/(k_BT)}\right). \tag{4.36}$$

We note that all the local operators $\mathcal{O}_i$ which we take into account are Hermitian [see Eqs. (4.28)–(4.30)], leading to real-valued $\langle\mathcal{O}_i\rangle$.

4.2.1 One-body sector

Now we determine the Wilson coefficients of the unit and one-body operators by the matching procedure mentioned in Section 4.1.1. We calculate the expectation values of both sides of Eq. (4.35) with respect to a one-body state $|\phi_P\rangle$, in which a boson has a set of energy and momentum P.

Step 1: Expectation values of local operators

The expectation values of the unit operator and one-body operators in the right hand side of Eq. (4.35) equal

$$\langle\phi_P|1|\phi_P\rangle = \langle\phi_P|\phi_P\rangle, \tag{4.37a}$$
$$\langle\phi_P|\mathcal{O}_{a,b}|\phi_P\rangle = -(P_0)^a(P_1)^b[G(P)]^2, \tag{4.37b}$$

respectively. These expectation values can be expressed in terms of Feynman diagrams as Figs 4.2(a) and 4.2(b). As a result, we obtain the expectation value of the right hand side:

$$\sum_i W_{nn}^{\mathcal{O}_i}(K)\langle\phi_P|\mathcal{O}_i|\phi_P\rangle = W_{nn}^{1}(K)\langle\phi_P|\phi_P\rangle + \sum_{a,b} W_{nn}^{\mathcal{O}_{a,b}}(K)\times(-1)(P_0)^a(P_1)^b[G(P)]^2. \tag{4.38}$$

Step 2: Expectation value of the operator product

The expectation value of the left-hand side of Eq. (4.35) is given by the diagrams in Fig. 4.2(c). The result is

$$\langle\phi_P|\mathcal{G}_{nn}(K)|\phi_P\rangle = -\left[G(K+P)+G(-K+P)\right][G(P)]^2. \tag{4.39}$$

Step 3: Expansion of $\langle\phi_P|\mathcal{G}_{nn}(K)|\phi_P\rangle$ in P

By expanding $G(\pm K+P)$ in powers of P, Eq. (4.39) reads

$$\langle\phi_P|\mathcal{G}_{nn}(K)|\phi_P\rangle = \sum_{a,b}\frac{1}{a!b!}\left(\frac{\partial^{a+b}G(K)}{\partial(K_0)^a\partial(K_1)^b}+(K\to -K)\right)(-1)(P_0)^a(P_1)^b[G(P)]^2. \tag{4.40}$$

Step 4: Matching both sides

By comparing Eq. (4.40) with Eqs. (4.38), the Wilson coefficients are determined as follows:

$$W_{nn}^{1} = 0, \tag{4.41}$$

$$W_{nn}^{\mathcal{O}_{a,b}}(K) = \frac{1}{a!b!}\frac{\partial^{a+b}G(K)}{\partial(K_0)^a\partial(K_1)^b}+(K\to -K). \tag{4.42}$$

In particular, the explicit forms of $\mathcal{O}_{a,b}$ with $\Delta_{\mathcal{O}_{a,b}}\le 4$ are

$$W_{nn}^{\mathcal{O}_{0,0}}(K) = G(K)+(K\to -K), \tag{4.43a}$$

$$W_{nn}^{\mathcal{O}_{0,1}}(K) = \frac{K_1}{m}[G(K)]^2+(K\to -K), \tag{4.43b}$$

$$W_{nn}^{\mathcal{O}_{0,2}}(K) = \frac{[G(K)]^2}{2m}+\left(\frac{K_1}{m}\right)^2[G(K)]^3+(K\to -K), \tag{4.43c}$$

$$W_{nn}^{\mathcal{O}_{0,3}}(K) = \frac{K_1}{m^2}[G(K)]^3+\left(\frac{K_1}{m}\right)^3[G(K)]^4+(K\to -K), \tag{4.43d}$$

$$W_{nn}^{\mathcal{O}_{1,0}}(K) = -[G(K)]^2+(K\to -K), \tag{4.43e}$$

$$W_{nn}^{\mathcal{O}_{1,1}}(K) = -\frac{2K_1}{m}[G(K)]^3+(K\to -K). \tag{4.43f}$$

The OPE (4.35) in the one-body sector can be expressed diagrammatically as shown in Fig. 4.4(a). Because of

$$-\frac{1}{\pi}\mathrm{Im}[G(K)] = -\frac{1}{\pi}\mathrm{Im}\left(\frac{1}{K_0-\frac{K_1^2}{2m}+i0^+}\right) = \delta\left(K_0-\frac{K_1^2}{2m}\right), \tag{4.44}$$

all the one-body operators make contributions to the large-K behavior of $S(K)$ [Eq. (4.36)] only at the single-particle peak $K_0 = K_1^2/(2m)$.

(a) (b)

Figure 4.3: (a) Diagram for the expectation value of the dimer density $\langle d^\dagger d\rangle_2$. (b) Diagram making a nontrivial contribution to $\langle \mathcal{O}_{a,b}\rangle_2$.

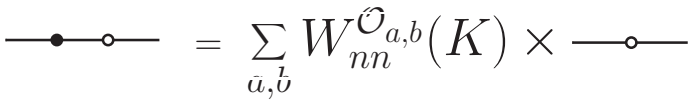

(a)

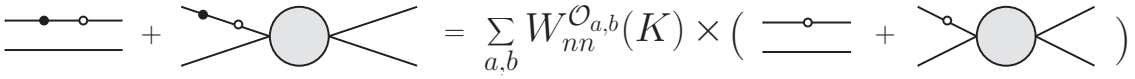

(b)

Figure 4.4: (a) Diagrammatic expression of OPE (4.35) in the one-body sector. This structure of the one-body sector is also included in OPE (4.35) in the two-body sector as shown in (b). The Wilson coefficients in Eqs. (4.41) make diagrams in both sides of (b) cancel with each other.

4.2.2 Two-body sector

To determine the Wilson coefficient of $d^\dagger d$, we calculate the expectation values of both sides of Eq. (4.35) with respect to two-body state $|\phi_{Q/2}, \phi_{Q/2}\rangle$, in which two bosons have the same energy $Q_0/2$ and momentum $Q_1/2$.

Step 1: Expectation values of local operators

First, we calculate the expectation values of local operators in the right-hand side of Eq. (4.35). The expectation value of $d^\dagger d$ is given by the diagram in Fig. 4.3(a):

$$\langle d^\dagger d\rangle_2 = \frac{4}{m^2a^2}[G(Q/2)]^4[D_B(Q)]^2 = \frac{m^2a^2}{4}[G(Q/2)]^4[A(Q)]^2, \tag{4.45}$$

where Eq. (4.20) was used and we define

$$\langle \mathcal{O}\rangle_2 \equiv \langle \phi_{Q/2}, \phi_{Q/2}|\mathcal{O}|\phi_{Q/2}, \phi_{Q/2}\rangle. \tag{4.46}$$

The Wilson coefficients $W_{nn}^{\mathcal{O}_{a,b}}(K)$ in Eq. (4.41) make some diagrams for the expectation value of the right-hand side canceled by those for the left-hand side [see Fig. 4.4(b)]. As a result, we should consider only one diagram shown in Fig. 4.3(b) to calculate the expectation values $\langle \mathcal{O}_{a,b}\rangle_2$:

$$\text{Fig. 4.3(b)} = [G(Q/2)]^4[A(Q)]^2 I_{\mathcal{O}_{a,b}}(Q), \tag{4.47}$$

where integrals corresponding to the loop in Fig. 4.3(b) are given by

$$I_{\mathcal{O}_{a,b}}(Q) = i \int \frac{d^2R}{(2\pi)^2} (Q_0 - R_0)^a (Q_1 - R_1)^b G(R)[G(Q-R)]^2. \tag{4.48}$$

The integrations can be carried out by the residue theorem, and thus their explicit forms with $\Delta_{\mathcal{O}_{a,b}} \leq 4$ are given by

$$I_{\mathcal{O}_{0,0}}(Q) = \frac{m^2}{4\beta_Q^3}, \tag{4.49a}$$

$$I_{\mathcal{O}_{0,1}}(Q) = \frac{m^2}{8\beta_Q^3} Q_1, \tag{4.49b}$$

$$I_{\mathcal{O}_{0,2}}(Q) = \frac{m^2}{4\beta_Q^3} (Q_1^2/4 + \beta_Q^2), \tag{4.49c}$$

$$I_{\mathcal{O}_{0,3}}(Q) = \frac{m^2}{32\beta_Q^3} Q_1 (Q_1^2 + 12\beta_Q^2), \tag{4.49d}$$

$$I_{\mathcal{O}_{1,0}}(Q) = \frac{m}{32\beta_Q^3} (Q_1^2 - 12\beta_Q^2), \tag{4.49e}$$

$$I_{\mathcal{O}_{1,1}}(Q) = \frac{m}{16\beta_Q^3} Q_1 \left(Q_1^2/4 - \beta_Q^2\right). \tag{4.49f}$$

For convenience, we define

$$\mathcal{N}_2 \equiv [G(Q/2)]^4 [A(Q)]^2. \tag{4.50}$$

The expectation value of the right-hand side of Eq. (4.35) divided by $\mathcal{N}_2$ is thus found to be

$$\sum_i \frac{W_{nn}^{\mathcal{O}_i}(K) \langle \mathcal{O}_i \rangle_2}{\mathcal{N}_2} = \frac{m^2 a^2}{4} W_{nn}^{d^\dagger d}(K) + \sum_{\Delta_{\mathcal{O}_{a,b}} \leq 4} W_{nn}^{\mathcal{O}_{a,b}}(K) I_{\mathcal{O}_{a,b}}(Q) + O(Q) \tag{4.51}$$

with $O(Q) \equiv O(\beta_Q) + O(Q_1)$. From Eqs. (4.43) and (4.49), the sum over $\Delta_{\mathcal{O}_{a,b}} \leq 4$ equals

$$\begin{aligned} \sum_{\Delta_{\mathcal{O}_{a,b}} \leq 4} W_{nn}^{\mathcal{O}_{a,b}}(K) I_{\mathcal{O}_{a,b}}(Q) = \frac{m^2 G(K)}{4\beta_Q^3} \Bigg[& 1 + \frac{Q_1}{2} \frac{K_1 G(K)}{m} + (Q_1^2/4 + \beta_Q^2) \left(\frac{K_1 G(K)}{m} \right)^2 \\ & + 2\beta_Q^2 \frac{G(K)}{m} + \frac{Q_1}{8} (Q_1^2 + 12\beta_Q^2) \left(\frac{K_1 G(K)}{m} \right)^3 + 2Q_1 \beta_Q^2 \frac{K_1 [G(K)]^2}{m^2} \Bigg] \\ & + (K \to -K). \end{aligned} \tag{4.52}$$

Step 2: Expectation value of the operator product

We turn to the expectation value $\langle \mathcal{G}_{nn}(K) \rangle_2$ of the left-hand side of Eq. (4.35). As mentioned above, $\langle \mathcal{G}_{nn}(K) \rangle_2$ includes diagrams which are canceled trivially by those of the right-hand

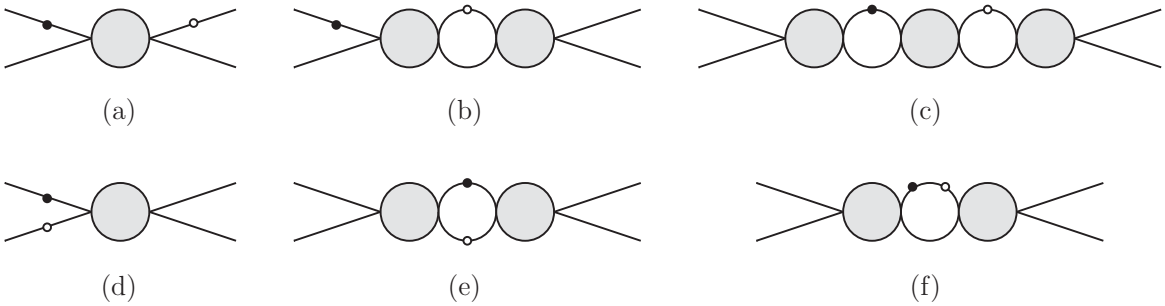

Figure 4.5: All graph topologies contributing to the expectation value $\langle \mathcal{G}_{nn}(K) \rangle_2$.

side through the result of the one-body sector [see Fig. 4.4(b)]. By neglecting these diagrams, $\langle \mathcal{G}_{nn}(K) \rangle_2$ is given by six types of diagrams in Fig. 4.5:

$$\begin{aligned} \langle \mathcal{G}_{nn}(K) \rangle_2 = \langle \mathcal{G}_{nn}(K) \rangle_{(\mathrm{a})} + \langle \mathcal{G}_{nn}(K) \rangle_{(\mathrm{b})} + \langle \mathcal{G}_{nn}(K) \rangle_{(\mathrm{c})} + \langle \mathcal{G}_{nn}(K) \rangle_{(\mathrm{d})} \\ + \langle \mathcal{G}_{nn}(K) \rangle_{(\mathrm{e})} + \langle \mathcal{G}_{nn}(K) \rangle_{(\mathrm{f})}. \end{aligned} \tag{4.53}$$

These diagrams make the following contributions:

$$\frac{\langle \mathcal{G}_{nn}(K) \rangle_{(\mathrm{a})}}{\mathcal{N}_2} = -4A(K+Q) \left(\frac{G(K+Q/2)}{A(Q)} \right)^2 + (K \to -K), \tag{4.54a}$$

$$\frac{\langle \mathcal{G}_{nn}(K) \rangle_{(\mathrm{b})}}{\mathcal{N}_2} = 4A(K+Q) \left(\frac{G(K+Q/2)}{A(Q)} \right) I_1(K,Q) + (K \to -K), \tag{4.54b}$$

$$\frac{\langle \mathcal{G}_{nn}(K) \rangle_{(\mathrm{c})}}{\mathcal{N}_2} = -A(K+Q)[I_1(K,Q)]^2 + (K \to -K), \tag{4.54c}$$

$$\frac{\langle \mathcal{G}_{nn}(K) \rangle_{(\mathrm{d})}}{\mathcal{N}_2} = -\frac{4G(K+Q/2)G(-K+Q/2)}{A(Q)}, \tag{4.54d}$$

$$\frac{\langle \mathcal{G}_{nn}(K) \rangle_{(\mathrm{e})}}{\mathcal{N}_2} = -I_2(K,Q), \tag{4.54e}$$

$$\frac{\langle \mathcal{G}_{nn}(K) \rangle_{(\mathrm{f})}}{\mathcal{N}_2} = I_3(K,Q) + (K \to -K), \tag{4.54f}$$

where integrals corresponding to loops in the Feynman diagrams are given by

$$I_1(K,Q) = i \int_R G(R)G(Q-R)G(K+Q-R), \tag{4.55a}$$

$$I_2(K,Q) = -i \int_R G(R)G(R+K)G(Q-R)G(Q-K-R), \tag{4.55b}$$

$$I_3(K,Q) = i \int_R G(R)[G(Q-R)]^2 G(Q+K-R). \tag{4.55c}$$

Analytical expressions of these integrals are shown in Appendix A.

Step 3: Expansion of $\langle \mathcal{G}_{nn}(K)\rangle_2$ in Q

Before expanding Eqs. (4.54) in Q, we define

$$\begin{aligned}\frac{\langle \mathcal{G}_{nn}(K)\rangle_{(\mathrm{a})+(\mathrm{b})+(\mathrm{c})}}{\mathcal{N}_2} &\equiv \frac{\langle \mathcal{G}_{nn}(K)\rangle_{(\mathrm{a})}}{\mathcal{N}_2} + \frac{\langle \mathcal{G}_{nn}(K)\rangle_{(\mathrm{b})}}{\mathcal{N}_2} + \frac{\langle \mathcal{G}_{nn}(K)\rangle_{(\mathrm{c})}}{\mathcal{N}_2} \\ &= -A(K+Q)\left(\frac{2}{A(Q)}G(K+Q/2) - I_1(K,Q)\right)^2 + (K\to -K), \qquad (4.56)\\ \frac{\langle \mathcal{G}_{nn}(K)\rangle_{(\mathrm{d})+(\mathrm{e})}}{\mathcal{N}_2} &\equiv \frac{\langle \mathcal{G}_{nn}(K)\rangle_{(\mathrm{d})}}{\mathcal{N}_2} + \frac{\langle \mathcal{G}_{nn}(K)\rangle_{(\mathrm{e})}}{\mathcal{N}_2} \\ &= -\frac{4G(K+Q/2)G(-K+Q/2)}{A(Q)} - I_2(K,Q). \qquad (4.57)\end{aligned}$$

As shown in Appendix A, the integrals, $I_1(K,Q)$, $I_2(K,Q)$ and $I_3(K,Q)$, can be expanded as follows [see Eqs. (A.3), (A.11), and (A.19)]:

$$I_1(K,Q) = -G(K)\left[\frac{m}{2\beta_K} + \frac{m}{2\beta_Q} + G(K)\beta_K + G(K)\frac{K_1Q_1}{4\beta_Q}\right] + O(Q), \qquad (4.58)$$

$$\begin{aligned}I_2(K,Q) = &\frac{mG(K)G(-K)}{\beta_Q}\left(1+\frac{K_1Q_1G(K)}{2m}\right)\left(1-\frac{K_1Q_1G(-K)}{2m}\right)\\ &+\frac{m[G(K)]^2}{2\beta_K} + \frac{m[G(-K)]^2}{2\beta_{-K}} + O(Q), \qquad (4.59)\end{aligned}$$

$$\begin{aligned}I_3(K,Q) + (K\to -K) = &\left[\left(K_1^2\beta_K - \frac{(mK_0)^2}{\beta_K}\right)\frac{[G(K)]^4}{2m} + (K\to -K)\right]\\ &+\sum_{\Delta_{\mathcal{O}_{a,b}}\le 4} W_{nn}^{\mathcal{O}_{a,b}}(K) I_{\mathcal{O}_{a,b}}(Q) + O(Q), \qquad (4.60)\end{aligned}$$

where the sum in the last line coincides with Eq. (4.52). Using these expressions combined with

$$\frac{2}{A(Q)} + \frac{m}{2\beta_Q} = \frac{ma}{2}, \qquad (4.61)$$

we can expand Eqs. (4.56), (4.57) and (4.54f) as

$$\frac{\langle \mathcal{G}_{nn}(K)\rangle_{(\mathrm{a})+(\mathrm{b})+(\mathrm{c})}}{\mathcal{N}_2} = -A(K)[G(K)]^2\left(\frac{ma}{2} + \frac{m}{2\beta_K} + G(K)\beta_K\right)^2 + (K\to -K) + O(Q), \qquad (4.62)$$

$$\frac{\langle \mathcal{G}_{nn}(K)\rangle_{(\mathrm{d})+(\mathrm{e})}}{\mathcal{N}_2} = \frac{m^2a}{K_1^2}G(K) - \frac{m[G(K)]^2}{2\beta_K} + (K\to -K) + O(Q), \qquad (4.63)$$

$$\frac{\langle \mathcal{G}_{nn}(K)\rangle_{(\mathrm{f})}}{\mathcal{N}_2} = \left[\left(K_1^2\beta_K - \frac{(mK_0)^2}{\beta_K}\right)\frac{[G(K)]^4}{2m} + (K\to -K)\right]$$

$$+\sum_{\Delta_{\mathcal{O}_{a,b}}\le 4} W_{nn}^{\mathcal{O}_{a,b}}(K) I_{\mathcal{O}_{a,b}}(Q) + O(Q), \tag{4.64}$$

respectively. Summing up Eqs. (4.62)–(4.64), we can obtain the expansion of $\langle \mathcal{G}_{nn}(K)\rangle_2$ with respect to Q:

$$\begin{aligned}
\frac{\langle \mathcal{G}_{nn}(K)\rangle_2}{\mathcal{N}_2} &= \Bigg[-A(K)[G(K)]^2 \left(\frac{ma}{2} + \frac{m}{2\beta_K} + G(K)\beta_K\right)^2 + \frac{m^2 a}{K_1^2} G(K) - \frac{m[G(K)]^2}{2\beta_K} \\
&\quad + \left(K_1^2\beta_K - \frac{(mK_0)^2}{\beta_K}\right)\frac{[G(K)]^4}{2m} + (K \to -K)\Bigg] \\
&\quad + \sum_{\Delta_{\mathcal{O}_{a,b}}\le 4} W_{nn}^{\mathcal{O}_{a,b}}(K) I_{\mathcal{O}_{a,b}}(Q) + O(Q) \\
&= \frac{m^3 a}{4}\left[\frac{1}{1-a\beta_K}\left(\frac{K_1 G(K)}{m}\right)^4 + \frac{4}{K_1^2}\frac{G(K)}{m} - 4\left(\frac{G(K)}{m}\right)^2 + (K \to -K)\right] \\
&\quad + \sum_{\Delta_{\mathcal{O}_{a,b}}\le 4} W_{nn}^{\mathcal{O}_{a,b}}(K) I_{\mathcal{O}_{a,b}}(Q) + O(Q).
\end{aligned} \tag{4.65}$$

Step 4: Matching both sides

In order to determine the Wilson coefficient of $d^\dagger d$, we compare the expectation values of both sides of the OPE (4.35). As shown in Eq. (4.51), the right hand side is evaluated as

$$\sum_i \frac{W_{nn}^{\mathcal{O}_i}(K)\langle \mathcal{O}_i\rangle_2}{\mathcal{N}_2} = \frac{m^2 a^2}{4} W_{nn}^{d^\dagger d}(K) + \sum_{\Delta_{\mathcal{O}_{a,b}}\le 4} W_{nn}^{\mathcal{O}_{a,b}}(K) I_{\mathcal{O}_{a,b}}(Q) + O(Q), \tag{4.66}$$

while the left hand side as Eq. (4.65). As a result, $W_{nn}^{d^\dagger d}(K)$ is found to be

$$W_{nn}^{d^\dagger d}(K) = \frac{m}{a}\left[\frac{1}{1-a\beta_K}\left(\frac{K_1 G(K)}{m}\right)^4 + \frac{4}{K_1^2}\frac{G(K)}{m} - 4\left(\frac{G(K)}{m}\right)^2\right] + (K \to -K). \tag{4.67}$$

4.2.3 Dynamic structure factor in the large-K limit

We now evaluate the high-energy-momentum behavior of $S(K)$ [Eq. 4.36] away from the single-particle peak. Since there is no contribution from the one-body operators to $S(K)$ for $K \neq K_1^2/(2m)$ as shown in Section 4.2.1, the imaginary part of $W_{nn}^{d^\dagger d}(K)$ dominates $S(K)$ in the large-K limit:

$$S(K) = -\frac{1}{\pi}\mathrm{Im}\left[W_{nn}^{d^\dagger d}(K)\right]\mathcal{C}_2 + O\left(K^{-7}\right) \tag{4.68}$$

with $\mathcal{C}_2 = \langle d^\dagger d\rangle$. The order of corrections can be estimated as follows: First, we focus on two-body operators $d^\dagger(i\overleftrightarrow{\partial_t})^a(-i\overleftrightarrow{\partial_x})^b d$ with scaling dimensions $\Delta = 2+2a+b$. The expectation value of the operator $d^\dagger(-i\overleftrightarrow{\partial_x})d$ with odd parity vanishes for a thermal equilibrium state. Therefore, the Wilson coefficients of $d^\dagger(i\overleftrightarrow{\partial_t})d$ and $d^\dagger(-i\overleftrightarrow{\partial_x})^2 d$ provide next-to-leading terms in Eq. (4.68).

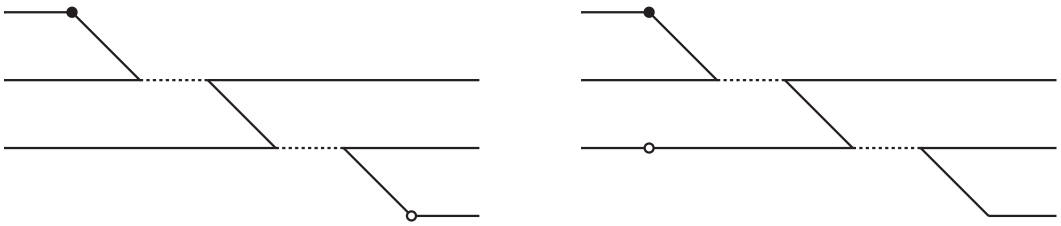

Figure 4.6: All graph topologies of diagrams contributing to the Wilson coefficient $W_{nn}^{\phi^{\dagger 3}\phi^3}(K)$ to leading order in K^{-1}. We note that the doted line denotes $iD_B^{(0)} = -ma$ and the boson-dimer vertex is $2i/(ma)$.

Because their scaling dimensions are higher than that of $d^\dagger d$ by 2, the corrections from these operators are found to be $O(K^{-7})$. On the other hand, the corrections from three- and higher-body operators can be evaluated in the perturbation theory. For instance, the Wilson coefficient of $\phi^{\dagger 3}\phi^3$ for large K is dominated by diagrams depicted in Fig. 4.6:

$$W_{nn}^{\phi^{\dagger 3}\phi^3}(K) = \frac{4}{m^2 a^2}\Big([G(K)]^3 + 4[G(K)]^2 G(-K) + (K \to -K)\Big) + O(K^{-7}). \tag{4.69}$$

However, the leading terms are real for $K_0 \neq K_1^2/(2m)$, and thus we can obtain $\mathrm{Im}[W_{nn}^{\phi^{\dagger 3}\phi^3}] = O(K^{-7})$. Similarly, Wilson coefficients of all the three- and higher-body operators are found to make contributions of the order of $O(K^{-7})$.

Since K_0 is assumed to be positive, the imaginary part of $W_{nn}^{d^\dagger d}(K)$ in Eq. (4.67) for $K_0 \neq K_1^2/(2m)$ reads

$$-\frac{1}{\pi}\mathrm{Im}\left[W_{nn}^{d^\dagger d}(K)\right] = \Theta(mK_0 - K_1^2/4) \times \frac{m}{\pi}\frac{\sqrt{mK_0 - K_1^2/4}}{1 + a^2(mK_0 - K_1^2/4)}\left(\frac{K_1 G(K)}{m}\right)^4. \tag{4.70}$$

The Heaviside step function $\Theta(mK_0 - K_1^2/4)$ represents the two-particle threshold, which is also pointed out in the 2D and 3D cases [115, 116]. The inequality $K_0 > K_1^2/(4m)$ follows from the fact that, in order to excite two particles with center-of-mass momentum K_1, the energy K_0 is required to be larger than their center-of-mass energy $K_1^2/(4m)$.

Substituting Eq. (4.70) into Eq. (4.68), we can obtain the large-K behavior of $S(K)$ above the two-particle threshold:

$$S(K) = \frac{m\mathcal{C}_2}{\pi}\frac{\sqrt{mK_0 - K_1^2/4}}{1 + a^2(mK_0 - K_1^2/4)}\left(\frac{K_1}{mK_0 - K_1^2/2}\right)^4 + O(K^{-7}). \tag{4.71}$$

This behavior holds when $\sqrt{mK_0}$ and K_1 are much larger than n, $1/|a|$, and $\sqrt{mk_BT}$. As mentioned in Section 2.2.1, the two-body contact density can be exactly calculated for arbitrary coupling strength and temperature by the Bethe ansatz method. Substituting this exact result of $\mathcal{C}_2$ into Eq. (4.71), we can completely determine the large-K behavior of $S(K)$ for any coupling strength and temperature.

In the end of this section, we prove that, with a and T fixed, the Bose-Fermi correspondence makes $S(K)$ for bosons identical to that for fermions with a contact interaction. By using a complete set of energy eigenstates $|\mu\rangle$ with number of particles N, the Lehmann representation of $S(K)$ defined by Eq. (4.32) can be obtained:

$$S(K) = \frac{1}{L}\sum_{\lambda,\mu}\frac{e^{-E_\lambda/(k_BT)}}{\mathcal{Z}}|\langle\lambda|\tilde{n}(K_1)|\mu\rangle|^2\delta(K_0+E_\lambda-E_\mu), \tag{4.72}$$

where L is the system size, E_μ is the energy of the state $|\mu\rangle$, and $\tilde{n}(K_1)$ is the Fourier transform of $n(0,x)$. The matrix element of $\tilde{n}(K_1)$ can be rewritten in terms of wave functions as follows:

$$\langle\lambda|\tilde{n}(K_1)|\mu\rangle = N\int dx_1\cdots dx_N\, e^{-iK_1x_1}\Psi^*_{B,\lambda}(x_1,\cdots,x_N)\Psi_{B,\mu}(x_1,\cdots,x_N), \tag{4.73}$$

where $\Psi_{B,\mu}(x_1,\cdots,x_N)$ is a wave function corresponding to $|\mu\rangle$. Because of the Bose-Fermi correspondence, a fermionic wave function corresponding to $\Psi_{B,\mu}$ is given by

$$\Psi_{F,\mu}(x_1,\cdots,x_N) = \prod_{1\le i<j\le N}\mathrm{sgn}(x_{ij})\Psi_{B,\mu}(x_1,\cdots,x_N), \tag{4.74}$$

leading to

$$\Psi^*_{F,\lambda}(x_1,\cdots,x_N)\Psi_{F,\mu}(x_1,\cdots,x_N) = \Psi^*_{B,\lambda}(x_1,\cdots,x_N)\Psi_{B,\mu}(x_1,\cdots,x_N). \tag{4.75}$$

Furthermore, $\Psi_{F,\mu}$ and $\Psi_{B,\mu}$ have the same energy E_μ. Consequently, the dynamic structure factor in Eq. (4.72) is found to be identical between bosons and fermions, and our result in Eq. (4.71) holds for fermions.

4.3 Current correlation

In this section, we study the large-K behavior of the current correlation function defined by

$$\mathcal{A}_j(K) = -\frac{\mathrm{Im}[\langle\mathcal{G}_{jj}(K)\rangle]}{\pi(1+e^{-K_0/(k_BT)})}, \tag{4.76}$$

where $j(X) = -i\phi^\dagger\overleftrightarrow{\partial_x}\phi(X)/m$ is a current operator and

$$\mathcal{G}_{jj}(K) = -i\int d^2X\, e^{iK\cdot X}\mathcal{T}\left[j(X)j(0)\right]. \tag{4.77}$$

Because of the U(1) symmetry of the system, $\mathcal{A}_j(K)$ is closely related to the dynamic structure factor $S(K)$ [116]. The U(1) symmetry gives the continuity equation for the number density and current operators:

$$\partial_t n(X) + \partial_x j(X) = 0. \tag{4.78}$$

Performing the Fourier transform and evaluating the matrix elements with respect to energy eigenstates $\langle\lambda|$ and $|\mu\rangle$ yields

$$\langle\lambda|\tilde{j}(K_1)|\mu\rangle = \frac{E_\mu - E_\lambda}{K_1}\langle\lambda|\tilde{n}(K_1)|\mu\rangle, \tag{4.79}$$

where $\tilde{j}(K_1)$ and $\tilde{n}(K_1)$ are the Fourier transforms of $j(0, X_1)$ and $n(0, X_1)$, respectively, and E_λ is the energy of $|\lambda\rangle$. The Lehmann representations of $\mathcal{A}_j(K)$ and $S(K)$ are

$$\mathcal{A}_j(K) = \frac{1}{L}\sum_{\lambda,\mu}\frac{e^{-E_\lambda/(k_BT)}}{\mathcal{Z}}|\langle\lambda|\tilde{j}(K_1)|\mu\rangle|^2\delta(K_0 + E_\lambda - E_\mu), \tag{4.80}$$

$$S(K) = \frac{1}{L}\sum_{\lambda,\mu}\frac{e^{-E_\lambda/(k_BT)}}{\mathcal{Z}}|\langle\lambda|\tilde{n}(K_1)|\mu\rangle|^2\delta(K_0 + E_\lambda - E_\mu), \tag{4.81}$$

respectively. Therefore, Eqs. (4.79)–(4.81) lead to a simple relation between $\mathcal{A}_j(K)$ and $S(K)$:

$$\mathcal{A}_j(K) = \left(\frac{K_0}{K_1}\right)^2 S(K). \tag{4.82}$$

From this relation, we can see that the Bose-Fermi correspondence makes $\mathcal{A}_j(K)$ identical between 1D bosons and fermions as well as $S(K)$. By substituting Eq. (4.71) into Eq. (4.82), the large-K behavior of $\mathcal{A}_j(K)$ above the two-particle threshold, $K_0 > K_1^2/(4m)$, is obtained as follows:

$$\mathcal{A}_j(K) = \frac{m\mathcal{C}_2}{\pi}\frac{\sqrt{mK_0 - K_1^2/4}}{1 + a^2(mK_0 - K_1^2/4)}\frac{K_0^2K_1^2}{(mK_0 - K_1^2/2)^4} + O(K^{-5}). \tag{4.83}$$

4.4 Single-particle correlation

This section is devoted to investigating the single-particle properties at large energy and momentum in thermal equilibrium. The single-particle Green function is defined as the canonical ensemble average of the following time-ordered operator product:

$$\mathcal{G}_{\phi\phi^\dagger}(K) = -i\int d^2X\, e^{iK\cdot X}\mathcal{T}\left[\phi(X)\phi^\dagger(0)\right]. \tag{4.84}$$

Its imaginary part provides the single-particle spectral density

$$\mathcal{A}_B(K) = -\frac{1}{\pi}\mathrm{Im}[\langle\mathcal{G}_{\phi\phi^\dagger}(K)\rangle]. \tag{4.85}$$

For large K, the operator product in Eq. (4.84) can be expressed in terms of local operators:

$$\mathcal{G}_{\phi\phi^\dagger}(K) = \sum_i W^{\mathcal{O}_i}_{\phi\phi^\dagger}(K)\mathcal{O}_i. \tag{4.86}$$

We determine Wilson coefficients up to the order of $O(K^{-6})$ because of $W^{d^\dagger d}_{\phi\phi^\dagger}(K) = O(K^{-6})$ as shown later.

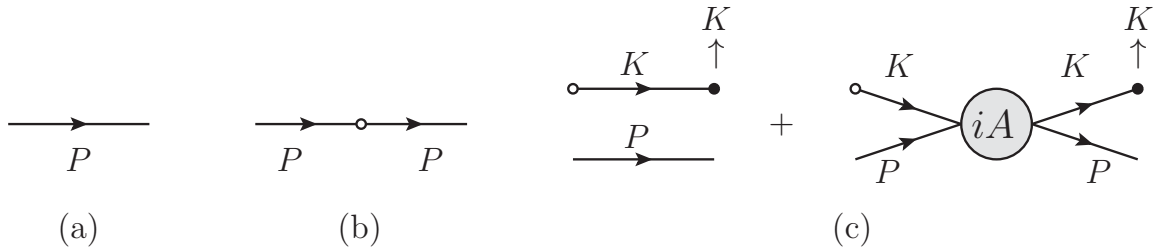

Figure 4.7: Diagrams contributing to (a) $\langle\phi_P|1|\phi_P\rangle$, (b) $\langle\phi_P|\mathcal{O}_{a,b}|\phi_P\rangle$, and (c) $\langle\phi_P|\mathcal{G}_{\phi\phi^\dagger}(K)|\phi_P\rangle$. In (b) and (c), operators at $X = 0$ are denoted by the open dots, while the Fourier transform of $\phi(X)$ by the filled dots. Energy and momentum are conserved at the filled dots.

4.4.1 One-body sector

To determine the Wilson coefficients by the matching procedure, we first take the expectation values of both sides of the OPE (4.86) with respect to a one-boson state $|\phi_P\rangle$.

Step 1: Expectation values of local operators

The expectation values of the unit operator and one-body operators in the right hand side of Eq. (4.86) are

$$\langle\phi_P|1|\phi_P\rangle = \langle\phi_P|\phi_P\rangle, \qquad \langle\phi_P|\mathcal{O}_{a,b}|\phi_P\rangle = -(P_0)^a(P_1)^b[G(P)]^2. \tag{4.87}$$

These expectation values can be expressed in terms of Feynman diagrams as Fig. 4.7(a) and (b). The expectation value of the right hand side thus reads

$$\sum_i W^{\mathcal{O}_i}_{\phi\phi^\dagger}(K)\langle\phi_P|\mathcal{O}_i|\phi_P\rangle = W^1_{\phi\phi^\dagger}(K)\langle\phi_P|\phi_P\rangle - \sum_{a,b} W^{\mathcal{O}_{a,b}}_{\phi\phi^\dagger}(K)\,(P_0)^a(P_1)^b[G(P)]^2. \tag{4.88}$$

Step 2: Expectation value of the operator product

The expectation value of the left-hand side depicted in Fig. 4.7(c) is given by

$$\langle\phi_P|\mathcal{G}_{\phi\phi^\dagger}(K)|\phi_P\rangle = \langle\phi_P|\phi_P\rangle G(K) + [G(P)]^2 A(K+P)[G(K)]^2. \tag{4.89}$$

Step 3: Expansion of $\langle\phi_P|\mathcal{G}_{\phi\phi^\dagger}(K)|\phi_P\rangle$ in P

By expanding $A(K+P)$ in powers of P, Eq. (4.89) reads

$$\langle\phi_P|\mathcal{G}_{\phi\phi^\dagger}(K)|\phi_P\rangle = G(K)\,\langle\phi_P|\phi_P\rangle + \sum_{a,b}\frac{1}{a!b!}\frac{\partial^{a+b}A(K)}{\partial(K_0)^a\partial(K_1)^b}[G(K)]^2(P_0)^1(P_1)^b[G(P)]^2. \tag{4.90}$$

Step 4: Matching both sides

By comparing Eq. (4.88) with Eqs. (4.90), the Wilson coefficients are determined as follows:

$$W^{1}_{\phi\phi^\dagger}(K) = G(K), \tag{4.91}$$

$$W^{\mathcal{O}_{a,b}}_{\phi\phi^\dagger}(K) = -\frac{1}{a!b!}\frac{\partial^{a+b}A(K)}{\partial(K_0)^a\partial(K_1)^b}[G(K)]^2. \tag{4.92}$$

Unlike $W^{\mathcal{O}_{a,b}}_{nn}(K)$ in Eq. (4.42) for the density correlation, $W^{\mathcal{O}_{a,b}}_{\phi\phi^\dagger}(K)$ is affected by the interaction through $A(K)$. As a result, the imaginary part of $W^{\mathcal{O}_{a,b}}_{\phi\phi^\dagger}(K)$ survives away from the single-particle peak, $K_0 \neq K_1^2/(2m)$. The orders of the Wilson coefficients for 1, $\mathcal{O}_{0,0} = \phi^\dagger\phi$, and $\mathcal{O}_{0,1} = \phi^\dagger(-i\overleftrightarrow{\partial_x})\phi$ are found to be

$$W^{1}_{\phi\phi^\dagger}(K) = O(K^{-2}), \tag{4.93}$$

$$W^{\mathcal{O}_{0,0}}_{\phi\phi^\dagger}(K) = O(K^{-4}), \tag{4.94}$$

$$W^{\mathcal{O}_{0,1}}_{\phi\phi^\dagger}(K) = O(K^{-6}), \tag{4.95}$$

respectively, while those for the other one-body operators are negligible within our accuracy.

4.4.2 Two-body sector

Next, consider the expectation values of both sides of OPE (4.86) with respect to a dimer state $|d_Q\rangle$, in which a dimer have a set of energy and momentum $Q = (Q_0, Q_1)$.

Step 1: Expectation values of local operators

The expectation values of local operators in the right hand side of Eq. (4.86) can be expressed in terms of Feynman diagrams as Figs. 4.8(a), (b) and (c), and they are evaluated as

$$\langle d_Q|1|d_Q\rangle = \langle d_Q|d_Q\rangle, \tag{4.96a}$$

$$\langle d_Q|d^\dagger d|d_Q\rangle = -[D_B(Q)]^2, \tag{4.96b}$$

$$\langle d_Q|\mathcal{O}_{a,b}|d_Q\rangle = -\frac{4}{m^2a^2}[D_B(Q)]^2 I_{\mathcal{O}_{a,b}}(Q), \tag{4.96c}$$

where $I_{\mathcal{O}_{a,b}}$ is defined by Eq (4.48). The expectation value of the right hand side thus reads

$$\begin{aligned}\sum_i W^{\mathcal{O}_i}_{\phi\phi^\dagger}(K)\,\langle d_Q|\mathcal{O}_i|d_Q\rangle &= G(K)\,\langle d_Q|d_Q\rangle - [D_B(Q)]^2 W^{d^\dagger d}_{\phi\phi^\dagger}(K) \\ &\quad - [D_B(Q)]^2\left(\frac{4}{m^2a^2}\sum_{\Delta_{\mathcal{O}_{a,b}}\leq 4} W^{\mathcal{O}_{a,b}}_{\phi\phi^\dagger}(K)\lim_{Q\to 0} I_{\mathcal{O}_{a,b}}(Q) + O(Q)\right),\end{aligned} \tag{4.97}$$

where $W^{1}_{\phi\phi^\dagger}(K) = G(K)$ was used. We note that the integrals $I_{\mathcal{O}_{a,b}}(Q)$ corresponding to the loops in Fig. 4.8 (c) are divergent in the limit of $Q \to 0$. These divergences are canceled by that in the left hand side.

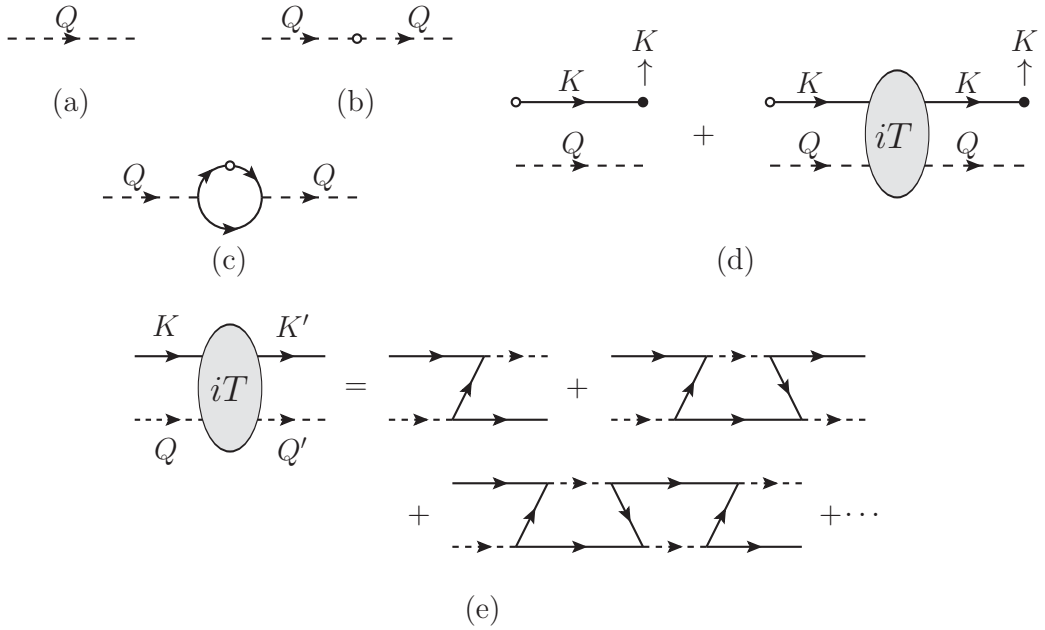

Figure 4.8: Diagrams contributing to (a) $\langle d_Q|1|d_Q\rangle$, (b) $\langle d_Q|d^\dagger d|d_Q\rangle$, (c) $\langle d_Q|\mathcal{O}_{a,b}|d_Q\rangle$, and (d) $\langle d_Q|\mathcal{G}_{\phi\phi^\dagger}(K)|d_Q\rangle$. (e) Boson-dimer scattering amplitude $iT(K,Q;K',Q')$.

Step 2: Expectation value of the operator product

The expectation value of the left-hand side of Eq. (4.86) is given by the diagrams in Fig. 4.8(d), and it is evaluated as

$$\langle d_Q|\mathcal{G}_{\phi\phi^\dagger}(K)|d_Q\rangle = G(K)\langle d_Q|d_Q\rangle + [D_B(Q)]^2[G(K)]^2 T(K,Q;K,Q), \tag{4.98}$$

where the boson-dimer scattering amplitude $T(K',Q';K,Q)$. As shown in Fig. 4.8(e), the amplitude can be expanded as follows:

$$T(K,Q;K',Q') = \sum_{n=0}^{\infty} T^{(n)}(K,Q;K',Q'), \tag{4.99}$$

where n is the number of loops in a Feynman diagram and the n-th term is given by the recurrence relations

$$T^{(0)}(K,Q;K',Q') = -\frac{4}{m^2a^2}G(Q'-K), \tag{4.100a}$$

$$T^{(n)}(K,Q;K',Q') = \frac{4i}{m^2a^2}\int_R T^{(n-1)}(K,Q;R,K+Q-R)G(R)G(Q'-R) \times D_B(K+Q-R). \tag{4.100b}$$

Step 3: Expansion of $\langle d_Q|\mathcal{G}_{\phi\phi^\dagger}(K)|d_Q\rangle$ in Q

Equation (4.98) can be expanded in Q as follows:

$$\langle d_Q|\mathcal{G}_{\phi\phi^\dagger}(K)|d_Q\rangle = G(K)\langle d_Q|d_Q\rangle + [D_B(Q)]^2[G(K)]^2\left[\lim_{Q\to 0} T(K,Q;K,Q) + O(Q)\right]. \quad (4.101)$$

From Eqs. (4.100), we can see that $\lim_{Q\to 0} T(K,Q;K,Q)$ has divergences coming from the loops in Fig 4.8 (e), which are canceled by those of the right hand side.

Step 4: Matching both sides

Comparing Eq. (4.97) with Eq. (4.101), the Wilson coefficient $W^{d^\dagger d}_{\phi\phi^\dagger}(K)$ is provided by

$$W^{d^\dagger d}_{\phi\phi^\dagger}(K) = -[G(K)]^2 T^{\rm reg}(K,0;K,0), \quad (4.102)$$

where the regularized amplitude is defined as

$$T^{\rm reg}(K,Q;K,Q) \equiv T(K,Q;K,Q) + \frac{4}{m^2a^2}\sum_{\Delta_{\mathcal{O}_{a,b}}\le 4}\frac{W^{\mathcal{O}_{a,b}}_{\phi\phi^\dagger}(K)}{[G(K)]^2} I_{\mathcal{O}_{a,b}}(Q) \quad (4.103)$$

and this is convergent at $Q=0$.

We now determine $W^{d^\dagger d}_{\phi\phi^\dagger}(K)$ to leading order in $1/K$. As mentioned in Section 4.1.1, the perturbation theory combined with dimensional analysis is available to compute Wilson coefficients for large K. By recalling

$$A(K) = -\frac{4}{m^2a^2}D_B(K) = \frac{4}{m}\frac{1}{a-1/\beta_K} = O(a^{-1}) \quad (4.104)$$

and

$$\frac{W^{\mathcal{O}_{a,b}}_{\phi\phi^\dagger}(K)}{[G(K)]^2} = -\frac{1}{a!b!}\frac{\partial^{a+b}A(K)}{\partial(K_0)^a\partial(K_1)^b}, \quad (4.105)$$

the sum in Eq. (4.103) is estimated as

$$\frac{4}{m^2a^2}\sum_{\Delta_{\mathcal{O}_{a,b}}\le 4}\frac{W^{\mathcal{O}_{a,b}}_{\phi\phi^\dagger}(K)}{[G(K)]^2} I_{\mathcal{O}_{a,b}}(Q) = O(a^{-3}). \quad (4.106)$$

On the other hand, Eqs. (4.100) lead to $T^{(n)}(K,Q;K',Q') = O(a^{-(n+2)})$. Therefore, Eq. (4.103) at $Q=0$ is evaluated as

$$\begin{aligned} T^{\rm reg}(K,0;K,0) &= T^{(0)}(K,0;K,0) + O(a^{-3}) \\ &= -\frac{4G(-K)}{m^2a^2} + O(a^{-3}). \end{aligned} \quad (4.107)$$

Because $T^{\rm reg}(K,0;K,0)$ has dimensions 0, dimensional analysis shows that the corrections in this equation have the order of $O(K^{-3})$. Consequently, $W^{d^\dagger d}_{\phi\phi^\dagger}(K)$ to leading order is obtained:

$$W^{d^\dagger d}_{\phi\phi^\dagger}(K) = \frac{4G(-K)}{m^2a^2}[G(K)]^2 + O(K^{-7}). \quad (4.108)$$

4.4.3 Single-particle properties at high energy

We turn to study the single-particle properties of 1D bosons in the large-K limit. In a similar way as in the OPE of $\mathcal{G}_{nn}(K)$, the perturbative theory allows us to see that only the Wilson coefficients of the local operators

$$1, \quad \mathcal{O}_{0,0} = \phi^\dagger \phi, \quad \mathcal{O}_{0,1} = \phi^\dagger (-i \overleftrightarrow{\partial_x}) \phi, \quad d^\dagger d \tag{4.109}$$

are dominant within our accuracy. By evaluating the canonical ensemble average of the OPE (4.86), the single-particle Green function for large K reads

$$\langle \mathcal{G}_{\phi\phi^\dagger}(K) \rangle = \sum_i W^{\mathcal{O}_i}_{\phi\phi^\dagger}(K) \langle \mathcal{O}_i \rangle. \tag{4.110}$$

Because the current density of the thermal equilibrium state $\langle \phi^\dagger (-i \overleftrightarrow{\partial_x}) \phi \rangle$ is zero, we obtain

$$\langle \mathcal{G}_{\phi\phi^\dagger}(K) \rangle = G_K + W^{\mathcal{O}_{0,0}}_{\phi\phi^\dagger}(K)\, n + W^{d^\dagger d}_{\phi\phi^\dagger}(K)\, \mathcal{C}_2 + O(K^{-7}) \tag{4.111}$$

with $n = \langle \phi^\dagger \phi \rangle = \langle \mathcal{O}_{0,0} \rangle$ and $\mathcal{C}_2 = \langle d^\dagger d \rangle$. The self-energy $\Sigma(K)$ defined by

$$\langle \mathcal{G}_{\phi\phi^\dagger}(K) \rangle = \frac{1}{K_0 - \frac{K_1^2}{2m} - \Sigma(K)} \tag{4.112}$$

is written as

$$\Sigma(K) = \frac{W^{\mathcal{O}_{0,0}}_{\phi\phi^\dagger}(K)}{[G(K)]^2} n + \frac{W^{d^\dagger d}_{\phi\phi^\dagger}(K)}{[G(K)]^2} \mathcal{C}_2 + O(K^{-3}). \tag{4.113}$$

By using Eq. (4.108) and

$$\frac{W^{\mathcal{O}_{0,0}}_{\phi\phi^\dagger}(K)}{[G(K)]^2} = -\frac{4}{ma} \left(1 + \frac{1}{a\beta_K} + \frac{1}{(a\beta_K)^2} \right) + O(K^{-3}), \tag{4.114}$$

the analytic form of $\Sigma(K)$ up to $O(K^{-2})$ is found to be

$$\Sigma(K) = -\frac{4n}{ma} \left(1 + \frac{1}{a\beta_K} + \frac{1}{(a\beta_K)^2} \right) + \frac{4\mathcal{C}_2\, G(-K)}{m^2 a^2} + O(K^{-3}). \tag{4.115}$$

The pole of the single-particle Green function gives the quasiparticle energy $E(K_1)$ and scattering rate $\Gamma(K_1)$:

$$E(K_1) = \mathrm{Re}[K_0^{(\mathrm{pole})}], \qquad \Gamma(K_1) = -2\mathrm{Im}[K_0^{(\mathrm{pole})}], \tag{4.116}$$

where the pole solves the following equation:

$$K_0^{(\mathrm{pole})} = \frac{K_1^2}{2m} + \Sigma(K_0^{(\mathrm{pole})}, K_1). \tag{4.117}$$

Expanding $K_0^{(\mathrm{pole})}$ in both sides with respect to $1/|K_1|$ as

$$K_0^{(\mathrm{pole})} = \frac{K_1^2}{2m} + \delta K_0 = \frac{K_1^2}{2m} + \sum_{n=0}^{\infty} \epsilon_{1-n} |K_1|^{1-n}, \tag{4.118}$$

we obtain

$$\begin{aligned} \delta K_0 &= \Sigma\left(\frac{K_1^2}{2m}, K_1\right) + O(K_1^{-3}). \\ &= -\frac{4n}{ma}\left(1 + \frac{2i}{a|K_1|} - \frac{4}{a^2 K_1^2}\right) - \frac{4\mathcal{C}_2}{ma^2 K_1^2} + O(K^{-3}). \end{aligned} \tag{4.119}$$

As a result, the quasiparticle energy and scattering rate in the high-energy regime are found to be

$$E(K_1) = \frac{K_1^2}{2m}\left[1 + 4\gamma\left(\frac{n}{K_1}\right)^2 - 2\gamma^2\left(2\gamma + \frac{\mathcal{C}_2}{n^2}\right)\left(\frac{n}{K_1}\right)^4 + O(K_1^{-5})\right], \tag{4.120}$$

$$\Gamma(K_1) = \frac{K_1^2}{2m}\left[8\gamma^2\left(\frac{n}{|K_1|}\right)^3 + O(K^{-5})\right], \tag{4.121}$$

where $\gamma = -2/(na)$ is a dimensionless coupling. We note that the quasi-particle residue $Z(K_1)$ within our accuracy is

$$Z^{-1} = 1 - \frac{\partial}{\partial K_0}\mathrm{Re}[\Sigma(K)]\Big|_{K_0 = K^2/(2m)} = 1 + O(K^{-3}). \tag{4.122}$$

The single-particle spectral density near the peak, $K_0 \approx K_0^{(\mathrm{pole})}$, takes the form

$$\mathcal{A}_B(K) \simeq \frac{1}{2\pi}\frac{\Gamma(K_1)}{[K_0 - E(K_1)]^2 + [\frac{1}{2}\Gamma(K_1)]^2}. \tag{4.123}$$

Finally, we compute the large K-behavior of $\mathcal{A}_B(K)$ away from the single-particle peak $K_0 \neq K_0^{(\mathrm{pole})}$. By substituting Eq. (4.111) into Eq. (4.85), $\mathcal{A}_B(K)$ can be expanded as

$$\mathcal{A}_B(K) = -\frac{1}{\pi}\mathrm{Im}\left[W_{\phi\phi^\dagger}^{\mathcal{O}_{0,0}}(K)\right] n - \frac{1}{\pi}\mathrm{Im}\left[W_{\phi\phi^\dagger}^{d^\dagger d}(K)\right] \mathcal{C}_2 + O(K^{-7}). \tag{4.124}$$

By evaluating the imaginary part of $W_{\phi\phi^\dagger}^{\mathcal{O}_{0,0}}(K)$ in Eq. (4.92), it is found to vanish below the two-particle threshold:

$$-\frac{1}{\pi}\mathrm{Im}\left[W_{\phi\phi^\dagger}^{\mathcal{O}_{0,0}}(K)\right] = \Theta(mK_0 - K_1^2/4) \times \frac{4m}{\pi}\frac{\sqrt{mK_0 - K_1^2/4}}{[1 + a^2(mK_0 - K_1^2/4)](mK_0 - K_1^2/2)^2}. \tag{4.125}$$

On the other hand, Eq. (4.108) shows that the leading term of $W_{\phi\phi^\dagger}^{d^\dagger d}(K)$ in the order of $O(K^{-6})$ is real away from the single-particle peak. As a result, we obtain the following asymptotic behavior of $\mathcal{A}_B(K)$ for $K_0 > K_1^2/(4m)$:

$$\mathcal{A}_B(K) = \frac{4mn\sqrt{mK_0 - K_1^2/4}}{\pi[1 + a^2(mK_0 - K_1^2/4)](mK_0 - K_1^2/2)^2} + O(K^{-7}). \tag{4.126}$$

We note that, unlike $S(K)$ and $\mathcal{A}_j(K)$, the single-particle spectral density is in general different between bosons and fermions. We will demonstrate this difference by investigating the OPE for fermions in the next chapter.

4.5 Summary

In this chapter, the large-energy-momentum behaviors of dynamic correlation functions in 1D bosons were studied by OPE. Above the two-particle threshold, the dynamic structure factor [Eq. (4.71)] and the current correlation function [Eq. (4.83)] are dominated by the contributions from the two-body contact density. These results hold for 1D fermions because of the Bose-Fermi correspondence and are measurable in ultracold atoms experiments through Bragg spectroscopy [108] or Fourier sampling of time-of-flight images [109].

We also computed OPE for the single-particle Green function. We determined the high-energy behaviors of the quasiparticle energy and the scattering rate near the single-particle peak [Eqs. (4.120) and (4.121)]. In addition, the single-particle spectral density away from the two-particle threshold [Eq. (4.126)] was found to be dominated by the number density in the large-energy-momentum limit.

As mentioned in Section 2.2.1, the two-body contact density can be exactly calculated for arbitrary coupling strength and temperature by the Bethe ansatz method. Combining this exact result of $\mathcal{C}_2$ with our results, we can completely determine the large-energy-momentum behaviors of the dynamic correlation functions for any coupling strength and temperature.

Chapter 5

Dynamic correlation functions for fermions

This chapter is devoted to the study of a quantum field theory for 1D fermions which is studied in Chapter 3 in a first-quantized formalism. As shown in Section 2.1.1, these 1D fermions should correspond to 1D bosons in Chapters 3 and 4 via the Bose-Fermi mapping. We first construct the quantum field theory for fermions in Section 5.1. In Section 5.1.1, we use the momentum shell renormalization group method to renormalize a coupling constant. In order to confirm that this renormalized theory is consistent with the first-quantized formalism in Chapter 3, we solve the three-body problem (Section 5.1.2) and rederive the energy relation (Section 5.1.3). In particular, we clarify why the three-body contact appears in the energy relation from the viewpoint of the renormalization group. In Section 5.2, OPE is applied to the constructed field theory in order to study the single-particle properties of fermions in the high-energy regime. Throughout this chapter, a system is assumed to be homogeneous, i.e., without a trapping potential.

5.1 Quantum field theory of fermions with contact interactions

In this section, we study a quantum field theory for spinless fermions with contact interactions, whose Lagrangian density is given by

$$\begin{aligned}\mathcal{L}_F = \psi^\dagger \left(i\partial_t + \frac{\partial_x^2}{2m} \right) \psi - \frac{1}{2mv_2} \varphi^\dagger \varphi \\ + \frac{1}{2m} \left[\varphi^\dagger \left(\psi (-i \overleftrightarrow{\partial_x}) \psi \right) + \left(\psi^\dagger (-i \overleftrightarrow{\partial_x}) \psi^\dagger \right) \varphi \right] + \frac{v_3}{m} \psi^\dagger \varphi^\dagger \varphi \psi. \end{aligned} \tag{5.1}$$

Here, ψ is a fermionic field and φ is an auxiliary bosonic field representing the degrees of freedom of a dimer. The coupling constant v_2 characterizes the coupling between two fermions that approach each other. In fact, when we focus on a two-fermion problem, we can neglect the last term in $\mathcal{L}_F$ and carry out the path integrals over φ and $\varphi^\dagger$, leading to the Lagrangian

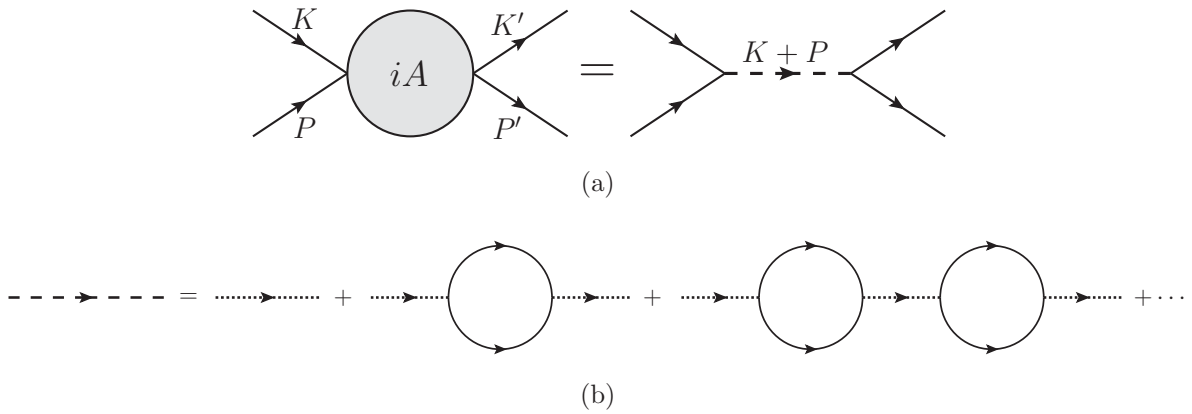

Figure 5.1: Feynman diagrams for (a) the two-body scattering amplitude $iA(K, P; K', P')$ and for (b) the full dimer propagator $iD_F(Q)$. The solid, dotted, and dashed lines indicate $iG(K)$, $iD_F^{(0)}$, and $iD_F(Q)$, respectively. The fermion-dimer vertex is i/m multiplied by the relative momentum of two fermions.

density in Eq. (2.31):

$$\mathcal{L}'_F = \psi^\dagger \left(i\partial_t + \frac{\partial_x^2}{2m} \right) \psi + \frac{v_2}{2m} \left| \psi \partial_x \psi \right|^2 . \tag{5.2}$$

On the other hand, the last term in Eq. (5.1) represents the coupling between a fermion and a dimer, which corresponds to a three-body coupling for fermions. Such a coupling does not appear in the Lagrangian density for bosons (4.13). This difference results from whether the quantum field theory for the zero-range model is required to be regularized or not. The field theory of bosons in the previous chapter is well defined without a regularization. On the other hand, we have to regularize the fermionic theory (5.1) by making v_2 and v_3 dependent on the ultraviolet cutoff scale Λ so that physical quantities at low energy become independent of Λ. Because we are considering the zero-range model describing the low-energy universal properties of fermions interacting via a short-range pairwise potential, the fermion-dimer coupling constant v_3 characterizing the three-fermion coupling vanishes at the ultraviolet scale Λ.

In order to renormalize v_2, we calculate the two-body scattering amplitude $iA(K, P; K', P')$ of two fermions, where K and P (K' and P') are sets of energy and momentum of incoming (outgoing) fermions. The energy and momentum conservation laws provide $K + P = K' + P'$. Figure 5.1(a) shows that $A(K, P; K', P')$ is related to the full propagator of a dimer $iD_F(Q)$ as follows:

$$A(K, P; K', P') = -\frac{1}{m^2} \frac{K_1 - P_1}{2} \frac{K'_1 - P'_1}{2} D_F(Q), \tag{5.3}$$

where $Q \equiv K + P$ denotes the set of the total energy Q_0 and the center-of-mass momentum Q_1.

The full propagator $iD_F(Q)$ is obtained by summing up all the bubble diagrams in Fig. 5.1(b):

$$\begin{aligned} iD_F(Q) &= iD_F^{(0)} + iD_F^{(0)}\Pi_F(Q)D_F^{(0)} + iD_F^{(0)}\left[\Pi_F(Q)D_F^{(0)}\right]^2 + \cdots \\ &= \frac{i}{1/D_F^{(0)} - \Pi_F(Q)}, \end{aligned} \tag{5.4}$$

where $D_F^{(0)} = -2mv_2$ is the bear propagator of a dimer. The dimer self-energy is given by

$$\Pi_F(Q) = \frac{i}{2m^2}\int_{-\infty}^{\infty}\frac{dR_0}{2\pi}\int_{-\Lambda}^{\Lambda}\frac{dR_1}{2\pi}\,G(Q/2+R)G(Q/2-R)R_1^2 \tag{5.5}$$

with the fermion propagator

$$G(K) = \frac{1}{K_0 - K_1^2/(2m) + i0^+}. \tag{5.6}$$

The integration in $\Pi_F(Q)$ can be performed as follows:

$$\begin{aligned} \Pi_F(Q) &= \frac{1}{2m^2}\int_{-\Lambda}^{\Lambda}\frac{dR_1}{2\pi}\frac{-mR_1^2}{R_1^2+\beta_Q^2} \\ &= -\frac{1}{2m}\left(\frac{\Lambda}{\pi} - \frac{\beta_Q}{2}\right), \end{aligned} \tag{5.7}$$

where $\beta_Q = \sqrt{Q_1^2/4 - mQ_0 - i0^+}$. We note that the momentum scale β_Q, which we are interested in, is much smaller than the cut off Λ. Substituting this into Eq. (5.4) yields

$$D_F(Q) = \frac{4m}{1/a - \beta_Q}, \tag{5.8}$$

where the scattering length a is defined by

$$\frac{1}{v_2} = \frac{\Lambda}{\pi} - \frac{1}{2a}. \tag{5.9}$$

This equation provides the dependence of v_2 on the ultraviolet scale Λ.

A pole of the scattering amplitude $A(K,P;K',P')$ in Eq. (5.3) provides the energy of a two-body bound state. Equation (5.3) shows that a pole of $A(K,P;K',P')$ is equivalent to that of $D_F(Q)$. We can find the bound state with binding energy $B_2 = |Q_0| = 1/(ma^2)$, which is consistent with the binding energy of Eq. (2.76) mentioned in Section 2.2.2.

5.1.1 Renormalization group analysis of v_3

To renormalize the fermion-dimer coupling v_3, we follow the momentum shell renormalization group method. We evaluate the variation of v_3 after integrating out the field operators in the partition function over the high momentum shell $\Lambda e^{-ds} < |Q_1| < \Lambda$. Hereafter, we adopt a shorthand

$$\int_Q' \equiv \int_{-\infty}^{\infty}\frac{dQ_0}{2\pi}\int_{\Lambda e^{-ds}<|Q_1|<\Lambda}\frac{dQ_1}{2\pi}. \tag{5.10}$$

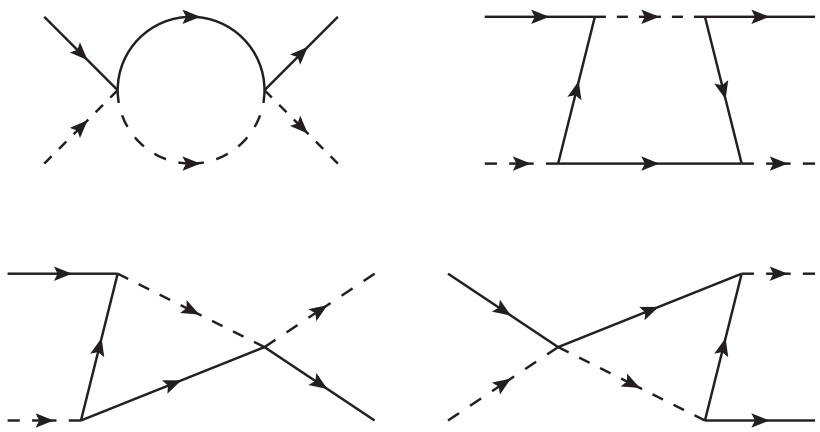

Figure 5.2: Diagrams renormalizing the coupling constant v_3. All the external energies and momenta can be set zero. The vertex at which a fermion (solid line) and a dimer (dashed line) collide with each other is iv_3/m.

There are three types of diagrams contributing to the variation of the coupling (see Fig. 5.2):

$$\frac{i\,dv_3}{m} = A_{\rm bub} + A_{\rm tri} + A_{\rm box}, \tag{5.11}$$

where contributions coming from a bubble diagram, two triangle diagrams, and a box diagram are provided by

$$A_{\rm bub} = \left(\frac{v_3}{m}\right)^2 \int_Q' G(-Q)D_F(Q) = \frac{8i}{\pi\sqrt{3}m} v_3^2 ds, \tag{5.12}$$

$$A_{\rm tri} = \frac{v_3}{m^3} \times 2 \int_Q' G(-Q)D_F(Q)G(Q)\frac{Q_1^2}{2} = -\frac{8i}{\sqrt{3}\pi m} v_3 ds, \tag{5.13}$$

$$A_{\rm box} = \frac{1}{m^4} \int_Q' G(-Q)D_F(Q)\left[G(Q)\frac{Q_1^2}{2}\right]^2 = \frac{2i}{\sqrt{3}\pi m} ds, \tag{5.14}$$

respectively. We thus obtain the renormalization group equation

$$\frac{dv_3}{ds} = \frac{8}{\sqrt{3}\pi}(v_3 - 1/2)^2, \tag{5.15}$$

which is solved by

$$v_3(s) = \frac{1}{2} + \left(\frac{1}{v_3(0) - 1/2} - \frac{8s}{\sqrt{3}\pi}\right)^{-1}. \tag{5.16}$$

As mentioned above, the fermion-dimer coupling must vanish at the ultraviolet scale, i.e., $v_3(0) = 0$. Therefore, the coupling flows into a non-zero value in the infrared limit $s \to \infty$:

$$v_3(s \to \infty) = \frac{1}{2}. \tag{5.17}$$

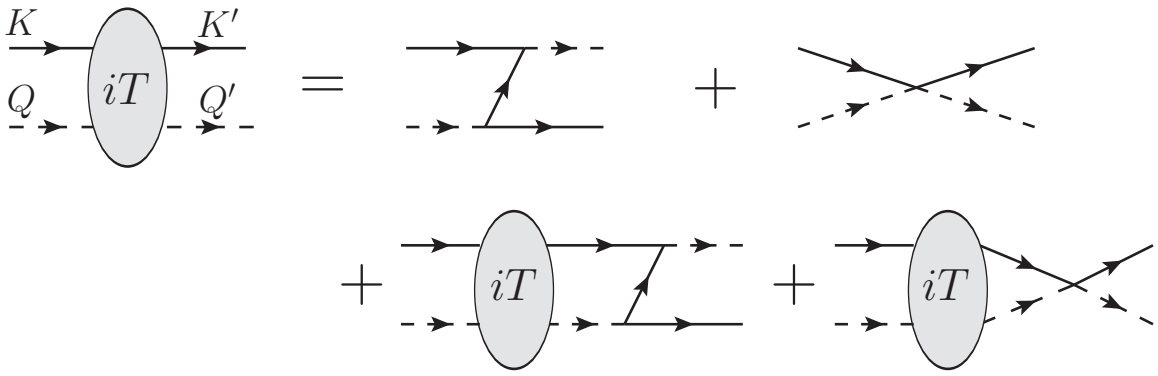

Figure 5.3: STM equation for the fermion-dimer scattering amplitude.

This means that, in the framework of local quantum field theory, the three-body coupling for fermions emerges at low energy scale even though the microscopic theory includes no three-body interaction. In Sections 5.1.2 and 5.1.3, we demonstrate that the fermionic quantum field theory constructed here is consistent with the first-quantized theory studied in Chapter 3.

5.1.2 Three-body bound state

We now study a three-fermion bound state and confirm its consistency with the prediction from the Bose-Fermi correspondence. We begin with a scattering problem for three fermions by using the method reviewed in Ref. [19]. The scattering of three fermions is equivalent to that between a fermion and a dimer. Therefore, we calculate the fermion-dimer scattering amplitude.

We assume that the incoming fermion and dimer have sets of energy and momentum, K and Q, respectively, and the outgoing fermion and dimer have K' and Q', respectively. The fermion-dimer scattering amplitude $iT(K,Q;K',Q')$ solves the Skornyakov–Ter-Martirosyan (STM) equation [see Fig. 5.3]:

$$\begin{aligned} mT(K,Q;K',Q') = \mathcal{M}(K,Q,K') - i\int_R T(K,Q;R,K+Q-R)G(R) \\ \times D(K+Q-R)\mathcal{M}(K',Q',R) \end{aligned} \tag{5.18}$$

where the inhomogeneous term is given by

$$\mathcal{M}(K,Q,K') = \frac{Q_1 - 2K_1'}{2}\frac{Q_1 - K_1 - K_1'}{2}\frac{G(Q-K')}{m} + v_3. \tag{5.19}$$

Note that the energy and momentum conservation laws provide $K + Q = K' + Q'$. Using Eq. (5.18), we can expand the amplitude as

$$T(K,Q;K',Q') = \sum_{n=0}^{\infty} T^{(n)}(K,Q;K',Q'), \tag{5.20}$$

where

$$mT^{(0)}(K,Q;K',Q') = \mathcal{M}(K,Q,K'), \tag{5.21}$$

$$mT^{(n)}(K,Q;K',Q') = -i\int_R T^{(n-1)}(K,Q;R,K+Q-R)G(R) \times D(K+Q-R)\mathcal{M}(K',Q',R). \tag{5.22}$$

The functions $D(K+Q-R)$ and $\mathcal{M}(K',Q',R)$ are analytic in the lower half plane in R_0. By using Eq. (5.22) iteratively, $T^{(n)}(K,Q;K',Q')$ for any n is also found to be analytic in the lower half plane. As a result, the integrand in Eq. (5.18) has only one pole $R_0 = R_1^2/(2m) - i0^+$ in the lower half plane in R_0, and Eq. (5.18) reads

$$mT(K,Q;K',Q') = \mathcal{M}(K,Q,K') - \int \frac{dR_1}{2\pi}\, T(K,Q;R,K+Q-R)D(K+Q-R)\mathcal{M}(K',Q',R)\Big|_{R_0=\frac{R_1^2}{2m}}. \tag{5.23}$$

Taking the center-of-mass frame and taking incoming and outgoing fermions on shell, we have

$$K = \left(\frac{k^2}{2m}, k\right), \quad Q = \left(E - \frac{k^2}{2m}, -k\right),$$
$$K' = \left(\frac{k'^2}{2m}, k'\right), \quad Q' = \left(E - \frac{k'^2}{2m}, -k'\right),$$

where E is the total energy, and k and k' are the incoming and outgoing relative momenta, respectively. The on-shell amplitude $T(K,Q;K',Q') = T(k,k',E)$ thus solves

$$mT(k,k',E) = \mathcal{M}(k,k',E) + \int dq\, \mathcal{K}(q,k',E)mT(k,q,E), \tag{5.24}$$

where the inhomogeneous term and the integral kernel reduce to

$$\mathcal{M}(k,k',E) = \frac{1}{4}\frac{-3kk' - 2mE}{k^2 + kk' + k'^2 - (mE + i0^+)} + v_3 - \frac{1}{2}, \tag{5.25}$$

$$\mathcal{K}(q,k',E) = \frac{2}{\pi}\frac{\mathcal{M}(q,k',E)}{\sqrt{\frac{3q^2}{4} - mE - i0^+} - 1/a}, \tag{5.26}$$

respectively.

If there is a three-body bound state with energy $E = -\kappa^2/m < 0$, the amplitude in the limit of $E \to -\kappa^2/m$ takes the following form [19]:

$$T(k,k',E) \to \frac{Z^*(k)Z(k')}{E + \kappa^2/m}. \tag{5.27}$$

Comparing the residues of both sides of Eq. (5.24) with respect to $E = -\kappa^2/m$, we find that κ is determined by solving the homogeneous integral equation

$$Z(k') = \int dq\, \mathcal{K}\left(q, k', -\frac{\kappa^2}{m}\right) Z(q). \tag{5.28}$$

By introducing a new function $z(q) = \frac{Z(q)}{\sqrt{\frac{3}{4}q^2+\kappa^2}-1/a}$, this reads

$$\left(1 - \frac{1}{a\sqrt{\frac{3}{4}k'^2+\kappa^2}}\right) z(k') = \frac{2}{\pi\sqrt{\frac{3}{4}k'^2+\kappa^2}} \int dq\, \mathcal{M}\left(q, k', -\frac{\kappa^2}{m}\right) z(q). \tag{5.29}$$

This equation has one solution $\kappa = 2/a$ and $z(k') = 1/[(k'a/2)^2+1]$ only when $a > 0$. The binding energy $B = \kappa^2/m = 4/(ma^2)$ is the same as that of a three-boson bound state in Eq. (2.76), which is consistent with the prediction from the Bose-Fermi correspondence in Section 2.2.2.

5.1.3 Rederivation of the energy relation

We now evaluate the canonical ensemble average of the Hamiltonian to reproduce the energy relation [Eq. (3.48)] for homogeneous systems ($E_{\rm trap} = 0$) within a quantum field theory framework. The Hamiltonian density operator of the system is given by

$$\begin{aligned}\mathcal{H}_F &= i\psi^\dagger\partial_0\psi - \mathcal{L}_F \\ &= \frac{|\partial_x\psi|^2}{2m} + \frac{1}{2mv_2}\varphi^\dagger\varphi - \frac{1}{2m}\left[\varphi^\dagger\left(\psi(-i\overleftrightarrow{\partial_x})\psi\right) + \left(\psi^\dagger(-i\overleftrightarrow{\partial_x})\psi^\dagger\varphi\right)\right] - \frac{v_3}{m}\psi^\dagger\varphi^\dagger\varphi\psi. \end{aligned}\tag{5.30}$$

By using the Euler-Lagrange equation for $\varphi^\dagger$,

$$\frac{1}{2mv_2}\varphi - \frac{1}{2m}\psi(-i\overleftrightarrow{\partial_x})\psi - \frac{v_3}{m}\psi^\dagger\varphi\psi = 0, \tag{5.31}$$

the canonical ensemble average of the Hamiltonian reads

$$E = \int dX_1 \langle\mathcal{H}_F\rangle = \int dX_1 \left[\frac{\langle|\partial_x\psi|^2\rangle}{2m} - \frac{1}{2mv_2}\langle\varphi^\dagger\varphi\rangle + \frac{v_3}{m}\langle\psi^\dagger\varphi^\dagger\varphi\psi\rangle\right]. \tag{5.32}$$

Substituting the running couplings (5.9) and (5.17) into this, we obtain

$$\begin{aligned} E &= \int dX_1 \left[\frac{\langle|\partial_x\psi|^2\rangle}{2m} - \frac{1}{2m}\left(\frac{\Lambda}{\pi} - \frac{1}{2a}\right)\langle\varphi^\dagger\varphi\rangle + \frac{1}{2m}\langle\psi^\dagger\varphi^\dagger\varphi\psi\rangle\right] \\ &= \lim_{\Lambda\to\infty}\int_{-\Lambda}^{\Lambda}\frac{dk}{2\pi}\frac{k^2}{2m}\left(\rho_F(k) - \frac{1}{k^2}\int dX_1\,\langle\varphi^\dagger\varphi\rangle\right) + \frac{1}{4ma}\int dX_1\,\langle\varphi^\dagger\varphi\rangle \\ &\quad + \frac{1}{2m}\int dX_1\,\langle\psi^\dagger\varphi^\dagger\varphi\psi\rangle, \end{aligned}\tag{5.33}$$

where the momentum distribution is expressed in terms of the field operators as

$$\rho_F(k) = L\int dX_1\, e^{-ikX_1}\langle\psi^\dagger(X)\psi(0)\rangle \tag{5.34}$$

with L being the system size.

As we will show in the next section, the following equal-time OPEs in coordinate space hold:

$$n(X)n(X_0, Y_1) = \frac{1}{4}\varphi^\dagger\varphi(X) + O(X_1 - Y_1), \tag{5.35}$$

$$\varphi^\dagger\varphi(X)n(X_0, Y_1) = \psi^\dagger\varphi^\dagger\varphi\psi(X) + O(X_1 - Y_1), \tag{5.36}$$

where the abbreviation $AB(X) \equiv A(X)B(X)$ is used hereafter. The two- and three-body contacts are thus written as

$$C_2 \equiv \int dX_1 \lim_{Y_1 \to X_1} \langle n(X) n(X_0, Y_1) \rangle = \frac{1}{4} \int dX_1 \, \langle \varphi^\dagger \varphi(X) \rangle, \tag{5.37a}$$

$$\begin{aligned} C_3 &\equiv \int dX_1 \lim_{Y_1, Z_1 \to X_1} \langle n(X) n(X_0, Y_1) n(X_0, Z_1) \rangle \\ &= \frac{1}{4} \int dX_1 \lim_{Z_1 \to X_1} \langle \varphi^\dagger \varphi(X) n(X_0, Z_1) \rangle \\ &= \frac{1}{4} \int dX_1 \, \langle \psi^\dagger \varphi^\dagger \varphi \psi(X) \rangle, \end{aligned} \tag{5.37b}$$

respectively. Therefore, Eq. (5.33) combined with Eqs. (5.37) reproduces the energy relation in Eq. (3.48) without a trapping potential:

$$E = \lim_{\Lambda \to \infty} \int_{-\Lambda}^{\Lambda} \frac{dk}{2\pi} \frac{k^2}{2m} \left(\rho(k) - \frac{4C_2}{k^2} \right) + \frac{C_2}{ma} + \frac{2C_3}{m}. \tag{5.38}$$

In the above derivation of the energy relation within the field theoretical formalism, we can see that the emergence of the three-body coupling at low energy scale [Eq. (5.17)] leads to the appearance of C_3 in the energy relation (5.38).

5.1.4 Equal-time OPE

In order to derive Eqs. (5.35) and (5.36), we calculate the Wilson coefficients in OPEs:

$$n(X) n(X_0, Y_1) = \sum_i \bar{W}^{\mathcal{O}_i}_{n,n}(X_1 - Y_1) \mathcal{O}_i(X), \tag{5.39}$$

$$\varphi^\dagger \varphi(X) n(X_0, Y_1) = \sum_i \bar{W}^{\mathcal{O}_i}_{\varphi^\dagger \varphi, n}(X_1 - Y_1) \mathcal{O}_i(X). \tag{5.40}$$

From dimensional analysis, the Wilson coefficient has the form

$$\bar{W}^{\mathcal{O}_i}_{AB}(X_1 - Y_1) = (X_1 - Y_1)^{\Delta_{O_i} - \Delta_A - \Delta_B} f\left(\frac{X_1 - Y_1}{a} \right), \tag{5.41}$$

where $\Delta_{\mathcal{O}}$ is a scaling dimension of an operator $\mathcal{O}(X)$. The scaling dimensions of the field operators ψ and φ are $\Delta_\psi = 1/2$ and $\Delta_\varphi = 1$, respectively.

We first turn to Eq. (5.39). Because all the matrix elements of $n(X)n(X_0, Y_1)$ in the one-fermion sector vanish, the Wilson coefficient of the unit and one-body operators are found to be zero. We then evaluate expectation values with respect to a dimer state $|\varphi_K\rangle$, in which a dimer has a set of energy and momentum K.

Step 1: Expectation values of local operators

The expectation value of a local operator $\varphi^\dagger \varphi(X)$ with $\Delta_{\varphi^\dagger \varphi} = 2$ equals

$$\langle \varphi_K | \varphi^\dagger \varphi(X) | \varphi_K \rangle = -[D_F(K)]^2, \tag{5.42}$$

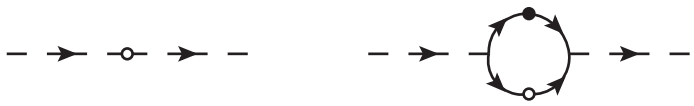

(a) (b)

Figure 5.4: Diagrams for the expectation values of (a) the local operator $\varphi^\dagger\varphi(X)$ and (b) the operator product $n(X)n(X_0,Y_1)$ with respect to a fermion-dimer state. The open dots denote operators at X, while the filled dot indicates the operator $n(X_0,Y_1)$

while those of the other local operators are $O(X_1-Y_1)$. As a result, the right hand side of Eq. (5.39) can be expanded as

$$\sum_i \bar{W}^{\mathcal{O}_i}_{n,n}(X_1-Y_1)\langle\varphi_K|\mathcal{O}_i(X)|\varphi_K\rangle = -\bar{W}^{\varphi^\dagger\varphi}_{n,n}(X_1-Y_1)\,[D_F(K)]^2 + O(X_1-Y_1). \tag{5.43}$$

Step 2: Expectation value of the operator product

The expectation value of $n(X)n(X_0,Y_1)$ depicted in Fig. 5.4(b) equals

$$\begin{aligned}\langle\varphi_K|n(X)n(X_0,Y_1)|\varphi_K\rangle &= \frac{[D_F(K)]^2}{m^2}\int_R R_1 G\left(\frac{K}{2}+R\right)G\left(\frac{K}{2}-R\right)e^{iR_1(X_1-Y_1)} \\ &\quad\times\int_{R'} R_1' G\left(\frac{K}{2}+R'\right)G\left(\frac{K}{2}-R'\right)e^{-iR_1'(X_1-Y_1)} \\ &= -[D_F(K)]^2\int\frac{dR_1}{2\pi}\frac{R_1 e^{iR_1\cdot(X_1-Y_1)}}{R_1^2+\beta_K^2}\int\frac{dR_1'}{2\pi}\frac{R_1' e^{-iR_1'\cdot(X_1-Y_1)}}{(R_1')^2+\beta_K^2} \\ &= -\frac{[D_F(K)]^2}{4}\times e^{-2|X_1-Y_1|\sqrt{K_1^2/4-m(K_0+i0^+)}}.\end{aligned} \tag{5.44}$$

Step 3: Expansion of $\langle\varphi_K|n(X)n(X_0,Y_1)|\varphi_K\rangle$ in X_1-Y_1

Equation (5.44) can be expanded as

$$\langle\varphi_K|n(X)n(X_0,Y_1)|\varphi_K\rangle = -\frac{[D_F(K)]^2}{4} + O(X_1-Y_1). \tag{5.45}$$

Step 4: Matching both sides

By comparing Eq. (5.45) with Eqs. (5.43), the Wilson coefficient of $\varphi^\dagger\varphi$ is found to be $\bar{W}^{\varphi^\dagger\varphi}_{n,n}(X_1-Y_1)=1/4$, leading to Eq. (5.35).

Next, we turn to Eq. (5.40). Because the expectation value of $\varphi^\dagger\varphi(X)n(X_0,Y_1)$ vanishes when a given state has only one fermion or one dimer, the Wilson coefficients of the unit, one-fermion, and one-dimer operators equal zero. We then focus on a fermion-dimer state $|\psi_K\varphi_Q\rangle$, in which K and Q are sets of energy and momentum of the fermion and dimer, respectively.

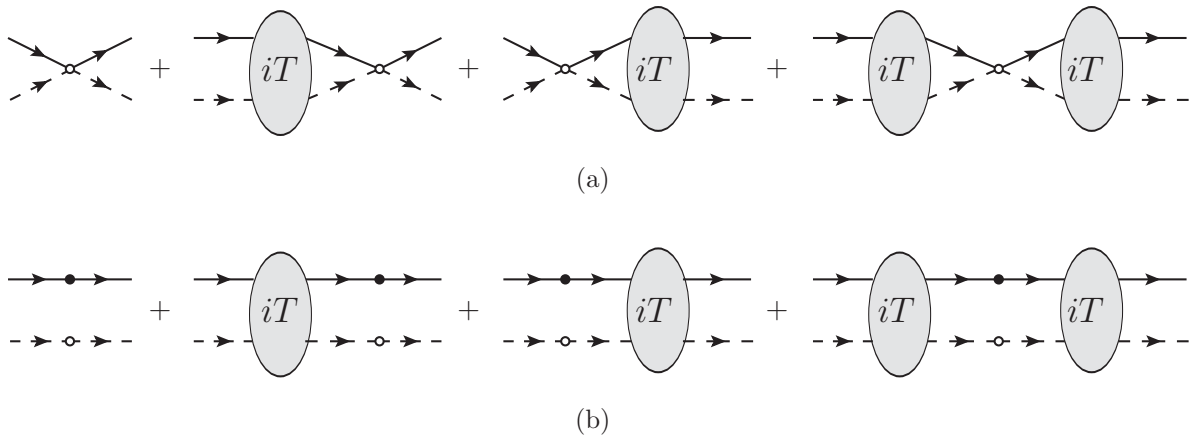

(a)

(b)

Figure 5.5: Diagrams contributing to the expectation values of (a) the local operator $\psi^\dagger\varphi^\dagger\varphi\psi(X)$ and (b) the operator product $\varphi^\dagger\varphi(X)n(X_0,Y_1)$ with respect to $|\psi_P\varphi_K\rangle$.

Step 1: Expectation values of local operators

The expectation value of the local operator $\psi^\dagger\varphi^\dagger\varphi\psi(X)$ with $\Delta_{\psi^\dagger\varphi^\dagger\varphi\psi}=3$ is given by diagrams in Fig. 5.5(a), and it is provided by

$$\begin{aligned}
&\langle\psi_K\varphi_Q|\psi^\dagger\varphi^\dagger\varphi\psi(X)|\psi_K\varphi_Q\rangle \\
&= [G(K)D_F(Q)]^2\left[1-i\int_R T(K,Q;R,K+Q-R)G(R)D(K+Q-R)\right] \\
&\quad\times\left[1-i\int_{R'} T(R',K+Q-R';K,Q)G(R')D(K+Q-R')\right],
\end{aligned} \tag{5.46}$$

while those of the other local operators are $O(X_1-Y_1)$. As a result, the expectation value of the right hand side of Eq. (5.40) can be evaluated as

$$\begin{aligned}
&\sum_i \bar{W}^{\mathcal{O}_i}_{\varphi^\dagger\varphi,n}(X_1-Y_1)\langle\psi_K\varphi_Q|\mathcal{O}_i(X)|\psi_K\varphi_Q\rangle \\
&= \bar{W}^{\psi^\dagger\varphi^\dagger\varphi\psi}_{\varphi^\dagger\varphi,n}(X_1-Y_1)\,\langle\psi_K\varphi_Q|\psi^\dagger\varphi^\dagger\varphi\psi(X)|\psi_K\varphi_Q\rangle + O(X_1-Y_1).
\end{aligned} \tag{5.47}$$

Step 2: Expectation value of the operator product

The expectation value of the left-hand side of Eq. (5.40) is given by the diagrams in Fig. 5.5(b):

$$\begin{aligned}
&\langle\psi_P\varphi_K|\varphi^\dagger\varphi(X)n(X_0,Y_1)|\psi_P\varphi_K\rangle \\
&= [G(K)D_F(Q)]^2 \\
&\quad\times\left[1-i\int_R T(K,Q;R,K+Q-R)G(R)D(K+Q-R)e^{i(R_1-K_1)(X_1-Y_1)}\right] \\
&\quad\times\left[1-i\int_{R'} T(R',K+Q-R';K,Q)G(R')D(K+Q-R')e^{-i(R'_1-K_1)(X_1-Y_1)}\right].
\end{aligned} \tag{5.48}$$

Step 3: Expansion of $\langle\psi_P\varphi_K|\varphi^\dagger\varphi(X)n(X_0,Y_1)|\psi_P\varphi_K\rangle$ in X_1-Y_1

Expanding Eq (5.48), we can see that its leading term coincides with Eq. (5.47):

$$\langle\psi_P\varphi_K|\varphi^\dagger\varphi(X)n(X_0,Y_1)|\psi_P\varphi_K\rangle = \langle\psi_K\varphi_Q|\psi^\dagger\varphi^\dagger\varphi\psi(X)|\psi_K\varphi_Q\rangle + O(X_1-Y_1). \tag{5.49}$$

Step 4: Matching both sides

By comparing Eq. (5.49) with Eqs. (5.47), the Wilson coefficient of $\psi^\dagger\varphi^\dagger\varphi\psi$ is found to be unity, leading to Eq. (5.36).

5.2 Single-particle correlation

This section is devoted to investigating the single-particle properties at large energy and momentum in thermal equilibrium. The single-particle Green function is defined as the canonical ensemble average of the following time-ordered operator product:

$$\mathcal{G}_{\psi\psi^\dagger}(K) = -i\int d^2X\, e^{iK\cdot X}\mathcal{T}\left[\psi(X)\psi^\dagger(0)\right]. \tag{5.50}$$

Its imaginary part provides the single-particle spectral density

$$\mathcal{A}_F(K) = -\frac{1}{\pi}\mathrm{Im}[\langle\mathcal{G}_{\psi\psi^\dagger}(K)\rangle]. \tag{5.51}$$

For large K, the operator product in Eq. (5.50) can be expressed in terms of local operators:

$$\mathcal{G}_{\psi\psi^\dagger}(K) = \sum_i W^{\mathcal{O}_i}_{\psi\psi^\dagger}(K)\mathcal{O}_i. \tag{5.52}$$

By recalling $\Delta_\psi = 1/2$ and $\Delta_\varphi = 1$, the local operators with scaling dimensions $\Delta_\mathcal{O} \leq 2$ are found as follows: the unit operator

$$1 \tag{5.53}$$

with $\Delta_\mathcal{O} = 0$, the number density operator

$$\psi^\dagger\psi \tag{5.54}$$

with $\Delta_\mathcal{O} = 1$, and the current density and dimer density operators

$$\psi^\dagger(-i\overleftrightarrow{\partial_x})\psi, \quad \varphi^\dagger\varphi \tag{5.55}$$

with $\Delta_\mathcal{O} = 2$. In the bosonic case in Section 4.4, Wilson coefficients for large K can be perturbatively calculated. This is because bosons are non-interacting in the limit of $1/a \to 0$. On the other hand, fermions strongly interact with each other in this limit. In order to determine the Wilson coefficient of $\varphi^\dagger\varphi$ in the large-K limit, we have to solve a three-body problem in a non-perturbative way, which is beyond the scope of this thesis. Hence, in this section, the local operators with $\Delta_\mathcal{O} = 0, 1$ in Eqs. (5.53) and (5.54) are taken into account.

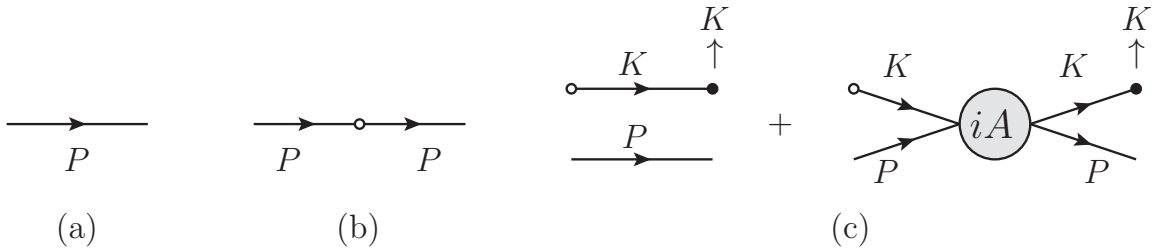

Figure 5.6: Diagrams contributing to (a) $\langle\psi_P|1|\psi_P\rangle$, (b) $\langle\psi_P|\psi^\dagger\psi|\psi_P\rangle$, and (c) $\langle\psi_P|\mathcal{G}_{\psi\psi^\dagger}(K)|\psi_P\rangle$. In (b) and (c), operators at $X = 0$ are denoted by the open dots, while the Fourier transform of $\psi(X)$ by the filled dots. Energy and momentum are conserved at the filled dots.

5.2.1 One-body sector

To determine the Wilson coefficients by the matching procedure, we take the expectation values of both sides of OPE (5.52) with respect to a one-fermion state $|\psi_P\rangle$.

Step 1: Expectation values of local operators

The expectation values of the unit operator and the number density operator in the right hand side of Eq. (5.52) equal

$$\langle\psi_P|1|\psi_P\rangle = \langle\psi_P|\psi_P\rangle, \qquad \langle\psi_P|\psi^\dagger\psi|\psi_P\rangle = -[G(P)]^2, \tag{5.56}$$

respectively. These expectation values can be expressed in terms of Feynman diagrams as Figs 5.6(a) and 5.6(b). As a result, we obtain the expectation value of the right hand side:

$$\sum_i W^{\mathcal{O}_i}_{\psi\psi^\dagger}(K)\langle\psi_P|\mathcal{O}_i|\psi_P\rangle = W^1_{\psi\psi^\dagger}(K)\langle\psi_P|\psi_P\rangle - W^{\psi^\dagger\psi}_{\psi\psi^\dagger}(K)\,[G(P)]^2 + O(K^{-4}). \tag{5.57}$$

Step 2: Expectation value of the operator product

The expectation value of the left-hand side of Eq. (5.52) is given by the diagrams in Fig. 5.6(c):

$$\langle\psi_P|\mathcal{G}_{\psi\psi^\dagger}(K)|\psi_P\rangle = G(K)\langle\psi_P|\psi_P\rangle + [G(P)G(K)]^2 A(K,P;K,P). \tag{5.58}$$

Form Eq. (5.3), the two-body scattering amplitude equals

$$A(K,P;K,P) = -\left(\frac{K_1 - P_1}{2m}\right)^2 D_F(P+K). \tag{5.59}$$

Step 3: Expansion of $\langle\psi_P|\mathcal{G}_{\psi\psi^\dagger}(K)|\psi_P\rangle$ in P

By expanding $A(K,P;K,P)$ in powers of P, Eq. (5.58) reads

$$\langle\psi_P|\mathcal{G}_{\psi\psi^\dagger}(K)|\psi_P\rangle = G(K)\langle\psi_P|\psi_P\rangle - \left(\frac{K_1 G(K)}{2m}\right)^2 D_F(K)[G(P)]^2 + O(K^{-4}). \tag{5.60}$$

Step 4: Matching both sides

Comparing Eq. (5.60) with Eqs. (5.57), we can obtain the Wilson coefficients

$$W^{1}_{\psi\psi^\dagger}(K) = G(K), \tag{5.61}$$

$$W^{\psi^\dagger\psi}_{\psi\psi^\dagger}(K) = \left(\frac{K_1 G(K)}{2m}\right)^2 D_F(K) = \frac{1}{m}\frac{K_1^2}{1/a-\beta_K}[G(K)]^2. \tag{5.62}$$

5.2.2 Single-particle properties in high energy regime

We turn to study the single-particle properties of 1D fermions in the large-K limit. By evaluating the canonical ensemble average of OPE (5.52), the single-particle Green function for large K reads

$$\langle \mathcal{G}_{\psi\psi^\dagger}(K)\rangle = G_K + n\, W^{\psi^\dagger\psi}_{\psi\psi^\dagger}(K) + O(K^{-4}) \tag{5.63}$$

with $n = \langle\psi^\dagger\psi\rangle$. The self-energy $\Sigma(K)$ defined by

$$\langle \mathcal{G}_{\phi\phi^\dagger}(K)\rangle = \frac{1}{K_0 - \frac{K_1^2}{2m} - \Sigma(K)} \tag{5.64}$$

is found to be

$$\Sigma(K) = \frac{n\, W^{\mathcal{O}_{0,0}}_{\psi\psi^\dagger}(K)}{[G(K)]^2} + O(1) = -\frac{nK_1^2}{m\beta_K} + O(1). \tag{5.65}$$

The pole of the single-particle Green function gives the quasiparticle energy $E(K_1)$ and scattering rate $\Gamma(K_1)$:

$$E(K_1) = \mathrm{Re}[K_0^{(\mathrm{pole})}], \qquad \Gamma(K_1) = -2\mathrm{Im}[K_0^{(\mathrm{pole})}], \tag{5.66}$$

where the pole solves the following equation:

$$K_0^{(\mathrm{pole})} = \frac{K_1^2}{2m} + \Sigma(K_0^{(\mathrm{pole})}, K_1). \tag{5.67}$$

Expanding $K_0^{(\mathrm{pole})}$ in both sides with respect to $1/|K_1|$ as

$$K_0^{(\mathrm{pole})} = \frac{K_1^2}{2m} + \delta K_0 = \frac{K_1^2}{2m} + \sum_{n=0}^{\infty} \epsilon_{1-n}|K_1|^{1-n}, \tag{5.68}$$

we obtain

$$\delta K_0 = \Sigma\left(\frac{K_1^2}{2m}, K_1\right) + O(1) = -\frac{2in|K_1|}{m} + O(1). \tag{5.69}$$

As a result, the quasiparticle energy and scattering rate in the high-energy regime are found to be

$$E(K_1) = \frac{K_1^2}{2m} + O(1), \tag{5.70}$$

$$\Gamma(K_1) = \frac{4n|K_1|}{m} + O(1). \tag{5.71}$$

We note that the quasi-particle residue $Z(K_1)$ within our accuracy is

$$Z^{-1} = 1 - \frac{\partial}{\partial K_0}\mathrm{Re}[\Sigma(K)]\Big|_{K_0=K^2/(2m)} = 1 + O(K^{-1}). \tag{5.72}$$

The single-particle spectral density near the peak, $K_0 \approx K_0^{(\mathrm{pole})}$, takes the form

$$\mathcal{A}_B(K) \simeq \frac{1}{2\pi}\frac{\Gamma(K_1)}{[K_0 - E(K_1)]^2 + [\frac{1}{2}\Gamma(K_1)]^2}. \tag{5.73}$$

While the leading term of $\Gamma(K_1)$ in Eq. (5.71) is dominated by the contribution from the number density operator, the corrections to $E(K_1)$ in Eq. (5.70) resulting from the interaction cannot be determined within the accuracy we are currently working. The $O(1)$ terms in $E(K_1)$ include not only the contribution from $\psi^\dagger\psi$ but also that from $\varphi^\dagger\varphi$. The Wilson coefficient of $\varphi^\dagger\varphi$ is expressed in terms of the fermion-dimer amplitude $T(K, Q; K', Q')$ in a way similar to $W^{d^\dagger d}_{\phi\phi^\dagger}(K)$ in Eq. (4.102). In order to determine $W^{\varphi^\dagger\varphi}_{\psi\psi^\dagger}(K)$, we have to solve the STM equation [Eq. (5.18)] in a non-perturbative way.

Finally, we compute the large K-behavior of $\mathcal{A}_F(K)$ away from the single-particle peak $K_0 \neq K_0^{(\mathrm{pole})}$. By substituting Eq. (5.63) into Eq. (5.51), $\mathcal{A}_F(K)$ for large K is found to be

$$\mathcal{A}_F(K) = -\frac{1}{\pi}\mathrm{Im}\left[n \cdot W^{\psi^\dagger\psi}_{\psi\psi^\dagger}(K)\right] + O(K^{-4}). \tag{5.74}$$

By evaluating the imaginary part of $W^{\psi^\dagger\psi}_{\psi\psi^\dagger}(K)$ in Eq. (5.62), it is found to vanish below the two-particle threshold:

$$-\frac{1}{\pi}\mathrm{Im}\left[W^{\psi^\dagger\psi}_{\psi\psi^\dagger}(K)\right] = \Theta(mK_0 - K_1^2/4) \times \frac{m}{\pi}\frac{a^2\sqrt{mK_0 - K_1^2/4}}{1 + a^2(mK_0 - K_1^2/4)^2}\frac{K_1^2}{(mK_0 - K_1^2/2)^2}. \tag{5.75}$$

As a result, the large-K behavior of $\mathcal{A}_F(K)$ for $K_0 > K_1^2/(4m)$ is found to be

$$\mathcal{A}_F(K) = \frac{mn}{\pi}\frac{a^2\sqrt{mK_0 - K_1^2/4}}{1 + a^2(mK_0 - K_1^2/4)^2}\frac{K_1^2}{(mK_0 - K_1^2/2)^2} + O(K^{-4}). \tag{5.76}$$

Comparing this with Eq. (4.126), we can find that the fermionic single-particle spectral density for $K_0 > K_1^2/(4m)$ is related to the bosonic one $\mathcal{A}_B(K)$:

$$\mathcal{A}_F(K) = \frac{(K_1 a)^2}{4}\mathcal{A}_B(K) + O(K^{-4}). \tag{5.77}$$

5.3 Summary

In this chapter, we studied the quantum field theory of 1D fermions near a two-body resonance. First, the renormalization of coupling constants in the field theory was investigated. As a result, not only the two-fermion coupling constant v_2 but also the fermion-dimer one v_3 were found to depend on the cut off scale. In order to confirm that this renormalized theory is consistent with the first-quantized formalism in Chapter 3, we solved the three-body problem in Section 5.1.2 and rederived the energy relation [Eq. (5.38)] in Section 5.1.3. In particular, we clarified that the emergence of the three-body coupling v_3 at low energy scale [Eq. (5.17)] leads to the apparence of the three-body contact in the energy relation.

Applying the constructed field theory to the determination of Wilson coefficients in OPE, we investigated the single-particle properties in high-energy regime. We computed the high-energy behaviors of the quasiparticle energy $E(K_1)$ and the scattering rate $\Gamma(K_1)$ near the single-particle peak within the accuracy of $O(1)$ [Eqs. (5.70) and (5.71)]. While the leading term of $\Gamma(K_1)$ was determined within our accuracy, the determination of the correction to $E(K_1)$ requires a non-perturbative calculation of the fermion-dimer amplitude. We leave this for future work. We also found the single-particle spectral density away from the two-particle threshold [Eq. (5.76)]. In addition, the relation between the bosonic and fermionic single-particle spectral densities [Eq. (5.77)] was found in the large-energy-momentum limit. Our results in Eqs. (5.70), (5.71), and (5.76) are essential properties of 1D fermions near a two-body resonance because they hold for arbitrary scattering length a and temperature T.

Chapter 6

Bosons with a resonant three-body attraction in 1D

In Section 2.3.1, it was shown that 1D bosons governed by a resonant three-body interaction can be realized as a low-energy effective theory of two-component bosons in an optical lattice. In this chapter, we turn to the effective field theory of 1D bosons near a three-body resonance and clarify what universal bound states are stabilized in this system. We first solve a three-boson problem to relate the coupling constant to a three-body scattering length in Section 6.1, so that the importance of quantum corrections in this system becomes obvious. Section 6.2 is devoted to a four-boson problem, leading to the discovery of three four-boson bound states. In Section 6.3, many bosons are found to form a droplet stabilized by the quantum effect and its binding energy is proven to grow exponentially with increasing particle number. At last, we summarize this chapter.

6.1 Quantum field theory near a three-body resonance

The Lagrangian density of 1D bosons interacting via a resonant three-body interaction is given by

$$\mathcal{L}_3 = \phi^\dagger \left(i\partial_t + \frac{\partial_x^2}{2m} \right) \phi - \frac{u_3}{6m} \phi^\dagger \phi^\dagger \phi^\dagger \phi \phi \phi, \tag{6.1}$$

leading to the corresponding Hamiltonian

$$H = \int dx \left(\frac{1}{2m} |\partial_x \phi(x)|^2 + \frac{u_3}{6m} [\phi^\dagger(x)]^3 [\phi(x)]^3 \right). \tag{6.2}$$

Here, the three-body interaction is attractive $u_3 < 0$.

To renormalize the three-body interaction, we solve a scattering problem of three bosons with their total energy K_0 and the center-of-mass momentum K_1. The three-body scattering

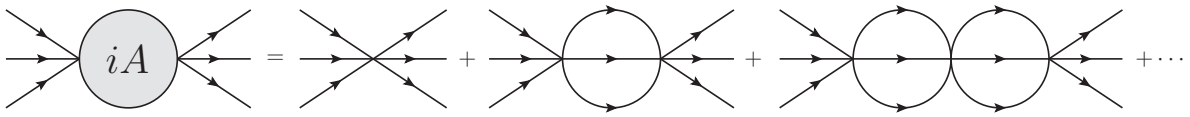

Figure 6.1: Three-body scattering amplitude. The solid line indicates the boson propagator $iG(P)$ and the vertex $-iu_3/m$.

amplitude $iA(K)$ with $K = (K_0, K_1)$ is written as a diagram in Fig. 6.1 and reads

$$\begin{aligned} iA(K) &= -\frac{6iu_3}{m} - \frac{6iu_3}{m}\frac{u_3}{m}\,\Pi_3(K) - \frac{6iu_3}{m}\left(\frac{u_3}{m}\,\Pi_3(K)\right)^2 + \cdots \\ &= -\frac{6iu_3}{m}\frac{1}{1-\frac{u_3}{m}\Pi_3(K)}, \end{aligned} \tag{6.3}$$

where the factor 6 comes from Bose-Einstein statistics. Here, $\Pi_3(K)$ can be expressed in terms of the boson propagator $G(Q) = 1/[Q_0 - Q_1^2/(2m) + i0^+]$ as

$$\begin{aligned} \Pi_3(K) &= -\int_{P,Q} G(K/3+Q)G(K/3-Q/2+P)G(K/3-Q/2-P) \\ &= \frac{m}{\sqrt{3}\pi}\log\left(\sqrt{\frac{K_1^2/6 - mK_0 - i0^+}{\Lambda^2}}\right), \end{aligned} \tag{6.4}$$

where Λ is a momentum cutoff. The scattering amplitude thus reads

$$A(K) = \frac{6\sqrt{3}\pi}{m}\frac{1}{\log\left(\sqrt{\frac{K_1^2/6-mK_0-i0^+}{\Lambda^2}}e^{-\sqrt{3}\pi/u_3}\right)}. \tag{6.5}$$

Since a pole of the scattering amplitude corresponds to the energy for a bound state, we can see that there is one three-body bound state with binding energy $B_3 = |K_0| = \frac{\Lambda^2}{m}e^{2\sqrt{3}\pi/u_3}$ in the center-of-mass frame ($K_1 = 0$). As shown in Eq. (2.93), the binding energy is expressed in terms of the three-body scattering length a_3 as $B_3 = 1/(ma_3^2)$. Therefore, the coupling strength u_3 must depend logarithmically on the product of the scale Λ and the scattering length a_3,

$$u_3 = -\frac{\sqrt{3}\pi}{\log(a_3\Lambda)}, \tag{6.6}$$

and thus $A(K)$ is found to be

$$A(K) = \frac{6\sqrt{3}\pi}{m}\frac{1}{\log\left(a_3\sqrt{K_1^2/6 - mK_0 - i0^+}\right)}. \tag{6.7}$$

As shown above, the quantum effect coming from loops in Fig. 6.1 plays a crucial role of in this quantum field theory. Dimensional analysis of Eq. (6.1) shows that u_3 is dimensionless and thus the classical action is invariant under the scale transformation:

$$x \to \lambda x, \quad t \to \lambda^2 t, \quad \phi(x) \to \lambda^{-1/2}\phi(x). \tag{6.8}$$

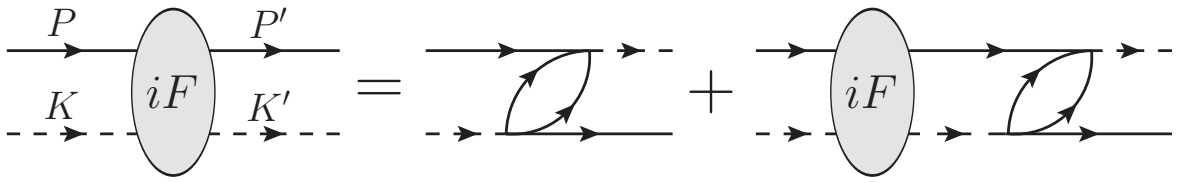

Figure 6.2: STM equation for the boson-trimer scattering [Eq. (6.11)]. The dashed line denotes the trimer propagator $iT(K)$.

This means that there is no length scale providing the size of a bound state within the classical field theory. However, this classical scale symmetry is broken by loop corrections in Fig. 6.1, so that a_3 provides a length scale to the quantum field theory. This emergence of the scale generating from the quantum effect is called dimensional transmutation [117].

6.2 Four-body bound states

Next, four-boson bound states are investigated. For convenience, we employ the auxiliary field method used in the previous two chapters: The Hubbard-Stratonovich transformation is performed to introduce a auxiliary trimer field $t \sim \frac{u_3}{m}\phi^3$. The Lagrangian after the transformation is written as

$$\mathcal{L}_3' = \phi^\dagger \left(\partial_t + \frac{\partial_x^2}{2m}\right)\phi + \frac{m}{6u_3}t^\dagger t - \frac{1}{6}(t^\dagger\phi^3 + \phi^{\dagger 3}t). \tag{6.9}$$

The propagator $iT(K)$ of a trimer coincides with the three-boson scattering amplitude $iA(K)$ up to a minus sign:

$$iT(K) = -iA(K). \tag{6.10}$$

Following the similar way as in the three-fermion problem in Section (5.1.2), we begin with a boson-trimer scattering problem. The incoming boson and trimer have sets of energy and momentum, $P = (P_0, P_1)$ and $K = (K_0, K_1)$, respectively, and the outgoing boson and trimer have $P' = (P_0', P_1')$ and $K' = (K_0', K_1')$, respectively. The boson-trimer scattering amplitude $iF(P, K; P', K')$ satisfies the Skorniakov–Ter-Martirosian (STM) equation [see Fig. 6.2]:

$$iF(P,K;P',K') = \frac{1}{2}\int_R G(R)G(K'-P-R) - i\int_Q F(P,K;Q,P+K-Q)T(P+K-Q)G(Q) \times \frac{1}{2}\int_R G(R)G(K'-Q-R). \tag{6.11}$$

We note that the energy and momentum conservation laws lead to $P + K = P' + K'$. The integrals over R can be easily evaluated by the residue theorem:

$$\frac{1}{2}\int_R G(R)G(K'-P-R) = \frac{im}{4\beta_{K'-P}}, \tag{6.12}$$

where $\beta_P = \sqrt{P_1^2/4 - m(P_0 + i0^+)}$. Equation (6.11) thus reduces to

$$iF(P,K;P',K') = \frac{im}{4\beta_{K'-P}} + \frac{m}{4}\int_Q \frac{F(P,K;Q,P+K-Q)T(P+K-Q)G(Q)}{\beta_{K'-Q}}. \tag{6.13}$$

In a similar way as in Eq. (5.18), we can prove that $F(P,K;Q,P+K-Q)$, $T(P+K-Q)$, and $1/\beta_{K'-Q}$ are analytic in the lower half plane in Q_0. The integrand in Eq. (6.13) has only one pole $Q_0 = Q_1^2/(2m) - i0^+$ in the lower half plane, and thus Eq. (6.13) reads

$$F(P,K;P',K') = \frac{m}{4\beta_{K'-P}} + \frac{m}{4}\int \frac{dQ_1}{2\pi} \left.\frac{F(P,K;Q,P+K-Q)T(P+K-Q)}{\beta_{K'-Q}}\right|_{Q_0=\frac{Q_1^2}{2m}}. \tag{6.14}$$

Taking the center-of-mass frame and taking the incoming and outgoing atoms on shell, we have

$$P = \left(\frac{p^2}{2m}, p\right), \quad K = \left(E - \frac{p^2}{2m}, -p\right), \tag{6.15}$$

$$P' = \left(\frac{p'^2}{2m}, p'\right), \quad K' = \left(E - \frac{p'^2}{2m}, -p'\right), \tag{6.16}$$

where E is the total energy, and p and p' are incoming and outgoing relative momenta, respectively. The amplitude $F(P,K;P',K') = F(p,p',E)$ under the on-shell conditions thus solves the following equation:

$$F(p,p',E) = m\mathcal{I}(p,p',E) + \int_{-\infty}^{\infty} dq\, \mathcal{K}(p',q,E)F(p,q,E), \tag{6.17}$$

where the exchange of integration valuable $Q_1 \to q$ was performed, and the inhomogeneous term and the kernel are provided by

$$\mathcal{I}(p,p',E) = \frac{1}{2\sqrt{3p'^2 + 2p'p + 3p^2 - 4mE - i0^+}}, \tag{6.18}$$

$$\mathcal{K}(p',q,E) = \frac{3\sqrt{3}\mathcal{I}(p',q,E)}{\log\left(a_3\sqrt{\frac{2}{3}q^2 - mE - i0^+}\right)}, \tag{6.19}$$

respectively.

We now turn to four-body bound states, which correspond to the poles of $F(p,p',E)$. If there is a four-body bound state with energy $E = -B_4 < 0$, the amplitude in the limit of $E \to -B_4$ takes the form

$$F(p,p',E) \to \frac{Z^*(p)Z(p')}{E + B_4}. \tag{6.20}$$

By comparing the residues of both sides of Eq. (6.17) with respect to $E = -B_4$, the binding energy is found to solve the homogeneous integral equation

$$Z(p') = \int_{-\infty}^{\infty} dq\, \mathcal{K}(p',q,-B_4)Z(q). \tag{6.21}$$

Since the kernel has the property $\mathcal{K}(p', q, -B_4) = \mathcal{K}(-p', -q, -B_4)$, even and odd sectors of the wave function are decoupled from each other:

$$Z_{\pm}(p') = \int_0^{\infty} dq \, [\mathcal{K}(p', q) \pm \mathcal{K}(-p', q)] Z_{\pm}(q), \tag{6.22}$$

where $Z_{\pm}(p') \equiv [Z(p') \pm Z(-p')]/2$. We numerically find three bound states in the even channel

$$\log(B_4/B_3) = 13.5447, \quad 4.91925, \quad 0.747826, \tag{6.23}$$

whereas there is no bound state in the odd channel. These four-boson bound states are universal in the sense that the ratios of their binding energies to B_3 are independent of the microscopic details.

6.3 Many-body droplet

In this section, we study a many-body droplet, which is the ground state of a large number of bosons. We use the method developed by Hammer and Son for self-bound bosons with a two-body attraction in 2D, which relies on the classical field theory applicable to a large number of bosons [118]. In this 2D case, the validity of the method was confirmed by solving the Schrödinger equation for up to 26 bosons [119]. Furthermore, in the case of two-body repulsion, the Gross-Pitaevskii equation with the right choice of coupling was proven to provide the ground state energy and number density exactly for trapped bosons both in 3D [120,121] and in 2D [122,123]. Here we proceed by considering the same to be true for self-bound attractive bosons in 1D, which can be confirmed explicitly in the case of two-body attraction[1] [124].

The ground state energy of $N \gg 1$ bosons is determined so as to minimize the energy functional

$$E = \int dx \left(\frac{1}{2m} |\partial_x \phi(x)|^2 + \frac{u_3}{6m} |\phi(x)|^6 \right) \tag{6.24}$$

with respect to $\phi(x)$ regarded as a c-number function satisfying $\int_{-\infty}^{\infty} dx \, |\phi(x)|^2 = N$. This normalization condition results from particle number conservation and is conveniently incorporated by expressing the wave function as

$$\phi(x) = \sqrt{\frac{N}{CR}} \, f\Big(\frac{x}{R}\Big), \tag{6.25}$$

where

$$C \equiv \int_{-\infty}^{\infty} d\rho \, [f(\rho)]^2 \tag{6.26}$$

[1] For one-dimensional bosons with a two-body attraction ($-1/a < 0$), the minimization of $E_N = \int dx \, \frac{1}{2m} |\partial \phi(x)|^2 - \frac{1}{ma} \int dx \, |\phi(x)|^4$ with respect to $\phi(x)$ under $\int_{-\infty}^{\infty} dx \, |\phi(x)|^2 = N$ leads to the binding energy $B_N = -E_N = \frac{N^3}{6ma^2}$, which is consistent with the large-N limit of the exact result in Eq. (2.76) [124].

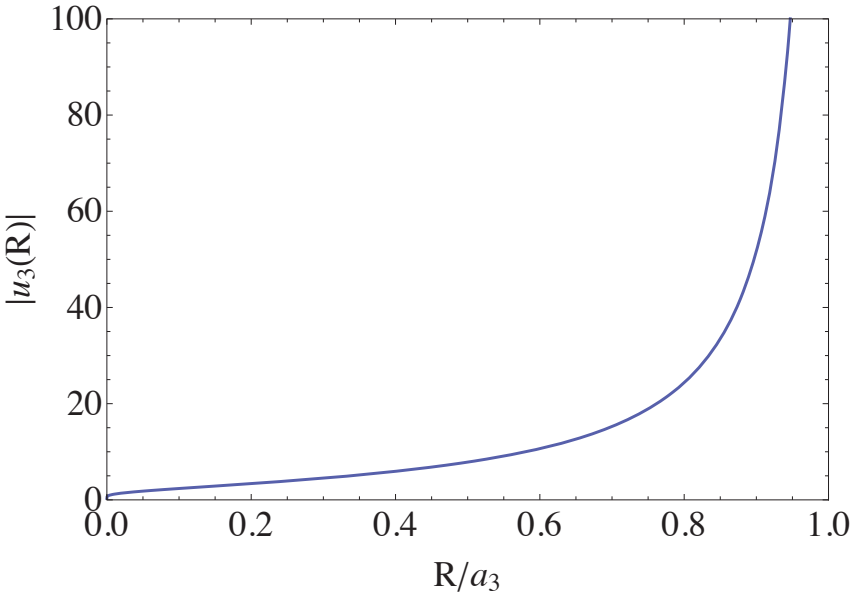

Figure 6.3: Strength of the scale dependent running coupling in Eq. (6.27). Because attractive bosons without repulsion and Pauli exclusion are considered, the size of the ground state is expected to be decreased monotonously with increasing N. Hence, we assume that the size of the N-boson droplet R is smaller than that of the three-boson bound state a_3, leading to $R/a_3 < 1$.

is a functional of $f(\rho)$. The dimensionless positive function $f(x/R)$ must vanish at $|x| \gg R$ for the convergent normalization integral and thus R sets the size of N-boson droplet. In order to minimize the energy with respect to R, it is essential to take into account the logarithmic scale dependence of coupling through the renormalization [118, 122, 123], which was shown in Eq. (6.6). Because a characteristic momentum scale of bosons confined in a droplet of size R is $\Lambda \sim R^{-1}$, the three-body coupling constant u_3 in Eq. (6.24) should have the form,

$$u_3(R) = -\frac{\sqrt{3}\pi}{\log(a_3/R)}, \tag{6.27}$$

to the leading logarithmic accuracy. By defining two functionals of $f(\rho)$,

$$A \equiv \int_{-\infty}^{\infty} d\rho\, [f'(\rho)]^2, \quad B \equiv \int_{-\infty}^{\infty} d\rho\, [f(\rho)]^6, \tag{6.28}$$

and using Eqs. (6.25) and (6.27), Eq. (6.24) reduces to

$$E = \frac{1}{2mR^2}\left(\frac{NA}{C} + \frac{N^3 B}{3C^3} u_3(R)\right). \tag{6.29}$$

We minimize this with respect to R and $f(\rho)$.

First, we fix the shape of the droplet $f(\rho)$ and minimize E with respect to R. As shown in Fig. 6.3, when R is large, the scale-dependent attraction in Eq. (6.27) becomes strong, which

favors smaller R. On the other hand, in the limit $R \to +0$ the coupling becomes weak and thus the energy is dominated by the kinetic energy, which tends to expand the droplet. As a result, E is minimized at a finite R, which can be determined by solving $dE/dR = 0$. The optimal size R_N and the corresponding binding energy $B_N = -E|_{R=R_N}$ for $N \gg 1$ are obtained as follows:

$$R_N = a_3 \exp\left[-\frac{\pi}{\sqrt{3}}\frac{B}{AC^2}N^2 + O(N)\right], \tag{6.30}$$

$$B_N = B_3 \exp\left[\frac{2\pi}{\sqrt{3}}\frac{B}{AC^2}N^2 + O(N)\right]. \tag{6.31}$$

The binding energy should be maximized further with respect to $f(\rho)$, which is achieved by maximizing the ratio B/AC^2 in the exponent of Eq. (6.31). The variation of B/AC^2 reads

$$\delta\left(\frac{B}{AC^2}\right) = \frac{-BC\delta A + AC\delta B - 2AB\delta C}{A^2C^3} \tag{6.32}$$

with

$$\delta A = \int_{-\infty}^{\infty} d\rho\,[-2f''(\rho)]\delta f, \tag{6.33}$$

$$\delta B = \int_{-\infty}^{\infty} d\rho\,6[f(\rho)]^5\delta f, \tag{6.34}$$

$$\delta C = \int_{-\infty}^{\infty} d\rho\,2f(\rho)\delta f. \tag{6.35}$$

Therefore, the extremization of B/AC^2 leads to the following differential equation for the optimal function to satisfy:

$$BCf''(\rho) + 3AC[f(\rho)]^5 - 2ABf(\rho) = 0, \tag{6.36}$$

where $f'(\rho)$ and $f''(\rho)$ denote the first and second derivatives of the shape function, respectively. Under the scale transformation

$$\rho \to \tilde{\rho} = \lambda\rho, \quad f(\rho) \to \tilde{f}(\tilde{\rho}) = \mu f(\rho), \tag{6.37}$$

the ratio B/AC^2 to be maximized is invariant as follows:

$$\begin{aligned}
\frac{B[\tilde{f}]}{A[\tilde{f}]\left(C[\tilde{f}]\right)^2} &= \frac{\int d\tilde{\rho}\,[\tilde{f}(\tilde{\rho})]^6}{\left(\int d\tilde{\rho}\,[\tilde{f}'(\tilde{\rho})]^2\right)\left(\int d\tilde{\rho}\,[\tilde{f}(\tilde{\rho})]^2\right)^2} \\
&= \frac{\int d(\lambda\rho)\,[\mu f(\rho)]^6}{\left(\int d(\lambda\rho)\,\left[\frac{\partial\mu f(\rho)}{\partial(\lambda\rho)}\right]^2\right)\left(\int d(\lambda\rho)\,[\mu f(\rho)]^2\right)^2} \\
&= \frac{\int d\rho\,[f(\rho)]^6}{\left(\int d\rho\,[f'(\rho)]^2\right)\left(\int d\rho\,[f(\rho)]^2\right)^2} \\
&= \frac{B[f]}{A[f]\left(C[f]\right)^2}.
\end{aligned} \tag{6.38}$$

The rescaling

$$\tilde{\rho} \equiv 2\sqrt{\frac{2A}{C}}\rho, \quad \tilde{f}(\tilde{\rho}) \equiv \left(\frac{C}{2B}\right)^{1/4} f(\rho), \tag{6.39}$$

reduces Eq. (6.36) to

$$4\tilde{f}''(\tilde{\rho}) + 3[\tilde{f}(\tilde{\rho})]^5 - \tilde{f}(\tilde{\rho}) = 0. \tag{6.40}$$

This nonlinear equation has a bright soliton solution

$$\tilde{f}(\tilde{\rho}) = \frac{1}{\sqrt{\cosh\tilde{\rho}}}, \tag{6.41}$$

leading to the maximum of the ratio

$$\frac{B[\tilde{f}]}{A[\tilde{f}]\left(C[\tilde{f}]\right)^2} = \frac{4}{\pi^2}. \tag{6.42}$$

Consequently, we find that the ground state has the size and binding energy

$$R_N = a_3 \exp\left[-\frac{4}{\sqrt{3}\pi}N^2 + O(N)\right] \approx a_3 \times (0.4794550206)^{N^2}, \tag{6.43}$$

$$B_N = B_3 \exp\left[\frac{8}{\sqrt{3}\pi}N^2 + O(N)\right] \approx B_3 \times (4.350150263)^{N^2}, \tag{6.44}$$

as well as the density distribution

$$n(x) = |\phi(x)|^2 = \frac{N}{\pi R_N \cosh(x/R_N)}. \tag{6.45}$$

We note that our results in Eqs. (6.43)–(6.45) are valid for $N \gg 1$ as long as the droplet is so dilute that the mean interparticle separation is much larger than the lattice constant l in the microscopic lattice theory in Section (2.3.1). This requires $R_N/N \gg l$, that is

$$1 \ll N \ll \sqrt{\frac{3\pi^2}{2}\frac{t_x}{|U_3|}}. \tag{6.46}$$

Here, Eq. (6.43) and the scattering length a_3 in terms of the microscopic lattice parameters [Eq. (2.91)] were used.

6.4 Summary

Universal few- and many-body properties of 1D bosons with a resonant three-body attraction were investigated in this chapter. In Section 6.1, we computed the three-body scattering amplitude and showed that quantum corrections results in the scale dependence of the coupling constant and the emergence of the length scale a_3. We found three four-body bound states by

solving the STM equation in Section 6.2 and a many-body ground state, in which bosons form a dilute droplet stabilized by the quantum effect. We clarified that the ratios of their binding energies to that of three bosons are universal and found that the size and energy of the dilute droplet grows exponentially with increasing particle number. These bound states can be in principle observed in ultracold-atom experiments with two-component bosons trapped in a 1D optical lattice.

Chapter 7

Conclusion and outlook

We studied universal properties of 1D quantum systems with resonant interactions, which can be realized with ultracold atoms by taking advantage of their high controllability. We first focused on bosons and fermions near two-body resonances. In Chapter 2, we reviewed essential properties of these two systems. These systems can be described by the zero-range models, in which particles interact with each other via contact interactions. In addition, we explained the Bose-Fermi correspondence, which is the interrelation between bosons and fermions with contact interactions. Because of the Bose-Fermi correspondence, these two systems have the same energy spectrum, thermodynamics and correlation functions including static and dynamic structure factors and a current correlation. However, other correlation functions such as a momentum distribution and a single-particle Green function are different between bosons and fermions. We also reviewed the method of the Bethe ansatz to solve the Schrödinger equations for the zero-range models without a trapping potential. By using this method, energy and contact densities can be exactly computed.

Chapters 3, 4, and 5 were devoted to deriving universal relations for bosons and fermions near two-body resonances. These relations hold for any energy eigenstates and any statistical ensembles of the eigenstates with or without a trapping potential, and the relations involve the contact parameters such as two- and three-body contacts. In Chapters 3, universal relations for static structure factors $S(k)$ and momentum distributions $\rho_\alpha(k)$ with $\alpha = B\,, F$ for both bosons and fermions were derived. The power-law tails of $S(k)$ [Eqs. (3.12)], $\rho_B(k)$ [Eq. (3.14)] and $\rho_F(k)$ [Eq. (3.19)] at large momentum were found, and the coefficients of these tails were proportional to the two-body contact. We also derived the energy relations in Eqs. (3.23) and (3.48), in which the sum of kinetic and interaction energies are expressed in terms of $\rho_\alpha(k)$ and contact parameters. We found the following three facts in these universal relations: $S(k)$ has the identical tail between bosons and fermions; the Bose-Fermi correspondence results in two nontrivial connections between $\rho_B(k)$ and $\rho_F(k)$ through their tails and through the energy relations; and the three-body contact makes no contribution to the energy relation for bosons, but it makes an essential contribution to that for fermions. Furthermore, our universal relations for the large-momentum tails together with the two-body contact calculated by the Bethe ansatz completely determine the large-k asymptotics of $S(k)$ and $\rho_\alpha(k)$ for uniform Bose and Fermi

gases at any temperature. We also computed $\rho_F(k)$ for the ground state of N fermions in the limit of $a \to \infty$ and confirmed Eqs. (3.19) and (3.48) in this case.

In Chapter 4, the large-energy-momentum behaviors of dynamic correlation functions for bosons were studied by using OPE in a field theoretical formalism. For bosons, the quantum field theory was well-defined without a regularization and perturbative calculations were applicable to determine Wilson coefficients in the large-energy-momentum limit. Above the two-particle threshold, the dynamic structure factor [Eq. (4.71)] and the current correlation function [Eq. (4.83)] are dominated by the contributions from the two-body contact density, while the single-particle spectral density by the contribution from the number density. We also determined the high-energy behaviors of the quasiparticle energy and the scattering rate near the single-particle peak [Eqs. (4.120) and (4.121)].

In order to derive universal relations for the single-particle spectral density of fermions, we constructed the quantum field theory for fermions in Chapter 5. Unlike for bosons, the quantum field theory for fermions was required to be regularized. Performing the renormalization group analysis, we found that not only the two-fermion coupling constant v_2 [Eq. (5.9)] but also the fermion-dimer one v_3 [Eq. (5.17)] characterizing the three-fermion coupling are scale dependent. To confirm that this renormalized theory is consistent with the first-quantized formalism in Chapter 3, we calculated the energy of the three-fermion bound state and rederived the energy relation. In particular, we clarified that, in the field theory framework, the emergence of the three-body coupling v_3 at low energy scale leads to the appearance of the three-body contact in the energy relation. Applying OPE to the constructed field theory, we investigated the single-particle properties in high-energy regime. We computed the high-energy behaviors of the quasiparticle energy $E(K_1)$ and the scattering rate $\Gamma(K_1)$ near the single-particle peak within the accuracy of $O(1)$ [Eqs. (5.70) and (5.71)]. While the leading term of $\Gamma(K_1)$ was determined within our accuracy, the determination of the correction to $E(K_1)$ requires a non-perturbative calculation of the fermion-dimer amplitude. We leave this for future work. We also found that the single-particle spectral density away from the two-particle threshold [Eq. (5.76)] is dominated by the contribution from the number density. In addition, the relation between the bosonic and fermionic single-particle spectral densities [Eq. (5.77)] was found in the large-energy-momentum limit.

One-dimensional bosons near a three-body resonance were also studied in this thesis. In Section 2.3, we presented the way to realize a 1D system governed by a resonant three-body interaction with two-component bosons in an optical lattice. We showed that, by tuning the detuning and Rabi frequency, effective two- and three-body interactions can be independently controlled. When the effective two-body interaction vanishes and the effective three-body interaction is weakly attractive, the low-energy physics of the system is described by the quantum field theory with a contact three-body attraction. Few- and many-body states in this theory were investigated in Chapter 6. We first computed the three-body scattering amplitude and showed that quantum corrections results in the scale dependence of the coupling constant and the emergence of the length scale, i.e., the three-body scattering length a_3. There was one three-body bound state with binding energy $B_3 = 1/(ma_3^2)$. We found three four-body bound

states as well as a many-body ground state, in which bosons form a dilute droplet stabilized by the quantum effect. We clarified that the ratios of their binding energies to that of three bosons are universal and found that the size and energy of the dilute droplet grows exponentially with increasing particle number. These bound states can be in principle observed in ultracold-atom experiments with two-component bosons trapped in a 1D optical lattice.

In order to deepen our unified understanding of interacting quantum many-body systems in various fields of physics, we in this thesis studied resonantly interacting 1D systems from the viewpoint of the universal properties near resonances. The properties we clarified are universal in the sense that they are independent of microscopic details of the interaction potentials. This means that our results can be applied to systems in the resonant regime, where microscopic length scales associated with interactions are much smaller than the scattering lengths, thermal de Broglie wavelengths, and mean interparticle distances. From this perspective, the exploration of 1D systems near resonances is an important, interesting future work common to atomic physics, condensed matter physics, nuclear physics, and particle physics. So far, a variety of ultracold atomic gases such as ^{7}Li, ^{23}Na, ^{39}K, ^{87}Rb, and ^{133}Cs have reached this resonant regime with the help of magnetic Feshbach resonances. Also, the ^{4}He atom in nature has s-wave scattering length $a_s \simeq 10$ nm and interaction range $r_0 \simeq 0.54$ nm, leading to the large ratio $a_s/r_0 \simeq 20$ without the use of Feshbach resonances [21]. Therefore, we can predict that a dilute ^{4}He gas at low temperature confined in 1D geometry exhibits the universal properties for correlation functions studied here. We expect that such universal properties are tested in future experiments. On the other hand, it is well known that, at atmospheric pressure, the liquid ^{4}He in low-temperature regime becomes a superfluid. It is interesting how correlations for ^{4}He in 1D change from the universal resonant regime to the superfluid-liquid regime with increasing number density. In condensed matter physics, the possibility that magnons in 3D quantum magnets reach the universal resonant regime is pointed out [27]. Similarly, magnons in 1D spin systems may exhibit the universal properties which we have studied in this thesis. We hope that our studies in resonantly interacting systems will become a new bridge among different subfields of physics.

Appendix A

Calculations of loop Integrals

In this appendix, integrals (4.55) corresponding to the loops in Fig. 4.5 are computed and expanded in Q. As mentioned in Section 4.2, $K_0 > 0$ and $K_1 > 0$ is assumed. We begin with the integral

$$I_1(K,Q) = i\int_R G(R)G(Q-R)G(K+Q-R). \tag{A.1}$$

By the residue theorem, $I_1(K,Q)$ can be evaluated as

$$I_1(K,Q) = \left(\frac{m^2}{2\beta_{K+Q}} + \frac{m^2}{2\beta_Q}\right)\frac{1}{(\beta_{K+Q}+\beta_Q)^{\,2} + K_1^2/4}. \tag{A.2}$$

Expanding this in Q yields

$$I_1(K,Q) = -G(K)\left[\frac{m}{2\beta_K} + \frac{m}{2\beta_Q} + G(K)\beta_K + G(K)\frac{K_1Q_1}{4\beta_Q}\right] + O(Q). \tag{A.3}$$

Next, we turn to the integral

$$I_2(K,Q) = -i\int_R G(R)G(R+K)G(Q-R)G(Q-K-R). \tag{A.4}$$

In order to compute $I_2(K,Q)$, it is convenient to evaluate the integral after the Wick rotation: First, we replace K_0 by iK_4 with $K_4 > 0$ and then calculate the integral over $R = (R_0, R_1)$. After the integration, we perform the analytic continuation $iK_4 \to K_0 + i0^+$. The integral after the Wick rotation can be evaluated as

$$\begin{aligned} I_2(\tilde{K},Q) &= -\int\frac{dR_1}{2\pi}\,G(R+\tilde{K})G(Q-R)G(Q-\tilde{K}-R)\Big|_{R_0=\frac{R_1^2}{2m}+i0} \\ &\quad + (\tilde{K}\to-\tilde{K}) \qquad\qquad (A.5)\\ &= I_{2,1}(\tilde{K},Q) + I_{2,2}(\tilde{K},Q) + (\tilde{K}\to-\tilde{K}), \qquad\qquad (A.6) \end{aligned}$$

where the first and second terms with $\tilde{K} \equiv (iK_4, K_1)$ are given by

$$I_{2,1}(\tilde{\tilde{K}}, Q) = \frac{m^3}{2\beta_Q} \frac{1}{K_1(\frac{K_1+Q_1}{2} - i\beta_Q) - miK_4} \frac{1}{(K_1/2 - i\beta_Q)^2 + \beta_{Q-K}^2}, \tag{A.7}$$

$$I_{2,2}(\tilde{K}, Q) = \frac{m^3}{2\beta_{Q-K}} \frac{1}{K_1(Q_1/2 - i\beta_{Q-K}) - miK_4} \frac{1}{(K_1/2 + i\beta_{Q-K})^2 + \beta_Q^2}. \tag{A.8}$$

Expanding $I_{2,1}(\tilde{K}, Q)$ and $I_{2,2}(\tilde{K}, Q)$ in Q yields

$$I_{2,1}(\tilde{K}, Q) = \frac{m^3}{2\beta_Q} \frac{G(\tilde{K})}{m} \left(1 + \frac{G(\tilde{K})}{m} K_1(Q_1/2 - i\beta_Q)\right) \times \frac{G(-\tilde{K})}{m} \left(1 - \frac{G(-\tilde{K})}{m} K_1(Q_1/2 + i\beta_Q)\right) + O(Q), \tag{A.9}$$

$$I_{2,2}(\tilde{K}, Q) = \frac{m[G(-\tilde{K})]^2}{2\beta_{-\tilde{K}}} + O(Q). \tag{A.10}$$

After the analytic continuation $iK_4 \to K_0 + i0^+$, the integral $I_2(K, Q)$ within the accuracy of $O(Q)$ is found to be

$$I_2(K, Q) = \frac{m}{\beta_Q} \times G(K)G(-K) \left(1 + \frac{K_1 Q_1 G(K)}{2m}\right) \left(1 - \frac{K_1 Q_1 G(-K)}{2m}\right) + \frac{m[G(K)]^2}{2\beta_K} + \frac{m[G(-K)]^2}{2\beta_{-K}} + O(Q). \tag{A.11}$$

At last, we calculate the integral

$$I_3(K, Q) = i \int_R G(R)[G(Q - R)]^2 G(Q + K - R). \tag{A.12}$$

By using the residue theorem, we have

$$I_3(K, Q) = I_{3,1}(K, Q) - I_{3,2}(K, Q), \tag{A.13}$$

where

$$I_{3,1}(K, Q) \equiv \frac{m^3}{4\beta_Q^3} \frac{2iK_1\beta_Q - \beta_{K+Q}^2 - K_1^2/4 + 3\beta_Q^2}{(iK_1\beta_Q - \beta_{K+Q}^2 - K_1^2/4 + \beta_Q^2)^2}, \tag{A.14}$$

$$I_{3,2}(K, Q) \equiv \frac{m^3}{2\beta_{K+Q}} \frac{1}{(-iK_1\beta_{K+Q} + \beta_{K+Q}^2 - K_1^2/4 - \beta_Q^2)^2}. \tag{A.15}$$

From $\beta_{K+Q}^2 = \beta_K^2 + \beta_Q^2 + K_1 Q_1/2$, $I_{3,1}(K, Q)$ can be expanded as follows:

$$I_{3,1}(K, Q) = \frac{m^2 G(K)}{4\beta_Q^3} \left(1 + \frac{K_1 G(K)}{m} \frac{Q_1}{2} + \frac{G(K)}{m} 2\beta_Q^2 + \left(\frac{K_1 G(K)}{m}\right)^2 (\beta_Q^2 + Q_1^2/4) + \left(\frac{K_1 G(K)}{m}\right)^3 Q_1 \left(\frac{3}{2}\beta_Q^2 + \frac{1}{8}Q_1^2\right) + 2Q_1\beta_Q^2 \frac{K_1[G(K)]^2}{m^2}\right) - i\left[\frac{K_1^3[G(K)]^4}{2m} + K_1[G(K)]^3\right] + O(Q). \tag{A.16}$$

Using Eq. (4.52), we have

$$I_{3,1}(K,Q)+(K\to -K)=-i\left[\frac{K_1^3[G(K)]^4}{2m}+K_1[G(K)]^3+(K\to -K)\right] + \sum_{\Delta_{\mathcal{O}_{a,b}}\le 4} W_{nn}^{\mathcal{O}_{a,b}}(K) I_{\mathcal{O}_{a,b}}(Q)+O(Q). \tag{A.17}$$

On the other hand, $I_{3,2}(K,Q)$ can be expanded as

$$I_{3,2}(K,Q)=\frac{1}{2\beta_K}\frac{[G(K)]^4}{m}(K_1/2-i\beta_K)^4+O(Q). \tag{A.18}$$

Therefore, we obtain

$$I_3(K,Q)+(K\to -K)=\frac{[G(K)]^4}{2m}\left(K_1^2\beta_K-\frac{(mK_0)^2}{\beta_K}+(K\to -K)\right) + \sum_{\Delta_{\mathcal{O}_{a,b}}\le 4} W_{nn}^{\mathcal{O}_{a,b}}(K) I_{\mathcal{O}_{a,b}}(Q)+O(Q). \tag{A.19}$$

Bibliography

[1] J. G. Bednorz and K. Müller, "Possible high-Tc superconductivity in the Ba-La-Cu-O system," Z. Physik B **64**, 189 (1986).

[2] D. Bailin and A. Love, "Superfluidity And Superconductivity In Relativistic Fermion Systems," Phys. Rep. **107**, 325 (1984).

[3] D. J. Dean and M. H.-Jensen, "Pairing in nuclear systems: from neutron stars to finite nuclei," Rev. Mod. Phys. **75**, 607 (2003).

[4] I. Arsene *et al.* [BRAHMS Collaboration], "Quark–gluon plasma and color glass condensate at RHIC? The perspective from the BRAHMS experiment," Nucl. Phys. A **757**, 1 (2005).

[5] K. Adcox *et al.* [PHENIX Collaboration], "Formation of dense partonic matter in relativistic nucleus–nucleus collisions at RHIC: Experimental evaluation by the PHENIX Collaboration," Nucl. Phys. A **757**, 184 (2005).

[6] B. B. Back *et al.* [PHOBOS Collaboration], "The PHOBOS perspective on discoveries at RHIC," Nucl. Phys. A **757**, 28 (2005).

[7] J. Adams *et al.* [STAR Collaboration], "Experimental and theoretical challenges in the search for the quark–gluon plasma: The STAR Collaboration's critical assessment of the evidence from RHIC collisions," Nucl. Phys. A **757**, 102 (2005).

[8] I. Bloch, J. Dalibard, and W. Zwerger, "Many-body physics with ultracold gases," Rev. Mod. Phys. **80**, 885 (2008).

[9] S. Giorgini, L. P. Pitaevskii, and S. Stringari, "Theory of ultracold atomic Fermi gases," Rev. Mod. Phys. **80**, 1215 (2008).

[10] *Ultracold Fermi Gases*, Proceedings of the International School of Physics "Enrico Fermi", edited by M. Inguscio, W. Ketterle, and C. Salomon (SIF, Bologna, 2007).

[11] H. J. Metcalf, and P. van der Straten, *Laser Cooling and Trapping* (Springer, New York) (1999).

[12] W. Ketterle, and N. J. van Druten, "Evaporative cooling of trapped atoms," Adv. At., Mol., Opt. Phys. **37**, 181 (1997).

[13] C. Chin, R. Grimm, P. Julienne, and E. Tiesinga, "Feshbach resonances in ultracold gases," Rev. Mod. Phys. **82**, 1225-1286 (2010).

[14] A. J. Moerdijk, B. J. Verhaar, and A. Axelsson, "Resonances in ultracold collisions of ^{6}Li,^{7} Li, and ^{23}Na," Phys. Rev. A **51**, 4852 (1995).

[15] C. D'Errico, M. Zaccanti, M. Fattori, G. Roati, M. Inguscio, G. Modugno, and A. Simoni, "Feshbach resonances in ultracold ^{39}K," New J. Phys. **9**, 223 (2007).

[16] C. Ticknor, C. A. Regal, D. S. Jin, and J. L. Bohn, "Multiplet structure of Feshbach resonances in nonzero partial waves," Phys. Rev. A **69**, 042712 (2004).

[17] *The BCS-BEC Crossover and the Unitary Fermi Gas*, Lecture Notes in Physics, edited by W. Zwerger, Chap. 6 (Springer, Berlin, 2012).

[18] V. Efimov, "Energy levels arising from resonant two-body forces in a three-body system," Phys. Lett. B **33**, 563 (1970); "Weakly-bound states of three resonantly-interacting particles," Sov. J. Nucl. Phys. **2**, 589 (1971); "Energy levels of three resonantly interacting particles," Nucl. Phys. A **210**, 157 (1973).

[19] E. Braaten and H.-W. Hammer, "Universality in few-body systems with large scattering length," Phys. Rep. **428** 259 (2006).

[20] E. Nielsen, D. V. Fedorov, A. S. Jensen, and E. Garrido, "The three-body problem with short- range interactions," Phys. Rep. **347**, 373 (2001).

[21] P. Naidon and S. Endo, "Efimov physics: a review," Rep. Prog. Phys. **80**, 056001 (2017).

[22] T. Kraemer, M. Mark, P. Waldburger, J. G. Danzl, C. Chin, B. Engeser, A. D. Lange, K. Pilch, A. Jaakkola, H.-C. Nagerl, and R. Grimm, "Evidence for Efimov quantum states in an ultracold gas of caesium atoms," Nature **440**, 315–318, (2006).

[23] A. Gardestig and D. R. Phillips, "Using chiral perturbation theory to extract the neutron-neutron scattering length from $\pi^- d \to nn\gamma$," Phys. Rev. C **73**, 014002 (2006).

[24] G. Bertsch, *Many-Body X Challenge*, in: Proc. X Conference on Recent Progress in Many-Body Theories, eds. R. F. Bishop *et al.* (World Scientific, Singapore, 2000).

[25] M. Kunitski, S. Zeller, J. Voigtsberger, A. Kalinin, L. P. H. Schmidt, M. Schöffler, A. Czasch, W. Schöllkopf, R. E. Grisenti, T. Jahnke, D. Blume, and R. Dörner, "Observa- tion of the Efimov state of the helium trimer," Science **348**, 551–555, (2015).

[26] A. S. Jensen, K. Riisager, D. V. Fedorov, and E. Garrido, "Structure and reactions of quantum halos," Rev. Mod. Phys. **76**, 215, (2004).

[27] Y. Nishida, Y. Kato, and C. D. Batista, "Efimov effect in quantum magnets," Nat. Phys. **9**, 93, (2013).

[28] S. Tan, "Energetics of a strongly correlated Fermi gas," Ann. Phys. (NY) **323**, 2952 (2008); "Large momentum part of a strongly correlated Fermi gas," *ibid.* **323**, 2971 (2008); "Generalized virial theorem and pressure relation for a strongly correlated Fermi gas," *ibid.* **323**, 2987 (2008).

[29] E. Braaten and L. Platter, "Exact Relations for a Strongly Interacting Fermi Gas from the Operator Product Expansion," Phys. Rev. Lett. **100**, 205301 (2008).

[30] E. Braaten, in *The BCS-BEC Crossover and the Unitary Fermi Gas*, Lecture Notes in Physics, edited by W. Zwerger, Chap. 6 (Springer, Berlin, 2012).

[31] E. Braaten, D. Kang, and L. Platter, "Universal Relations for Identical Bosons from Three-Body Physics," Phys. Rev. Lett. **106**, 153005 (2011).

[32] F. Werner and Y. Castin, "General relations for quantum gases in two and three dimensions: Two-component fermions," Phys. Rev. A **86**, 013626 (2012); "General relations for quantum gases in two and three dimensions. II. Bosons and mixtures," *ibid.* **86**, 053633 (2012).

[33] M. Barth and W. Zwerger, "Tan relations in one dimension," Ann. Phys. (NY) **326**, 2544 (2011).

[34] J. Hofmann, "Quantum Anomaly, Universal Relations, and Breathing Mode of a Two-Dimensional Fermi Gas," Phys. Rev. Lett. **108**, 185303 (2012).

[35] M. Valiente, N. T. Zinner, and K. Mølmer, "Universal relations for the two-dimensional spin-1/2 Fermi gas with contact interactions," Phys. Rev. A **84**, 063626 (2011); "Universal properties of Fermi gases in arbitrary dimensions," *ibid.* **86**, 043616 (2012).

[36] S. M. Yoshida and M. Ueda, "Universal High-Momentum Asymptote and Thermodynamic Relations in a Spinless Fermi Gas with a Resonant p-Wave Interaction," Phys. Rev. Lett. **115**, 135303 (2015).

[37] Z. Yu, J. H. Thywissen, and S. Zhang, "Universal Relations for a Fermi Gas Close to a p-Wave Interaction Resonance," Phys. Rev. Lett. **115**, 135304 (2015).

[38] M. He, S. Zhang, H. M. Chan, and Q. Zhou, "Concept of a Contact Spectrum and Its Applications in Atomic Quantum Hall States," Phys. Rev. Lett. **116**, 045301 (2016).

[39] R. Weiss, B. Bazak, and N. Barnea, "Nuclear Neutron-Proton Contact and the Photoabsorption Cross Section," Phys. Rev. Lett. **114**, 012501 (2015); "Generalized nuclear contacts and momentum distributions," Phys. Rev. C **92**, 054311 (2015).

[40] J. T. Stewart, J. P. Gaebler, T. E. Drake, and D. S. Jin, "Verification of Universal Relations in a Strongly Interacting Fermi Gas," Phys. Rev. Lett. **104**, 235301 (2010).

[41] C. Luciuk, S. Trotzky, S. Smale, Z. Yu, S. Zhang, and J. H. Thywissen, "Evidence for universal relations describing a gas with p-wave interactions," Nat. Phys. **12**, 599 (2016).

[42] E. H. Lieb, D. C. Mattis, *Mathematical Physics in One Dimension: Exactly Soluble Models of Interacting Particles* (Academic Press, 1966).

[43] B. Sutherland, *Beautiful Models* (World Scientific Publishing, 2004).

[44] E. H. Lieb and W. Liniger, "Exact Analysis of an Interacting Bose Gas. I. The General Solution and the Ground State," Phys. Rev. **130**, 1605 (1963); E. H. Lieb, "Exact Analysis of an Interacting Bose Gas. II. The Excitation Spectrum," *ibid.* **130**, 1616 (1963).

[45] M. A. Cazalilla, R. Citro, T. Giamarchi, E. Orignac, and M. Rigol, "One dimensional bosons: From condensed matter systems to ultracold gases," Rev. Mod. Phys. 83, 1405-1466 (2011).

[46] M. Girardeau, "Relationship between Systems of Impenetrable Bosons and Fermions in One Dimension," J. Math. Phys. **1**, 516 (1960).

[47] C. N. Yang and C. P. Yang, "Thermodynamics of a One-Dimensional System of Bosons with Repulsive Delta-Function Interaction," J. Math. Phys. (N.Y.) **10**, 1115 (1969).

[48] J. B. McGuire, "Study of exactly soluble one-dimensional N-body problems," J. Math. Phys. **5**, 622-636 (1964).

[49] M. Olshanii, "Atomic Scattering in the Presence of an External Confinement and a Gas of Impenetrable Bosons," Phys. Rev. Lett. **81**, 938 (1998).

[50] T. Kinoshita, T. Wenger, D. S. Weiss, "Observation of a One-Dimensional Tonks-Girardeau Gas," Science **305**, 1125 (2004).

[51] B. E. Granger and D. Blume, "Tuning the Interactions of Spin-Polarized Fermions Using Quasi-One-Dimensional Confinement," Phys. Rev. Lett. **92**, 133202 (2004).

[52] T. Cheon and T. Shigehara, "Fermion-Boson Duality of One-Dimensional Quantum Particles with Generalized Contact Interactions," Phys. Rev. Lett. **82**, 2536 (1999).

[53] M. D. Girardeau and M. Olshanii, "Theory of spinor Fermi and Bose gases in tight atom waveguides," Phys. Rev. A **70**, 023608 (2004).

[54] V. E. Korepin, N. M. Bogoliubov, and A. G. Izergin, *Quantum Inverse Scattering Method and Correlation Functions* (Cambridge University Press, Cambridge, England, 1993).

[55] F. D. M. Haldane, "Effective Harmonic-Fluid Approach to Low-Energy Properties of One-Dimensional Quantum Fluids," Phys. Rev. Lett. **47**, 1840 (1981); "Demonstration of the "Luttinger liquid" character of Bethe-ansatz-soluble models of 1-D quantum fluids," Phys. Lett. **81A**, 153 (1981).

[56] H. Primakoff and T. Holstein, "Many-body interactions in atomic and nuclear systems," Phys. Rev. **55**, 1218-1234 (1939).

[57] B. M. Axilrod and E. Teller, "Interaction of the van der Waals type between three atoms," J. Chem. Phys. **11**, 299-300 (1943).

[58] Y. Muto, "Force between nonpolar molecules," J. Phys.-Math. Soc. Japan **17**, 629-631 (1943).

[59] J. Fujita and H. Miyazawa, "Pion theory of three-body forces," Prog. Theor. Phys. **17**, 360-365 (1957).

[60] H.-W. Hammer, A. Nogga, and A. Schwenk, "Colloquium: Three-body forces: From cold atoms to nuclei," Rev. Mod. Phys. **85**, 197-217 (2013).

[61] E. Braaten, H.-W. Hammer, and T. Mehen, "Dilute Bose-Einstein Condensate with Large Scattering Length," Phys. Rev. Lett. **88**, 040401 (2002).

[62] N. R. Cooper, "Exact Ground States of Rotating Bose Gases Close to a Feshbach Resonance," Phys. Rev. Lett. **92**, 220405 (2004).

[63] H. P. Büchler, A. Micheli, and P. Zoller, "Three-body interactions with cold polar molecules," Nat. Phys. **3**, 726 (2007).

[64] A. J. Daley, J. M. Taylor, S. Diehl, M. Baranov, and P. Zoller, "Atomic Three-Body Loss as a Dynamical Three-Body Interaction," Phys. Rev. Lett. **102**, 040402 (2009).

[65] M. Roncaglia, M. Rizzi, and J. I. Cirac, "Pfaffian State Generation by Strong Three-Body Dissipation," Phys. Rev. Lett. **104**, 096803 (2010).

[66] L. Mazza, M. Rizzi, M. Lewenstein, and J. I. Cirac, "Emerging bosons with three-body interactions from spin-1 atoms in optical lattices," Phys. Rev. A **82**, 043629 (2010).

[67] K. W. Mahmud and E. Tiesinga, "Dynamics of spin-1 bosons in an optical lattice: Spin mixing, quantum-phase-revival spectroscopy, and effective three-body interactions," Phys. Rev. A **88**, 023602 (2013).

[68] A. J. Daley and J. Simon, "Effective three-body interactions via photon-assisted tunneling in an optical lattice," Phys. Rev. A **89**, 053619 (2014).

[69] D. S. Petrov, "Three-body interacting bosons in free space," Phys. Rev. Lett. **112**, 103201 (2014).

[70] D. S. Petrov, "Elastic multibody interactions on a lattice," Phys. Rev. A **90**, 021601(R) (2014).

[71] S. Paul, P. R. Johnson, and E. Tiesinga, "Hubbard model for ultracold bosonic atoms interacting via zero-point-energy–induced three-body interactions," Phys. Rev. A **93**, 043616 (2016).

[72] A. Bulgac, "Dilute Quantum Droplets," Phys. Rev. Lett. **89**, 050402 (2002).

[73] L. Radzihovsky, J. Park, and P. B. Weichman, "Superfluid Transitions in Bosonic Atom-Molecule Mixtures near a Feshbach Resonance," Phys. Rev. Lett. **92**, 160402 (2004); L. Radzihovsky, P. B. Weichman, and J. I. Park, "Superfluidity and phase transitions in a resonant Bose gas," Ann. Phys. (NY) **323**, 2376 (2008).

[74] M. W. J. Romans, R. A. Duine, S. Sachdev, and H. T. C. Stoof, "Quantum Phase Transition in an Atomic Bose Gas with a Feshbach Resonance," Phys. Rev. Lett. **93**, 020405 (2004).

[75] Y.-W. Lee and Y.-L. Lee, "Quantum phase transition in an atomic Bose gas near a Feshbach resonance," Phys. Rev. B **70**, 224506 (2004).

[76] S. Basu and E. J. Mueller, "Stability of bosonic atomic and molecular condensates near a Feshbach resonance," Phys. Rev. A **78**, 053603 (2008).

[77] C. Nayak, S. H. Simon, A. Stern, M. Freedman, and S. D. Sarma, "Non-Abelian anyons and topological quantum computation," Rev. Mod. Phys. **80**, 1083 (2008).

[78] Y. Nishida, "Semisuper Efimov effect of two-dimensional bosons at a three-body resonance," Phys. Rev. Lett. **118**, 230601 (2017).

[79] V. Gurarie, "One-dimensional gas of bosons with Feshbach-resonant interactions," Phys. Rev. A **73**, 033612 (2006).

[80] X. Cui, "Universal one-dimensional atomic gases near odd-wave resonance," Phys. Rev. A **94**, 043636 (2016).

[81] K. V. Kheruntsyan, D. M. Gangardt, P. D. Drummond, and G. V. Shlyapnikov, "Pair Correlations in a Finite-Temperature 1D Bose Gas," Phys. Rev. Lett. **91**, 040403 (2003).

[82] D. M. Gangardt and G. V. Shlyapnikov, "Stability and Phase Coherence of Trapped 1D Bose Gases," Phys. Rev. Lett. **90**, 010401 (2003); "Local correlations in a strongly interacting one-dimensional Bose gas," New J. Phys. **5**, 79 (2003).

[83] V. V. Cheianov, H. Smith, and M. B. Zvonarev, "Exact results for three-body correlations in a degenerate one-dimensional Bose gas," Phys. Rev. A **73**, 051604(R) (2006); "Three-body local correlation function in the Lieb-Liniger model: bosonization approach," J. Stat. Mech. (2006) P08015.

[84] M. Kormos, G. Mussardo, and A. Trombettoni, "Expectation Values in the Lieb-Liniger Bose Gas," Phys. Rev. Lett. **103**, 210404 (2009); "One-dimensional Lieb-Liniger Bose gas as nonrelativistic limit of the sinh-Gordon model," Phys. Rev. A **81**, 043606 (2010).

[85] M. Kormos, Y.-Z. Chou, and A. Imambekov, "Exact Three-Body Local Correlations for Excited States of the 1D Bose Gas," Phys. Rev. Lett. **107**, 230405 (2011).

[86] M. Gaudin, *La fonction d'onde de Bethe*, Masson, Paris (1983).

[87] T. M. Hanna, E. Tiesinga, and P. S. Julienne, "Creation and manipulation of Feshbach resonances with radiofrequency radiation," New J. Phys. **12**, 083031 (2010).

[88] M. Lysebo and L. Veseth, "Feshbach resonances and transition rates for cold homonuclear collisions between ^{39}K and ^{41}K atoms," Phys. Rev. A **81**, 032702 (2010).

[89] Y. Sekino, and Y. Nishida, "Quantum droplet of one-dimensional bosons with a three-body attraction," Phys. Rev. A **97**, 011602(R) (2018).

[90] M. Olshanii and V. Dunjko, "Short-Distance Correlation Properties of the Lieb-Liniger System and Momentum Distributions of Trapped One-Dimensional Atomic Gases," Phys. Rev. Lett. **91**, 090401 (2003).

[91] S. A. Bender, K. D. Erker, and B. E. Granger, "Exponentially Decaying Correlations in a Gas of Strongly Interacting Spin-Polarized 1D Fermions with Zero-Range Interactions," Phys. Rev. Lett. **95**, 230404 (2005).

[92] M. D. Girardeau and A. Minguzzi, "Bosonization, Pairing, and Superconductivity of the Fermionic Tonks-Girardeau Gas," Phys. Rev. Lett. **96**, 080404 (2006).

[93] A. Yu. Cherny and J. Brand, "Polarizability and dynamic structure factor of the one-dimensional Bose gas near the Tonks-Girardeau limit at finite temperatures," Phys. Rev. A **73**, 023612 (2006); "Dynamic and static density-density correlations in the one-dimensional Bose gas: Exact results and approximations," *ibid.* **79**, 043607 (2009).

[94] M. Valiente, "Exact equivalence between one-dimensional Bose gases interacting via hard-sphere and zero-range potentials," Europhys. Lett. **98**, 10010 (2012).

[95] R. Combescot, F. Alzetto, and X. Leyronas, "Particle distribution tail and related energy formula," Phys. Rev. A **79**, 053640 (2009).

[96] Y. Hao, Y. Zhang, J. Q. Liang, and S. Chen, "Ground-state properties of one-dimensional ultracold Bose gases in a hard-wall trap," Phys. Rev. A **73**, 063617 (2006).

[97] Y. Hao, Y. Zhang, and S. Chen, "One-dimensional fermionic gases with attractive p-wave interaction in a hard-wall trap," Phys. Rev. A **76**, 063601 (2007).

[98] M. Rigol, V. Dunjko, V. Yurovsky, and M. Olshanii, "Relaxation in a Completely Integrable Many-Body Quantum System: An Ab Initio Study of the Dynamics of the Highly Excited States of 1D Lattice Hard-Core Bosons," Phys. Rev. Lett. **98**, 050405 (2007).

[99] G. E. Astrakharchik and S. Giorgini, "Correlation functions and momentum distribution of one-dimensional Bose systems," Phys. Rev. A **68**, 031602(R) (2003).

[100] J.-S. Caux and P. Calabrese, "Dynamical density-density correlations in the one-dimensional Bose gas," Phys. Rev. A **74**, 031605(R) (2006).

[101] J.-S. Caux, P. Calabrese, and N. A. Slavnov, "One-particle dynamical correlations in the one-dimensional Bose gas," J. Stat. Mech. (2007) P01008.

[102] T. Jacqmin, B. Fang, T. Berrada, T. Roscilde, and I. Bouchoule, "Momentum distribution of one-dimensional Bose gases at the quasicondensation crossover: Theoretical and experimental investigation," Phys. Rev. A **86**, 043626 (2012).

[103] M. Panfil, and J.-S. Caux, "Finite-temperature correlations in the Lieb-Liniger one-dimensional Bose gas," Phys. Rev. A **89**, 033605 (2014).

[104] F. F. Bellotti, T. Frederico, M. T. Yamashita, D. V. Fedorov, A. S. Jensen, and N. T. Zinner, "Dimensional effects on the momentum distribution of bosonic trimer states," Phys. Rev. A **87**, 013610 (2013).

[105] A. Imambekov, A. A. Lukyanov, L. I. Glazman, and V. Gritsev, "Exact Solution for 1D Spin-Polarized Fermions with Resonant Interactions," Phys. Rev. Lett. **104**, 040402 (2010).

[106] R. Qi and X. Guan, "Many-body properties of quasi-one-dimensional boson gas across a narrow CIR," Europhys. Lett. **101**, 40002 (2013).

[107] X. Cui and H. Dong, "High-momentum distribution with a subleading k^3 tail in odd-wave interacting one-dimensional Fermi gases," Phys. Rev. A **94**, 063650 (2016).

[108] J. Stenger, S. Inouye, A. P. Chikkatur, D. M. Stamper-Kurn, D. E. Pritchard, and W. Ketterle, "Bragg Spectroscopy of a Bose-Einstein Condensate," Phys. Rev. Lett. **82**, 4569 (1999).

[109] L.-M. Duan, "Detecting Correlation Functions of Ultracold Atoms through Fourier Sampling of Time-of-Flight Images," Phys. Rev. Lett. **96**, 103201 (2006).

[110] T.-L. Dao, A. Georges, J. Dalibard, C.—Salomon, and I. Carusotto, "Measuring the One-Particle Excitations of Ultracold Fermionic Atoms by Stimulated Raman Spectroscopy," Phys. Rev. Lett. **98**, 240402 (2007).

[111] A. Altland and B. Simons, *Condensed Matter Field Theory*, Chap. 7 (Cambridge University Press, Cambridge, 2010).

[112] L. P. Kadanoff, "Operator Algebra and the Determination of Critical Indices," Phys. Rev. Lett. **23**, 1430 (1969).

[113] A. Polyakov, "Properties of Long and Short Range Correlations in the Critical Region," Sov. Phys. JETP **30**, 151 (1970).

[114] K. G. Wilson, "Non-Lagrangian Models of Current Algebra," Phys. Rev. **179**, 1499 (1969).

[115] D. T. Son and E. G. Thompson, "Short-distance and short-time structure of a unitary Fermi gas," Phys. Rev. A **81**, 063634 (2010).

[116] J. Hofmann, "Current response, structure factor and hydrodynamic quantities of a two- and three-dimensional Fermi gas from the operator-product expansion," Phys. Rev. A **84**, 043603 (2011).

[117] S. Coleman and E. Weinberg, "Radiative corrections as the origin of spontaneous symmetry breaking," Phys. Rev. D **7**, 1888-1910 (1973).

[118] H.-W. Hammer and D. T. Son, "Universal properties of two-dimensional boson droplets," Phys. Rev. Lett. **93**, 250408 (2004).

[119] B. Bazak and D. S. Petrov, "Energy of N two-dimensional bosons with zero-range interactions," New J. Phys. **20**, 023045 (2018).

[120] E. H. Lieb and J. Yngvason, "Ground state energy of the low density Bose gas," Phys. Rev. Lett. **80**, 2504-2507 (1998).

[121] E. H. Lieb, R. Seiringer, and J. Yngvason, "Bosons in a trap: A rigorous derivation of the Gross-Pitaevskii energy functional," Phys. Rev. A **61**, 043602 (2000).

[122] E. H. Lieb and J. Yngvason, "The ground state energy of a dilute two-dimensional Bose gas," J. Stat. Phys. 509-526, **103** (2001).

[123] E. H. Lieb, R. Seiringer, and J. Yngvason, "A rigorous derivation of the Gross-Pitaevskii energy functional for a two-dimensional Bose gas," Commun. Math. Phys. **224**, 17-31, (2001).

[124] Y. Castin and C. Herzog, "Bose-Einstein condensates in symmetry breaking states," C. R. Acad. Sci. Paris **2**, 419-443 (2001).